NASA TECHNICAL REPORT

NASA TR R-333

COUPLED THERMALLY-INDUCED TRANSVERSE PLUS TORSIONAL VIBRATIONS OF A THIN-WALLED CYLINDER OF OPEN SECTION

by Harold P. Frisch

Goddard Space Flight Center
Greenbelt, Md. 20771

1. Report No. NASA TR R-333	2. Government Accession No.	3. Recipient's Catalog No.	
4. Title and Subtitle Coupled Thermally-Induced Transverse Plus Torsional Vibrations of a Thin-Walled Cylinder of Open Section		5. Report Date March 1970	
		6. Performing Organization Code	
7. Author(s) Harold P. Frisch		8. Performing Organization Report No. G-952	
9. Performing Organization Name and Address Goddard Space Flight Center Greenbelt, Maryland 20771		10. Work Unit No. 124-08-25-07	
		11. Contract or Grant No.	
		13. Type of Report and Period Covered	
12. Sponsoring Agency Name and Address National Aeronautics and Space Administration Washington, D. C. 20546		Technical Report	
		14. Sponsoring Agency Code	

15. Supplementary Notes

16. Abstract

    Long thin-walled cylinders of open section (STEM type booms) have been used on many satellites either for experimentation or Gravity Gradient stabilization. Equations for the coupled transverse plus torsional oscillations of a long open section cylinder in direct sunlight are derived. Numerical results show that unstable thermally induced oscillations can be excited solely by the impinging thermal energy of the sun. It is shown that this is a direct result of the boom's extreme weakness in torsion. By literally zippering the boom's open section, to increase its torsional rigidity, the problem can be eliminated. Flight data from OGO IV, V, VI and RAE are cited to support the theoretical findings.

17. Key Words Suggested by Author Gravity Gradient Satellites Beam vibrations Oscillation of satellite bodies Thermoelasticity Thermally Induced Vibrations OGO		18. Distribution Statement Unclassified - Unlimited		
19. Security Classif. (of this report) Unclassified	20. Security Classif. (of this page) Unclassified		21. No. of Pages 114	22. Price * $3.00

SUMMARY

Recent satellites have carried long extendable appendages of the type classified as thin-walled cylinders of open section for such diverse applications as dipole antennas, gravity-gradient stabilization booms, and electric-field probes. Actual flight data show that several satellites which deploy these long appendages (or antennas, as they will be referred to) exhibit varying degrees of anomalous spacecraft body motion while exposed to direct sunlight. NASA/GSFC hypothesis is that in many cases the observed oscillations are thermally induced.

This document presents the equations which describe the coupled non-planar transverse and torsional vibrations of such an antenna when it is exposed to a directional solar thermal field (sunlight). To obtain a numerical solution, the equations are specialized to the case of a clamped-free cylinder of open section having the nominal characteristics of the antennas in orbit. Comparison of results with actual flight data shows that this hypothesis leads to conclusions consistent with the observed phenomena. The numerical examples show that the problem of thermally-induced vibration can be eliminated by literally zippering the open section of the antenna, in various fashions, so as to effectively increase its torsional rigidity. Flight data from the Radio Astronomy Explorer satellite (which has four 750-foot stable zippered antennas) and the Orbiting Geophysical Observatory, OGO VI, (which has two 30-foot stable torsionally rigid electron probes) support this conclusion.

CONTENTS

COUPLED THERMALLY-INDUCED TRANSVERSE PLUS TORSIONAL VIBRATIONS OF A THIN-WALLED CYLINDER OF OPEN SECTION

by
Harold P. Frisch
Goddard Space Flight Center

INTRODUCTION

Prior to the flight of RAE* all satellites having long extendable appendages used the basic STEM† type boom, shown in Figure 1, for storage and deployment. It is made from a long, thin prestressed tape which is rolled on a drum for storage and when extended takes on a tubular shape. Such booms have been used on OGO‡ IV and V as electric field probes, on ATS-A,§ OV1-10, GGSE‖ III, V and VI and several other Navy and Air Force satellites as gravity-gradient booms.

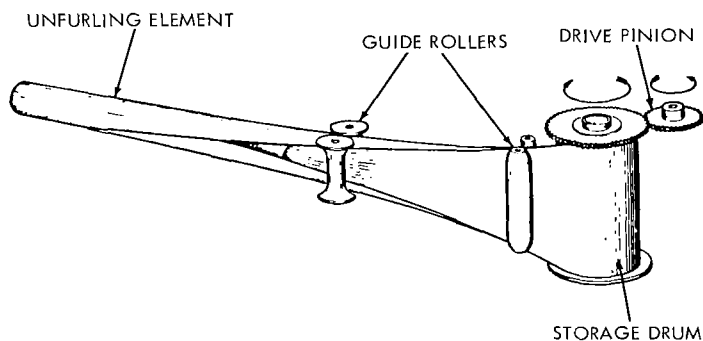
Figure 1—The STEM principle.

Anomolous Motion of Booms

On each of the aforementioned satellites, with the exception of RAE, varying degrees of anomalous spacecraft body motion has been observed. This motion is known to be excited only when the satellite is in full sunlight and its magnitude has at times been large enough to impair severely the performance and stability of the satellite.**

The problem first manifested itself during the initial phases of the flight of OGO IV. Soon after the deployment of the 60' open-section cylinder, used as an electric-field probe on this satellite, in full sunlight, a disturbance was noted by the control-system sensors. They indicated that the satellite body was oscillating ±1.5° about the axis of maximum moment of inertia at the fundamental bending frequency of the satellite boom system. Furthermore, the oscillation persisted whenever the satellite was in sunlight and rapidly damped down every time it entered eclipse. From a knowledge of the elastic modes of vibration of OGO IV it has been calculated[*] that a ±1.5° oscillation of the satellite body corresponded to a ±20-foot oscillation of the antenna tip.

Before the launch of OGO IV, a study had been completed (Reference 1) which showed that, because of the extreme weakness of the boom in torsion, the static-thermal-equilibrium shape that the boom could assume in a solar thermal field was not unique. It was postulated[†] that, if torsional motion were excited, the thermal equilibrium position toward which the antenna was moving would be continually changing in time. It was further hypothesized that, if the proper relationship existed between the motion of the position of thermal equilibrium and the motion of the boom, the observed anomalous motion could be thermally-induced.

This paper is intended to be a complete documentation of the theory of thermally-induced vibration of spacecraft booms; the basic findings have been previously published in a highly condensed form.[‡§]

Soon after the initial postulation that the anomalous motion on OGO IV could be caused by a thermally-induced oscillation of the attached boom, two other variations of the theory were postulated by other personnel[∥] of Goddard Space Flight Center.

The first variation, set down by G. Banks,[**] showed that a cantilevered beam could be driven unstable by solar energy if the source were oriented behind the clamped root. The solution was obtained by investigating the stability characteristics of the equation which defined the motion of a single-degree-of-freedom analogy of the system. Results of this analysis indicated also that only a small amount of damping is needed to stabilize the system. This variation was therefore dismissed as not practically applicable to present spacecraft problems.

The second variation, set down by J. Donohue,[††] uses a unique representation of the coupling between torsional and transverse displacement to derive a single-degree-of-freedom analogy of the system. While some of the assumptions made must be termed gross simplifications of the problem, the treatment is a perfect example of how sound engineering judgment can be incorporated

[*]GSFC Memo 732-46, H. P. Frisch to H. C. Hoffman, Aug. 18, 1967, "Transfer Function, Tip Deflection and Root Bending Stress of OGO-D Boom As Derived from Flexible Body Analysis."

[†]GSFC Memo 732-56, H. P. Frisch to H. C. Hoffman, Aug. 29, 1967, "Thermally Induced Vibrations of the OGO-D Boom With Inference to ATS."

[‡]J. H. Donohue and H. P. Frisch, "Thermoelastic Instability of Open Section Booms," Symposium on Gravity Gradient Attitude Control, Dec. 3-5, 1968, Los Angeles, Calif. Also, NASA Technical Note TN D-5310, Dec. 1969.

[§]H. P. Frisch, "Thermally Induced Vibrations of Long Thin Walled Cylinders of Open Section," ASME/AIAA 10th Structures, Structural Dynamics and Materials Conference, April 14-16, 1969, New Orleans, La.

[∥]J. Donohue, H. Hoffman, H. Price, B. Zimmerman, and G. Banks.

[**]GSFC Memo, Sept. 1, 1967, G. F. Banks to R. J. Darcey, "Boom Flutter Due to Thermal Lag."

[††]GSFC Memo 732-194, J. H. Donohue to H. C. Hoffman, "Preliminary Review of Lumped Parameter Simulation of OGO Thermally Induced Boom Oscillations," Feb. 29, 1968.

into a simple model to yield useful and reasonably accurate answers to an extremely complex problem.

Unknown to GSFC at the time, G. Augusti at the University of Naples simultaneously initiated an investigation into the stability of elastic structures loaded by non-conservative forces, namely, radiant heat.* The problem solved by Augusti was virtually the same as that solved by Banks. Both investigators arrived at the same basic conclusions.

Subsequent to the initial work done by NASA/GSFC, Y. Y. Yu[†] made use of G. Banks' original idea and extended it to the continuous-beam case. His results, however, are 180° out of phase with the results obtained from the single-degree-of-freedom analogies presented by Banks and Augusti. The present author believes that the results of the single-degree-of-freedom analogy are correct and that the results of the continuous-beam analysis should be closely approximated by its lumped-parameter analogy.[‡]

The work to be presented herein derives the equations which define the dynamic response of a clamped-free thin-walled cylinder in a solar thermal field. The equations are specialized to the case of a cylinder of open section; however, modifications can be introduced which enable one to study cylinders of closed section. Cylinders of zippered section, that is, cylinders of open section which have had their seams literally zippered, also can be studied by the proper adjustment of the torsional stiffness parameters and by the introduction of a reasonable thermal model.

While it is recognized that the simplifying assumptions to be introduced will prevent describing the dynamic response of the boom exactly, it must be emphasized that the purpose of this analysis is to define the basic cause of the observed oscillations and to obtain an approximate estimate of its steady state amplitude. Furthermore, considerable scatter in experimentally determined values of stiffness, damping, and thermal characteristics imply that there is no point in an overly refined analysis.

The results obtained by numerical solution of the derived equations show that the postulated theory[§] (if accepted) leads to conclusions which are consistent with observed phenomena.

The question of the validity of the theory of thermally-induced vibration as proposed by Goddard Space Flight Center to explain this phenomena (and presented herein) was the subject of a session at the Symposium on Gravity Gradient Attitude Control sponsored by the Air Force and Aerospace Corporation in December 1968. It was the general conclusion at the symposium that this theory is valid and does indeed define the cause of the anomalous motion observed on OGO IV and other satellites deploying long flexible cylinders of open section.

---

*G. Augusti, "Instability of Struts Subject to Radiant Heat," 12th International Congress of Applied Mechanics, Stanford University, Aug. 26-31, 1968; in *Meccanica,* No. 3, 1968.
[†]Y. Y. Yu, "Thermally Induced Vibration and Flutter of a Flexible Boom," AIAA 7th Aerospace Science Meeting, New York, Jan. 20-22, 1969. Also, Journal of Spacecraft and Rockets, Aug. 1969.
[‡]See forthcoming technical comments by Jordan and Augusti in *Journal of Spacecraft and Rockets.*
[§]GSFC Memo 732-56, H. P. Frisch to H. C. Hoffman, Aug. 29, 1967, "Thermally Induced Vibrations of the OGO-D Beam with Inference to ATS."

Mathematical Model and Outline of Solution

The model which is assumed to adequately describe the boom is a long, uniform, continuous, thin-walled cylinder of open cross-section. It is assumed to be clamped at one end both in two-axis bending and in torsion. The other end is free to warp and deflect and has attached to it a tip weight which has both translational and rotational inertia. The effect of the shear center axis being displaced from the centroidal axis is assumed to be negligible, and the bending stiffness about any axis passing through the centroid of the cross-section is assumed to be constant.

The system is assumed to be free of all disturbances except those arising from the translational and torsional motion of the cylinder relative to an inertially fixed coordinate system, those arising from viscoelastic damping both in two-axis transverse bending and in torsion, and those arising from the continual attempts of the cylinder to relieve its state of thermal stress by bending and twisting toward a position of thermal equilibrium.

The response of the cylinder to a time-varying non-uniform thermal stress distribution is ascertained by applying the techniques of elementary strength of materials. This approach is justified by Boley in Reference 2 (Chapter 10).

Accordingly, the Timoshenko theory of bending and torsion of thin-walled members of open section as expounded in References 3 and 4 is directly applied. That is, for small-angle bending and torsion the equations are separable and can be solved independently. Furthermore, the stress couples that produce pure bending are proportional to curvature, and the stress couple that produces pure torsion is countered by the resistance of the cylinder to both torsion and warping.

The equations of vibration are derived by making use of two coordinate systems; one is fixed at the clamped end and the other slides with constant rate along the boom. The use of vector techniques as discussed by Landau and Lifshitz (Reference 5) and A. E. H. Love (Reference 6) makes it possible to derive these equations relative to the sliding coordinate system.

When long rods are to be studied, special consideration must be given to the development of the equations that define the forces associated with the kinetic reactions of accelerating mass elements. Since the antennas under study may be of arbitrary length, and non-planar transverse motion is assumed to occur, the deflected shape of the boom at each instant of time must be considered when such forces are computed. From the computation it is seen that significant coupling exists between translational and torsional motion. This coupling defines, for relatively long booms, the principal mechanism by which transverse and torsional motion are coupled together. For booms of short length, however, this effect becomes of decreasing importance compared to such neglected effects as the shear center being offset from the centroid and the non-symmetry of the cross-section.

With torsional motion existing in a solar thermal field, there will be a continuous change in the flow of heat around the perimeter of the boom. The rate at which heat will flow from the illuminated side to the dark side is governed by the thermal time constants of the boom. The overall temperature distribution and hence the thermal loading is therefore a non-linear function of the boom's torsional response and its thermal time constants.

4

It is assumed that there is zero heat flow along the length of the boom and that the heat flow around the perimeter is describable by the standard equation for heat conduction and radiation in a one-dimensional solid. Heat is assumed to be radiated uniformly around the entire perimeter, and to be absorbed only on the sunlit side according to a cosine law. By solving the thermodynamic equation at a sufficient number of thermal stations along the length of the boom, an accurate description of the overall temperature distribution, and hence the thermal loading, is obtainable.

The three equations that define the motion of the cylinder in the transverse and torsional directions and the thermodynamic equation that is defined at each thermal station are partial differential equations of the type which may have their solutions expressed in terms of orthogonal functions. That is, the solutions to the vibration equations are expressed in terms of their normal modes of vibration and the corresponding generalized displacement coordinates; similarly, the solutions to the thermodynamic equations are expressed in terms of the normalized thermal modes and the corresponding generalized thermal coordinates.

The actual solutions to be presented are obtained by numerically solving simultaneously the equations which define the generalized displacement and thermal coordinates associated with the most significant vibration and thermal modes. The solutions show that the theoretically predicted amplitudes of the antennas on OGO IV and OGO V are consistent with those observed from actual flight data.

Solutions are included that show how variations in various significant and controllable parameters can affect the steady state amplitude of the thermally-induced vibrations. From these solutions it becomes evident that the problem of thermally-induced vibrations can be eliminated by increasing the torsional rigidity of the boom by two to three orders of magnitude. This improvement can and has been made by various manufacturers by zippering the seams of the open-section cylinder.

Both RAE, launched September 1968, and OGO-VI, launched June 1969, have torsionally rigid booms. As predicted, the four 750-foot booms on RAE and the two 30-foot booms on OGO-VI are stable.

THE THERMODYNAMIC MODEL

The accurate prediction of whether or not thermally-induced vibrations can be excited depends upon the thermal model used to describe the thermal loading. The model to be used must be capable of taking into account large-angle torsional motion of the boom relative to a fixed sun line. It must also be capable of taking into account the thermal properties of the boom material, which cause heat to flow at a finite rate.

The development of the thermal model to be used will be based upon the fundamental hypothesis governing the conduction of heat in solids as discussed by Carslaw and Jaeger in Reference 7.

Since the amount of twist per unit length is restricted to small values by the assumptions of linear elasticity, and since the temperature gradients across and along the boom are small compared to its mean temperature, the assumption that zero heat is conducted along the length of the boom can be made and the equation linearized. It is thus possible to determine the entire temperature profile by solving the one-dimensional equation of heat conduction and radiation at a sufficient number of thermal stations along the boom length. The thermal profile between each thermal station is easily determined by linear or higher-order interpolation techniques.

The question to be answered before this method is used to describe the thermal loading is whether or not the detail it provides is necessary. To answer this the thermal response of a unit boom element is studied when it is made to oscillate at predefined rates and amplitudes in a solar thermal field. The results show clearly that it would be very difficult to construct and justify a reasonably simple model approximating the complete thermal profile for arbitrary torsional motion.

Accordingly, the equation describing the temperature change around a unit element of boom length is derived for arbitrary rotational motion of the sun relative to the cross-sectional principal axes of inertia. Once this equation has been obtained, it is a simple matter to:

1. Study the thermal response due to a predefined sun motion.

2. Study the thermal response at any thermal station along the boom.

By defining a thermodynamic equation at each thermal station and by solving each simultaneously with the vibration equations so that the sun's relative orientation can be continually updated, it is possible to obtain a continuous and accurate record of the thermal loading. This information can in turn be used in the vibration equations to update the effective forcing function due to thermal loading.

Thermodynamic Equation of Heat Conduction and Radiation

Figure 2 depicts the type of thin-walled cylinder of open section which is studied in this report. It has arbitrary length and radius, its wall thickness must be definable as thin (i.e., it cannot support a thermal gradient), and the angular amount of overlap should be not less than 0° nor greater than 180°.

The assumptions upon which the thermodynamic equation of heat conduction and radiation is based are identical with those set down in Reference 1 and used to study static thermal bending plus twist of long thin-walled cylinders of open section. These assumptions are:

1. Heat is conducted only in a circumferential direction around the entire perimeter.

2. The entire cross-section loses heat by radiation.

3. The heat absorbed at a point on the sunlit side of the boom element is proportional to the cosine of the angle between the surface normal and the sun line.

6

4. Heat transfer across the interior of the cylinder is assumed to be negligible; however, heat transfer from the overlapping surface to the overlapped surface is approximated by a radiation term because no smooth flush contact exists between the surfaces.
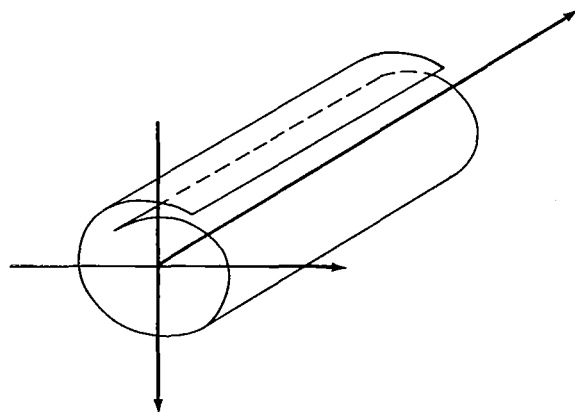
While slight differences exist between these assumptions, especially in the treatment of the overlap region, and those used by Florio and Hobbs (Reference 8) for their analytic model, both analyses lead to results that are consistent with experimental findings and with each other.

Figure 2—Thin-walled cylinder of open section (a typical boom segment).

It follows from the fundamental hypothesis for the mathematical theory of conduction of heat in solids (Reference 7) that, if there is no heat generated within or radiated away, the differential equation that defines the heat flow around a unit length of the boom shown in Figure 2 is

$$K_T h \frac{\partial^2 \tilde{T}(s, z, t)}{\partial s^2} - \rho c h \frac{\partial \tilde{T}(s, z, t)}{\partial t} = 0 , \qquad (1)$$

where the conditions at the boundaries are

$$\left. \frac{\partial \tilde{T}(s, z, t)}{\partial s} \right|_{s=0} = \left. \frac{\partial \tilde{T}(s, z, t)}{\partial s} \right|_{s=P} = 0 \qquad (2)$$

and the symbols used are defined as:

K_T = thermal conductivity, Btu/(sec-in.-°F)

h = cylinder wall thickness, in.

ρ = weight density of material, lbs/in.³

c = specific heat of material, Btu/(lb-°F)

s = arc length measured from outer to inner seam around the cross-section, in.

P = total perimeter of cross-section, in.

z = coordinate used to measure arc length along longitudinal axis of boom, in.

t = coordinate used to measure time, sec

$\tilde{T}(s, z, t)$ = absolute temperature at the position s, z at time t, °R.

If it is assumed that the boom radiates as a black body and that the heat input can be defined by the function $\Upsilon(s, z, t)$ then the thermodynamic equation of heat conduction and radiation is

given by

$$K_T h \frac{\partial^2 \widetilde{T}(s, z, t)}{\partial s^2} - \rho ch \frac{\partial \widetilde{T}(s, z, t)}{\partial t} = \sigma \epsilon \widetilde{T}^4 (s, z, t) - \Upsilon(s, z, t), \tag{3}$$

where

σ = Stefan-Boltzmann constant, Btu/(sec-in.^{2}-°F^4),

ϵ = emissivity,

$\Upsilon(s, z, t)$ = heat input at position (s, z) and at time t, Btu/(sec-in.^{2}).

The heat input function $\Upsilon(s, z, t)$ can be written as a function of the sun's orientation relative to the cross-sectional principal axes of inertia. Using Figure 3 as a guide, we let

$\overline{SL}(z, t)$ = unit vector emanating from the geocenter of the cross-section to the sun's relative position at (z, t),

$\vec{n}(s)$ = unit vector normal to the surface of the boom at position s
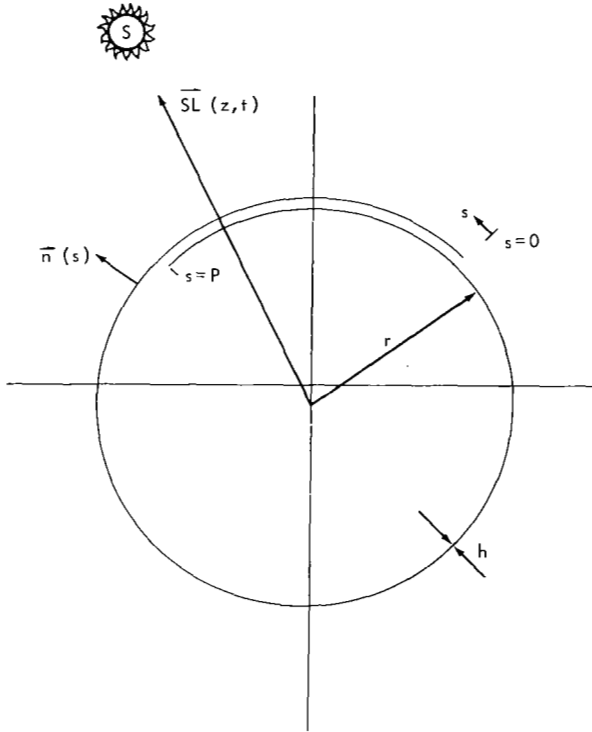
Figure 3—Boom cross-section at station z.

$$\Xi(s, z, t) = \begin{cases} 1 & \text{if} \quad \overline{SL}(z, t) \cdot \vec{n}(s) > 0 \\ 0 & \text{if} \quad \overline{SL}(z, t) \cdot \vec{n}(s) \leq 0 \end{cases} \tag{4}$$

(this function is used to distinguish mathematically between the sunlit and shaded sides of the boom),

J_s = solar radiation intensity, Btu/(sec-in.^{2}),

α_s = surface absorptivity,

r = radius of cylinder, in.,

and define the heat input function by the expression

$$\Upsilon(s, z, t) = \begin{cases} J_s \alpha_s \Xi(s, z, t) \overline{SL}(z, t) \cdot \vec{n}(s) & \text{for} \quad 0 \leq s \leq 2\pi r \\ \sigma \epsilon \alpha_s \widetilde{T}^4 (s - 2\pi r, z, t) & \text{for} \quad 2\pi r \leq s \leq P \end{cases} \tag{5}$$

This function is analogous to that used in Reference 1 to study static thermal deflection, and yields results which are consistent with the experimentally obtained data reported in Reference 8.

Making use of the fact that the maximum temperature difference between any two points on the boom surface for any sun orientation is small compared to the steady state mean temperature, the thermodynamic equation of heat conduction and radiation (Equation 3) can be linearized. Let

$$\tilde{T}(s, z, t) = T_0 + T(s, z, t),$$

(6)

where

T_0 = steady state mean temperature of cross-section, °R,

$T(s, z, t)$ = temperature deviation from T_0, °R,

and express $\tilde{T}^4(s, z, t)$ as a truncated binomial series expansion about T_0. A direct substitution of

$$\tilde{T}^4(s, z, t) \cong T_0^4 + 4T_0^3 T(s, z, t)$$

and Equation 6 into Equation 3 leads to the one-dimensional linearized thermodynamic equation of heat conduction and radiation along with its appropriate boundary conditions. That is,

$$\frac{\partial^2 T(s, z, t)}{\partial s^2} - \frac{\rho c}{K_T} \frac{\partial T(s, z, t)}{\partial t} - \frac{4\sigma\epsilon T_0^3}{K_T h} T(s, z, t) = \frac{\sigma\epsilon}{K_T h} T_0^4 - \frac{1}{K_T h} \Upsilon(s, z, t),$$

(7)

where

$$\left.\frac{\partial T(s, z, t)}{\partial s}\right|_{s=0} = \left.\frac{\partial T(s, z, t)}{\partial s}\right|_{s=P} = 0.$$

(8)

This equation can be solved for arbitrary sun motion by expressing the solution in terms of the orthogonal functions which satisfy its homogeneous part and their associated generalized coordinates.

By defining $\overrightarrow{SL}(z, t)$ to be a function of the torsional motion of the boom at thermal station z, a time history of the thermal loading at z can be obtained. To determine the thermal loading along the entire length of the boom, $\overrightarrow{SL}(z, t)$ must be defined, and the thermodynamic equation must be solved, at a sufficient number of thermal stations to obtain a piecewise continuous description of it.

Solution to Linearized Thermodynamic Equation

The linearized thermodynamic equation of heat conduction and radiation,

$$\frac{\partial^2 T(s, z, t)}{\partial s^2} - \frac{\rho c}{K_T} \frac{\partial T(s, z, t)}{\partial t} - \frac{4\sigma\epsilon T_0^3}{K_T h} T(s, z, t) = \frac{\sigma\epsilon T_0^4 - \Upsilon(s, z, t)}{K_T h},$$

(7)

9

may have its solution expressed in terms of the orthogonal functions that are solutions to its homogeneous part and that satisfy the stated boundary conditions

$$\frac{\partial T(s, z, t)}{\partial s}\bigg|_{s=0} = \frac{\partial T(s, z, t)}{\partial s}\bigg|_{s=P} = 0 .$$ (8)

The orthogonal functions that satisfy the homogeneous equation

$$\frac{\partial^2 T(s, z, t)}{\partial s^2} - \frac{\rho c}{K_T} \frac{\partial T(s, z, t)}{\partial t} - \frac{4\sigma \epsilon T_0^3}{K_T h} T(s, z, t) = 0$$ (9)

may be obtained by separation of variables. If a solution of the form

$$T(s, z, t) = e^{-\lambda t} T(s)$$ (10)

is assumed and substituted into Equation 9, a standard-type eigenvalue problem is obtained. That is, the function $T(s)$ must be a solution to the equation

$$\frac{d^2 T(s)}{ds^2} - \Omega_T^2 T(s) = 0$$ (11)

and satisfy the boundary conditions

$$\frac{dT(s)}{ds}\bigg|_{s=0} = \frac{dT(s)}{ds}\bigg|_{s=P} = 0 ,$$ (12)

where

$$\Omega_T^2 = \frac{4\sigma \epsilon T_0^3}{K_T h} - \frac{\rho c}{K_T} \lambda .$$ (13)

For a non-trivial solution to Equation 11 to exist, it can be shown, by substituting its general solution

$$T(s) = D_1 e^{\Omega_T s} + D_2 e^{-\Omega_T s}$$ (14)

into the boundary condition equations, that Ω_T must be a solution to the characteristic equation

$$e^{\Omega_T P} - e^{-\Omega_T P} = 0$$ (15)

10

and that the integration constants D_1 and D_2 must satisfy the relation

$$D_1 - D_2 = 0 . \tag{16}$$

It is easily seen that the characteristic equation, (15), is satisfied for all values of Ω_T given by

$$\Omega_T = \Omega_n = \frac{in\pi}{P}, \quad \text{where} \quad n = 0, \pm 1, \pm 2, \cdots , \tag{17}$$

while the eigenvector

$$T(s) = T_n(s) = D_{1n} \left[e^{\Omega_n s} + e^{-\Omega_n s} \right] \tag{18}$$

associated with the eigenvalue Ω_n is a solution to the equation

$$\frac{d^2 T_n(s)}{ds^2} - \Omega_n^2 T_n(s) = 0 \tag{19}$$

and satisfies the boundary conditions

$$\left. \frac{dT_n(s)}{ds} \right|_{s=0} = \left. \frac{dT_n(s)}{ds} \right|_{s=P} = 0 . \tag{20}$$

The constants of integration D_{1n} are arbitrary, but can be made unique by requiring the eigenvectors to satisfy the orthogonality relationship

$$\frac{1}{P} \int_0^P T_m(s) T_n(s) \, ds = \delta_{m,n} , \tag{21}$$

where

$$\delta_{m,n} = \begin{cases} 1 & \text{if} \quad m = n \\ 0 & \text{if} \quad m \neq n \end{cases} . \tag{22}$$

One is thus led to the expression

$$T_n(s) = \begin{cases} 1 & \text{for} \quad n = 0 \\ \sqrt{2} \cos \frac{n\pi}{P} s & \text{for} \quad n = 1, 2, 3, \cdots \end{cases} \tag{23}$$

These eigenvectors, referred to as the "thermal modes" of the system, define the set of orthogonal functions which will be used to solve the non-homogeneous equation (Equation 7).

The values of λ that satisfy both Equations 13 and 17 are given by

$$\lambda_n = \frac{4\sigma\epsilon T_0^3}{\rho ch} + \frac{K_T}{\rho c}\left(\frac{n\pi}{P}\right)^2 , \tag{24}$$

and are referred to as the "thermal decay constants." The quantities defined by

$$\tau_n = \frac{1}{\lambda_n} \tag{25}$$

are referred to as the "thermal time constants" and define the time it takes the nth thermal mode to decay 63.21% in the absence of thermal input.

These functions and relationships developed with respect to the homogeneous equation, (9), can be used as a basis for solving the non-homogeneous equation of heat conduction and radiation, (7).

Assume a solution to Equation 7 of the form

$$T(s, z, t) = \sum_{n=0}^{\infty} q_n(z, t) T_n(s) , \tag{26}$$

where

$q_n(z, t)$ = the time-dependent generalized thermal coordinate at thermal station z and time t associated with the nth thermal mode $T_n(s)$.

By directly substituting the assumed solution into the non-homogeneous equation, (7), and by making use of the functional relationships given by Equations 13 and 19, an infinite series representation of Equation 7 can be obtained. That is,

$$\sum_{n=0}^{\infty} \left\{\frac{dq_n(z, t)}{dt} + \lambda_n q_n(z, t)\right\} \frac{T_n(s)}{P} = \frac{\Upsilon(s, z, t) - \sigma\epsilon T_0^4}{\rho chP} . \tag{27}$$

Since the thermal modes $T_n(s)$ are orthogonal functions and are normalized according to Equation 21, Equation 27 can be decoupled to obtain a set of linearly independent equations that define the generalized thermal coordinates. These equations are derived by multiplying both sides of Equation 27 by $T_m(s)$ and integrating around the cross-section. The resulting equations for

$n = 0, 1, 2, \cdots$ are:

$$\frac{dq_n(z, t)}{dt} + \lambda_n(z, t) = Q_n(z, t),\qquad(28)$$

where the "generalized thermal input" $Q_n(z, t)$ is defined by

$$Q_n(z, t) = \frac{\displaystyle\int_0^P \left[\Upsilon(s, z, t) - \sigma\epsilon T_0^4\right] T_n(s)\, ds}{\rho chP}.\qquad(29)$$

Generalized Thermal Input

The generalized thermal input $Q_n(z, t)$ associated with the nth generalized thermal coordinate $q_n(z, t)$ was defined in the previous section by the equation

$$Q_n(z, t) = \frac{\displaystyle\int_0^P \left[\Upsilon(s, z, t) - \sigma\epsilon T_0^4\right] T_n(s)\, ds}{\rho chP}.\qquad(29)$$

The heat input $\Upsilon(s, z, t)$ was assumed to be adequately described by the equation

$$\Upsilon(s, z, t) = \begin{cases} J_s \, \alpha_s \, \Xi(s, z, t)\, \overline{SL}(z, t) \cdot \vec{n}(s) & \text{for} \quad 0 \le s \le 2\pi r \\[2mm] \sigma\epsilon\alpha_s \, \tilde{T}^4(s - 2\pi r, z, t) & \text{for} \quad 2\pi r < s \le P \end{cases},\qquad(5)$$

where the sun-line vector $\overline{SL}(z, t)$ is an arbitrary but definable function of time at any particular thermal station z along the boom.

Figure 4, showing the position of the sun-line vector $\overline{SL}(z, t)$ relative to the principal cross-sectional axes of inertia at the thermal station z, makes use of the following symbols:

ϕ = angular amount of overlap

Y-axis = cross-sectional principal axis of inertia parallel to the axis of symmetry and directed away from the overlap area

X-axis = cross-sectional principal axis of inertia normal to the Y-axis and passing through the centroid of the cross-section, directed in the direction shown

$\psi(z, t)$ = angle between the negative Y-axis and the sun-line vector at thermal station z and time t. $\psi(z, t)$ is measured positive in the direction of increasing s.
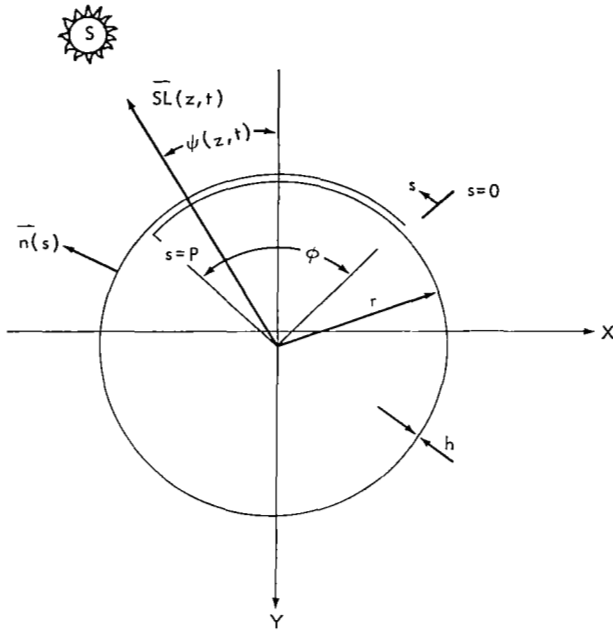
13

Figure 4—Orientation of boom cross-section at station z relative to sun.

From these definitions and the geometrical relationships shown in Figure 4 it can be seen that

$$\overrightarrow{SL}(z,\,t) \cdot \vec{n}(s) \;=\; \cos\left[\psi(z,\,t) - \frac{s}{r} + \frac{\phi}{2}\right], \qquad (30)$$

and thus Equation (5) may be rewritten as

$$\Upsilon(s,\,z,\,t) \;=\; \begin{cases} J_s\,\alpha_s\,\Xi(s,\,z,\,t)\cos\left[\psi(z,\,t) - \frac{s}{r} + \frac{\phi}{2}\right] \\ \qquad\qquad \text{for} \qquad 0 \le s \le 2\pi r \\[4pt] \sigma\epsilon\alpha_s\left[T_0^4 + 4T_0^3\,T(s - 2\pi r,\,z,\,t)\right] \\ \qquad\qquad \text{for} \qquad 2\pi r < s \le P \end{cases}, \qquad (31)$$

where

$$\Xi(s,\,z,\,t) \;=\; \begin{cases} 1 & \text{if} \quad \cos\left[\psi(z,\,t) - \frac{s}{r} + \frac{\phi}{2}\right] > 0 \\[6pt] 0 & \text{if} \quad \cos\left[\psi(z,\,t) - \frac{s}{r} + \frac{\phi}{2}\right] \le 0 \end{cases}. \qquad (32)$$

By introducing the following definitions,

$$B_{1n}(z,\,t) \;=\; \int_0^{2\pi r} \Xi(s,\,z,\,t)\cos\left[\psi(z,\,t) - \frac{s}{r} + \frac{\phi}{2}\right] T_n(s)\,ds. \qquad (33)$$

$$B_{2n} \;=\; \int_0^P T_n(s)\,ds, \qquad (34)$$

$$E_{1n} \;=\; \int_{2\pi r}^P T_n(s)\,ds, \qquad (35)$$

$$E_{2mn} \;=\; \int_{2\pi r}^P T_m(s - 2\pi r)\,T_n(s)\,ds, \qquad (36)$$

14

the generalized thermal input $Q_n(z, t)$ may be rewritten as

$$Q_n(z, t) = \frac{1}{\rho \text{chP}} \left\{ J_s \alpha_s B_{1n}(z, t) - \sigma \epsilon T_0^4 B_{2n} + \sigma \epsilon T_0^3 \alpha_s \left[T_0 E_{1n} + 4 \sum_{m=0}^{\infty} E_{2mn} q_m(z, t) \right] \right\} . \qquad (37)$$

By recalling that

$$\tilde{T}(s, z, t) = T_0 + \sum_{m=0}^{\infty} q_m(z, t) T_m(s) ,$$

one sees that $T_0 E_{1n}$ is proportional to the heat that would be radiated by the overlap if the entire overlap had a uniform constant temperature equal to the mean T_0, and that

$$\sum_{m=0}^{\infty} E_{2mn} q_m(z, t)$$

is a correction factor which accounts for the actual non-uniformity of the temperature distribution. Since the mean T_0 is two orders of magnitude greater than the maximum temperature deviation from T_0, one may write

$$T_0 E_{1n} + 4 \sum_{m=0}^{\infty} E_{2mn} q_m(z, t) \cong T_0 E_{1n} . \qquad (38)$$

The generalized thermal input is thus independent of all generalized thermal coordinates and can be expressed as

$$Q_n(z, t) \cong \frac{J_s \alpha_s B_{1n}(z, t) - \sigma \epsilon T_0^4 \left[B_{2n} - \alpha_s E_{1n} \right]}{\rho \text{chP}} ; \qquad (39)$$

and it will be shown that $B_{1n}(z, t)$ can be written as an analytic function of $\psi(z, t)$.

It is therefore possible to arrive at an analytic expression that defines the quantity $Q_n(z, t)$ for an arbitrary piecewise continuous function of the angle $\psi(z, t)$.

It is recalled that $\psi(z, t)$ is the angle between the sun line and the cross-sectional axis of symmetry and hence is directly proportional to the magnitude of the torsional oscillation at thermal station z and time t.

By defining $\psi(z, t)$ to be a particular function of time, the thermal response of a unit element of boom length oscillating, relative to a fixed sun, about its longitudinal axis can be determined. By

15

defining $\psi(z, t)$ to be proportional to the torsional oscillation of the vibrating boom, the thermal loading at thermal station z can be determined as a function of time.

In addition to the above expression which defines the generalized thermal input $Q_n(z, t)$, it will be shown that, in order to arrive at the expressions which define the thermal loading completely, the derivative of $Q_n(z, t)$ with respect to the sun angle $\psi(z, t)$ must also be determined. That is,

$$\frac{\partial Q_n(z, t)}{\partial \psi(z, t)} = \frac{J_s \alpha_s}{\rho chP} \frac{\partial B_{1n}(z, t)}{\partial \psi(z, t)} \tag{40}$$

is defined so that the equation

$$\frac{d}{dt}\left(\frac{\partial q_n(z, t)}{\partial \psi(z, t)}\right) + \lambda_n \left(\frac{\partial q_n(z, t)}{\partial \psi(z, t)}\right) = \frac{\partial Q_n(z, t)}{\partial \psi(z, t)} \tag{41}$$

(to be derived subsequently) can be solved.

Recalling that the thermal mode shape $T_n(s)$ is given by

$$T_n(s) = \begin{cases} 1 & \text{for} & n = 0 \\ \sqrt{2} \cos \dfrac{n\pi}{P} s & \text{for} & n = 1, 2, 3, \cdots \end{cases} \tag{23}$$

enables one to evaluate the integral equations defining

$$B_{1n}(z, t), \qquad B_{2n}, \qquad E_{1n}, \qquad \text{and} \qquad \frac{\partial B_{1n}(z, t)}{\partial \psi(z, t)}$$

as analytic functions of $\psi(z, t)$. A summary of these expressions follows:

$$B_{20} = P \tag{42}$$

$$B_{2n} = 0 \qquad n = 1, 2, \cdots \tag{43}$$

$$E_{10} = r\phi \tag{44}$$

$$E_{1n} = -\frac{\sqrt{2}P}{n\pi} \sin \frac{2n\pi^2 r}{P} \qquad n = 1, 2, \cdots. \tag{45}$$

16

For $n = 0$; $\phi \geq 0$; $-\phi/2 \leq \psi(z, t) \leq 2\pi - \phi/2$:

$$B_{10}(z, t) = 2r ,$$

$$\frac{\partial B_{10}(z, t)}{\partial \psi(z, t)} = 0 .$$

For $n = 2$; $\phi = 0$; $-\phi/2 \leq \psi(z, t) \leq 2\pi - \phi/2$:

$$B_{12}(z, t) = \frac{\sqrt{2}\,\pi r}{2} \cos \psi(z, t) ,$$

$$\frac{\partial B_{12}(z, t)}{\partial \psi(z, t)} = -\frac{\sqrt{2}\,\pi r}{2} \sin \psi(z, t) .$$

For $n = 1, 2, \cdots$; $\phi \geq 0$; $-\phi/2 \leq \psi(z, t) < \pi/2 - \phi/2$; with the exception of $n = 2$ for $\phi = 0$:

$$
B_{1n}(z, t) = \frac{\sqrt{2}\,rP^2}{P^2 - (n\pi r)^2} \left\{ \sin\left[\psi(z, t) + \frac{\phi}{2}\right] + \cos\frac{n\pi r}{P}\left[\psi(z, t) + \frac{\phi}{2} + \frac{\pi}{2}\right] \right.
$$

$$
+ \cos\frac{n\pi r}{P}\left[\psi(z, t) + \frac{\phi}{2} + \frac{3\pi}{2}\right] - \sin\left[\psi(z, t) + \frac{\phi}{2}\right] \cos\frac{2n\pi^2 r}{P}
$$

$$
\left. - \frac{n\pi r}{P} \cos\left[\psi(z, t) + \frac{\phi}{2}\right] \sin\frac{2n\pi^2 r}{P} \right\} ,
$$

$$
\frac{\partial B_{1n}(z, t)}{\partial \psi(z, t)} = \frac{\sqrt{2}\,rP^2}{P^2 - (n\pi r)^2} \left\{ \cos\left[\psi(z, t) + \frac{\phi}{2}\right] \right.
$$

$$
- \frac{n\pi r}{P} \sin\frac{n\pi r}{P}\left[\psi(z, t) + \frac{\phi}{2} + \frac{\pi}{2}\right]
$$

$$
- \frac{n\pi r}{P} \sin\frac{n\pi r}{P}\left[\psi(z, t) + \frac{\phi}{2} + \frac{3\pi}{2}\right]
$$

$$
- \cos\left[\psi(z, t) + \frac{\phi}{2}\right] \cos\frac{2n\pi^2 r}{P}
$$

$$
\left. + \frac{n\pi r}{P} \sin\left[\psi(z, t) + \frac{\phi}{2}\right] \sin\frac{2n\pi^2 r}{P} \right\} .
$$

For $n = 1, 2, \cdots$; $\phi \geq 0$; $\pi/2 - \phi/2 \leq \psi(z, t) \leq 3\pi/2 - \phi/2$; with the exception of $n = 2$ for $\phi = 0$:

$$B_{1n}(z, t) = \frac{2\sqrt{2}\, rP^2}{P^2 - (n\pi r)^2} \cos \frac{n\pi r}{P} \left[\psi(z, t) + \frac{\phi}{2}\right] \cos \frac{n\pi^2 r}{2P},$$

$$\frac{\partial B_{1n}(z, t)}{\partial \psi(z, t)} = -\frac{2\sqrt{2}\, n\pi r^2 P}{P^2 - (n\pi r)^2} \sin \frac{n\pi r}{P} \left[\psi(z, t) + \frac{\phi}{2}\right] \cos \frac{n\pi^2 r}{2P}.$$

For $n = 1, 2, \cdots$; $\phi \geq 0$; $3\pi/2 - \phi/2 < \psi(z, t) \leq 2\pi - \phi/2$; with the exception of $n = 2$ for $\phi = 0$:

$$B_{1n}(z, t) = \frac{\sqrt{2}\, rP^2}{P^2 - (n\pi r)^2} \left\{ \sin \left[\psi(z, t) + \frac{\phi}{2}\right] \right.$$

$$+ \cos \frac{n\pi r}{P} \left[\psi(z, t) + \frac{\phi}{2} - \frac{3\pi}{2}\right]$$

$$+ \cos \frac{n\pi r}{P} \left[\psi(z, t) + \frac{\phi}{2} - \frac{\pi}{2}\right]$$

$$- \sin \left[\psi(z, t) + \frac{\phi}{2}\right] \cos \frac{2n\pi^2 r}{P}$$

$$\left. - \frac{n\pi r}{P} \cos \left[\psi(z, t) + \frac{\phi}{2}\right] \sin \frac{2n\pi^2 r}{P} \right\},$$

$$\frac{\partial B_{1n}(z, t)}{\partial \psi(z, t)} = \frac{\sqrt{2}\, rP^2}{P^2 - (n\pi r)^2} \left\{ \cos \left[\psi(z, t) + \frac{\phi}{2}\right] \right.$$

$$- \frac{n\pi r}{P} \sin \frac{n\pi r}{P} \left[\psi(z, t) + \frac{\phi}{2} - \frac{3\pi}{2}\right]$$

$$- \frac{n\pi r}{P} \sin \frac{n\pi r}{P} \left[\psi(z, t) + \frac{\phi}{2} - \frac{\pi}{2}\right]$$

$$- \cos \left[\psi(z, t) + \frac{\phi}{2}\right] \cos \frac{2n\pi^2 r}{P}$$

$$\left. + \frac{n\pi r}{P} \sin \left[\psi(z, t) + \frac{\phi}{2}\right] \sin \frac{2n\pi^2 r}{P} \right\}.$$

18

Thermal Loading Associated With Non-Uniform Temperature Distribution

Since all booms of practical interest are made of materials that have finite coefficients of thermal expansion, a non-uniform temperature distribution around and along the boom will give rise to a non-uniform thermal stress distribution. This condition the boom will attempt to relieve by bending and twisting to a position of static thermal equilibrium.

As previously stated, the deflection analysis of beams subjected to thermal loading is performed on the basis of elementary strength of materials theory. From this basis it is shown in References 1 and 2 that the thermal loading may be adequately described by a resultant thermal bending moment distribution that produces pure bending and a resultant thermal torque distribution that produces pure torsion.

Both the thermal bending moment and the thermal torque at any thermal station z can be defined in terms of the generalized thermal coordinates. The corresponding distributions can be obtained by numerically differentiating with respect to z.

It was shown that the solution to the thermodynamic equation of heat conduction and radiation

$$K_T h \frac{\partial^2 \tilde{T}(s, z, t)}{\partial s^2} - \rho ch \frac{\partial \tilde{T}(s, z, t)}{\partial t} - \sigma \epsilon \tilde{T}^4(s, z, t) = -\Upsilon(s, z, t) \tag{3}$$

was given by Equation 6 combined with 26:

$$\tilde{T}(s, z, t) = T_0 + \sum_{n=0}^{\infty} q_n(z, t) T_n(s), \tag{46}$$

where the generalized thermal coordinates $q_n(z, t)$ can be obtained by solving the ordinary differential equation

$$\frac{dq_n(z, t)}{dt} + \lambda_n q_n(z, t) = Q_n(z, t). \tag{47}$$

The magnitude of T_0 was not specified, but T_0 was defined to be the steady state mean temperature of the cross-section. Its magnitude can therefore be derived from the expression

$$\lim_{t \to \infty} q_0(z, t) = \frac{Q_0(z, t)}{\lambda_0} = 0. \tag{48}$$

Since

$$Q_0(z, t) = \frac{2J_s \alpha_s r - \sigma \epsilon T_0^4 [P - \alpha_s r\phi]}{\rho chP} \tag{49}$$

19

and

$$\lambda_0. = \frac{4\sigma\epsilon T_0^3}{\rho ch} ,$$

(50)

it follows that

$$T_0^4 = \frac{2rJ_s \alpha_s}{\sigma\epsilon\left[P - \alpha_s r\phi\right]} .$$

(51)

In Reference 1 and in Appendix A it is shown that the thermal bending moment components at thermal station z about the local cross-sectional principal axes of inertia are given by

$$BM_x (z, t) = e_c Eh \int_0^P \widetilde{T}(s, z, t) y_c (s) ds$$

(52)

$$BM_y (z, t) = - e_c Eh \int_0^P \widetilde{T}(s, z, t) x_c (s) ds$$

(53)

and that the thermal torque about an axis normal to the cross-sectional plane at thermal station z is given by

$$T_{sc} (z, t) = e_c Ehr \frac{\partial V(z, t)}{\partial \psi(z, t)} \frac{\partial \psi(z, t)}{\partial \varphi(z, t)} \frac{d\varphi(z, t)}{dz} ,$$

(54)

where

$BM_x (z, t)$ = component of the thermal bending moment vector in the X-direction, i.e. normal to the axis of symmetry (see Figure 4),

$BM_y (z, t)$ = component of the thermal bending moment vector in the Y-direction, i.e. parallel to the axis of symmetry (see Figure 4),

e_c = coefficient of thermal expansion,

E = Young's modulus of elasticity,

$x_c (s)$ = distance of the point s on the cross-section to the Y-axis;

$$x_c (s) = - r \sin\left(\frac{s}{r} - \frac{\phi}{2}\right) ,$$

(55)

20

$y_c(s)$ = distance of the point s on the cross-section to the X-axis;

$$y_c(s) = -r \cos\left(\frac{s}{r} - \frac{\phi}{2}\right) + \delta_c , \tag{56}$$

δ_c = distance between the centroid and the geometrical center of the cross-section;

$$\delta_c = \frac{r \sin\frac{\phi}{2}}{\pi + \frac{\phi}{2}} , \tag{57}$$

$\varphi(z, t)$ = angular amount the cross-section at thermal station z has rotated at time t from its zero position,

$$V(z, t) = \left[e_s \sin\frac{\phi}{2} + \frac{P}{2}\right] \int_0^P \tilde{T}(s, z, t)\,ds$$

$$- \int_0^P \left[\frac{e_s}{r} \cos\left(\frac{s}{r} - \frac{\phi}{2}\right) + 1\right] \int_0^s \tilde{T}(\xi, z, t)\,d\xi\,ds , \tag{58}$$

e_s = distance between the shear center and the geometrical center of the cross-section;

$$e_s = P \left[\frac{\cos\frac{\phi}{2} - \frac{\sin\frac{\phi}{2}}{\pi + \frac{\phi}{2}}}{\pi + \frac{\phi}{2} - \frac{1}{2}\sin\phi}\right] \tag{59}$$

A direct substitution of Equation 46 into Equations 52, 53, and 54 leads to the equations which define the bending moment components and the thermal torque as infinite series. That is,

$$BM_x(z, t) = e_c Eh \int_0^P \left[T_0 + \sum_{n=0}^{\infty} q_n(z, t) T_n(s)\right] y_c(s)\,ds , \tag{60}$$

$$BM_y(z, t) = -e_c Eh \int_0^P \left[T_0 + \sum_{n=0}^{\infty} q_n(z, t) T_n(s)\right] x_c(s)\,ds , \tag{61}$$

$$T_{sc}(z, t) = e_c Ehr \left\{\left[e_s \sin\frac{\phi}{2} + \frac{P}{2}\right] \int_0^P \sum_{n=0}^{\infty} \frac{\partial q_n(z, t)}{\partial \psi(z, t)} T_n(s)\,ds \right.$$

$$\left. - \int_0^P \left[\frac{e_s}{r} \cos\left(\frac{s}{r} - \frac{\phi}{2}\right) + 1\right] \int_0^s \sum_{n=0}^{\infty} \frac{\partial q_n(z, t)}{\partial \psi(z, t)} T_n(\xi)\,d\xi\,ds \right\} \frac{\partial \psi(z, t)}{\partial \varphi(z, t)} \frac{d\varphi(z, t)}{dz} , \tag{62}$$

where

$$\frac{d}{dt}\left(\frac{\partial q_n(z,t)}{\partial \psi(z,t)}\right) + \lambda_n \left(\frac{\partial q_n(z,t)}{\partial \psi(z,t)}\right) = \left(\frac{\partial Q_n(z,t)}{\partial \psi(z,t)}\right). \tag{63}$$

By introducing the definition of the thermal mode shape $T_n(s)$ given by Equation 23 and carrying out the obvious integrations, one is led to the following:

$$BM_x(z,t) = 2\sqrt{2} e_c Ehr^2 P^2 \sin \frac{\phi}{2} \sum_{\substack{n=2 \\ n \text{ even}}}^{\infty} \frac{q_n(z,t)}{(n\pi r)^2 - P^2}, \tag{64}$$

$$BM_y(z,t) = -2\sqrt{2} e_c Ehr^2 P^2 \cos \frac{\phi}{2} \sum_{\substack{n=1 \\ n \text{ odd}}}^{\infty} \frac{q_n(z,t)}{(n\pi r)^2 - P^2}, \tag{65}$$

$$T_{sc}(z,t) = 2\sqrt{2} e_c EhrP \left\{ \sum_{\substack{n=1 \\ n \text{ odd}}}^{\infty} \frac{1}{n\pi} \left[\frac{n\pi P r e_s \cos \frac{\phi}{2}}{P^2 - (n\pi r)^2} - \frac{P}{n\pi} \right] \frac{\partial q_n(z,t)}{\partial \psi(z,t)} \right\} \frac{\partial \psi(z,t)}{\partial \varphi(z,t)} \frac{d\varphi(z,t)}{dz}. \tag{66}$$

It is thus possible to obtain infinite series expressions for the thermal bending moment components and the thermal torque in terms of the generalized thermal coordinates which can be readily obtained at every thermal station.

Special note is made of the fact that these quantities are derived relative to the principal cross-sectional axes of inertia at thermal station z.

Thermal Response of Unit Boom Length to Predefined Torsional Oscillation

Before an attempt is made to define the thermal loading along the entire length of the boom and include this thermal loading in the vibration equation, a prerequisite study will be made.

Two fundamental points must be studied. That is, we must first determine the number of thermal modes needed to adequately define the thermal loading, and must then show that the thermal model as defined does indeed predict a physically realizable representation of it.

With regard to the first point, it suffices to state that by comparing results obtained using 2, 4, 6, and 20 thermal modes (excluding the $n = 0$ mode) it has been found that the use of 4 modes is optimum from the standpoints of accuracy and computer running time.

The second point is studied by investigating the change in the thermal load on a unit element of boom length due to a predefined change in the sun position with time.

The nominal parameters used to define the geometric and physical properties of the boom element are all obtained from the extensive experimental work carried on at NASA/GSFC on booms of

Table 1

Antenna material	= beryllium copper, silver-plated
Perimeter of cross-section	$= P = 2$ in.
Total overlap angle	$= \phi = 90$ deg.
Wall thickness	$= h = .002$ in.
Weight density of material	$= \rho = .2714$ lb/in.^{3}
Young's modulus	$= E = .19 \times 10^8$ lb/in.^{2}
Thermal conductivity	$= K_T = 4.167$ Btu/(hr-in.-°F)
Specific heat	$= c = .1$ Btu/(lb-°F)
Solar radiation intensity	$= J_s = 3.065$ Btu/(hr-in.^{2})
Thermal expansion coefficient	$= e_c = .104 \times 10^{-4}$ in./(in.-°F)
Emissivity	$= \epsilon = .035$
Absorptivity	$= \alpha_s = .13$

flight quality. These parameters are listed in Table 1.

The hypothetical case of a spinning sun is studied in Figure 5. The curves labeled A, B, and C correspond to the particular cases defined by

$$\psi(z, t) = .05 t$$

$$\psi(z, t) = .50 t$$

$$\psi(z, t) = 5.0 t \ (\text{radians})$$

respectively. The change in the thermal load is illustrated by plotting the components of the effective thermal bending moment vector (BM_x vs BM_y as defined by Equations 64, 65) after a steady state response has been achieved.

As expected, for the slow-spin case the thermal model does yield results consistent with those obtained in the static analysis. This

A. $\psi(z,t) = 0.05t$
B. $\psi(z,t) = 0.5$
C. $\psi(z,t) = 5.0t$

Figure 5—Variation in thermal bending moment for three spinning sun cases.

fact may be verified by comparing curve A with its analogous counterpart in Reference 1. As spin rate increases, a temperature-averaging or "barbecuing" effect is to be expected and is evidenced by curves B and C. The offset point about which the three curves appear to be centered is a result of the fact that the overlapped portion of the cylinder is never exposed to direct radiation.
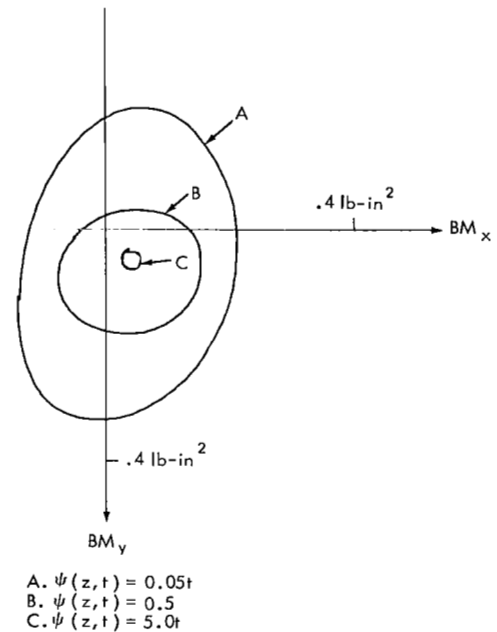
Figures 6 through 14 are included to demonstrate the need for a rather detailed thermal model in this analysis.

In the actual problem, the boom oscillates torsionally in the directional thermal field. To study the steady state thermal response of a torsionally oscillating unit element, the sun's relative orientation is described by

$$\psi(z, t) \;=\; \psi^* \sin(\omega^* t - \psi_0) \;\text{(radians)}$$

for particular values of ψ^*, ω^*, and ψ_0.

As in Figure 5, each curve corresponds to the motion of the tip of the effective thermal bending moment vector after a steady state thermal response has been achieved.
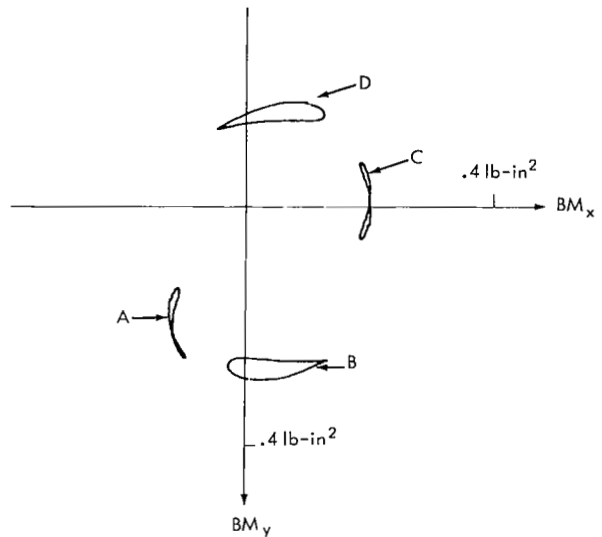
On all figures from 6 through 14, the curves labeled A, B, C, and D correspond to $\psi_0 = 0$, $\pi/2$, π, and $3\pi/2$ respectively.

Table 2 lists the respective magnitudes of ω^* and ψ^* used in each figure.
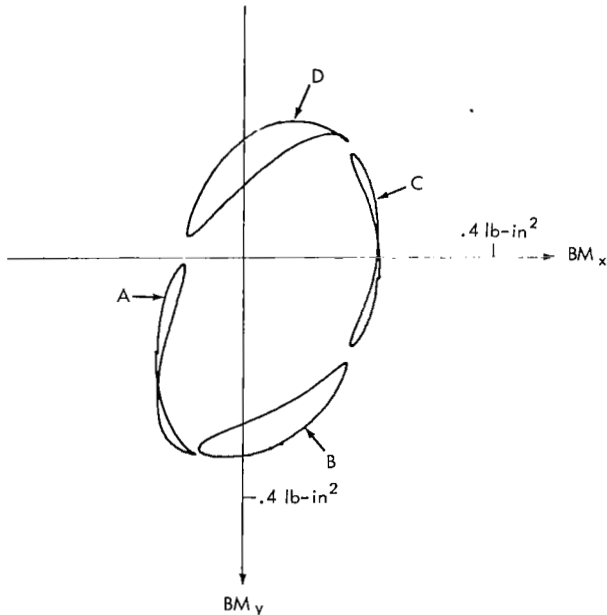
A. $\psi(z,t) = \pi/4 \sin(.05t - 0)$
B. $\psi(z,t) = \pi/4 \sin(.05t - \pi/2)$
C. $\psi(z,t) = \pi/4 \sin(.05t - \pi)$
D. $\psi(z,t) = \pi/4 \sin(.05t - 3\pi/2)$

Figure 6—Variation in thermal bending moment for oscillating sun cases.

A. $\psi(z,t) = \pi/4 \sin(0.5t - 0)$
B. $\psi(z,t) = \pi/4 \sin(0.5t - \pi/2)$
C. $\psi(z,t) = \pi/4 \sin(0.5t - \pi)$
D. $\psi(z,t) = \pi/4 \sin(0.5t - 3\pi/2)$
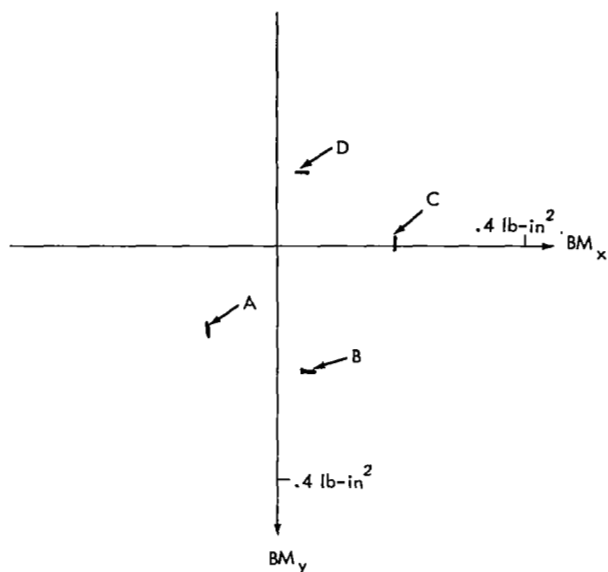
Figure 7—Variation in thermal bending moment for oscillating sun cases.

A. $\psi(z,t) = \pi/4 \sin(5t - 0)$
B. $\psi(z,t) = \pi/4 \sin(5t - \pi/2)$
C. $\psi(z,t) = \pi/4 \sin(5t - \pi)$
D. $\psi(z,t) = \pi/4 \sin(5t - 3\pi/2)$

Figure 8—Variation in thermal bending moment for oscillating sun cases.

A. $\psi(z,t) = \pi/2 \sin(.05t - 0)$
B. $\psi(z,t) = \pi/2 \sin(.05t - \pi/2)$
C. $\psi(z,t) = \pi/2 \sin(.05t - \pi)$
D. $\psi(z,t) = \pi/2 \sin(.05t - 3\pi/2)$

Figure 9—Variation in thermal bending moment for oscillating sun cases.

A. $\psi(z,t) = \pi/2 \sin(0.5t - 0)$
B. $\psi(z,t) = \pi/2 \sin(0.5t - \pi/2)$
C. $\psi(z,t) = \pi/2 \sin(0.5t - \pi)$
D. $\psi(z,t) = \pi/2 \sin(0.5t - 3\pi/2)$

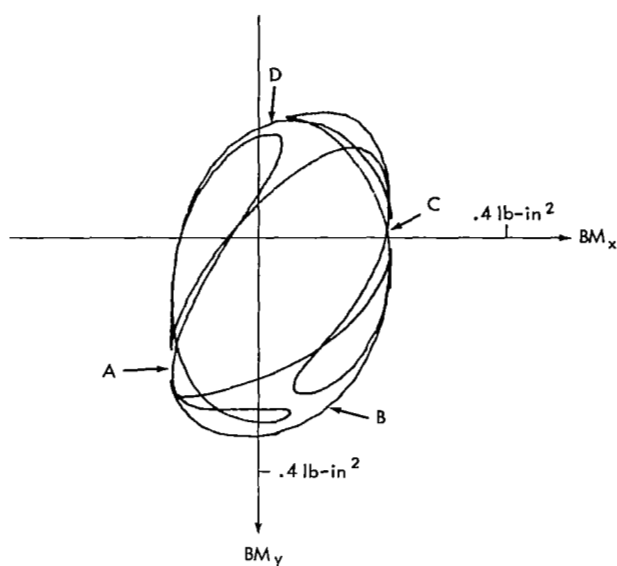Figure 10—Variation in thermal bending moment for oscillating sun cases.

A. $\psi(z,t) = \pi/2 \sin(5t - 0)$
B. $\psi(z,t) = \pi/2 \sin(5t - \pi/2)$
C. $\psi(z,t) = \pi/2 \sin(5t - \pi)$
D. $\psi(z,t) = \pi/2 \sin(5t - 3\pi/2)$

Figure 11—Variation in thermal bending moment for oscillating sun cases.

25

A. $\psi(z,t) = \pi \sin(.05t - 0)$
B. $\psi(z,t) = \pi \sin(.05t - \pi/2)$
C. $\psi(z,t) = \pi \sin(.05t - \pi)$
D. $\psi(z,t) = \pi \sin(.05t - 3\pi/2)$

Figure 12—Variation in thermal bending moment for oscillating sun cases.

A. $\psi(z,t) = \pi \sin(0.5t - 0)$
B. $\psi(z,t) = \pi \sin(0.5t - \pi/2)$
C. $\psi(z,t) = \pi \sin(0.5t - \pi)$
D. $\psi(z,t) = \pi \sin(0.5t - 3\pi/2)$

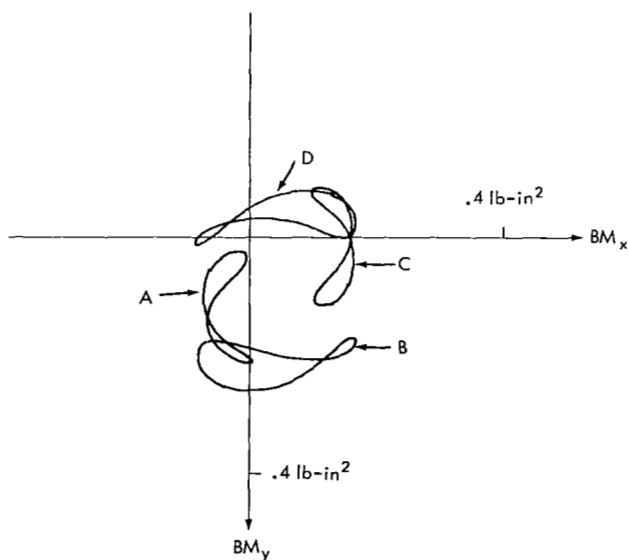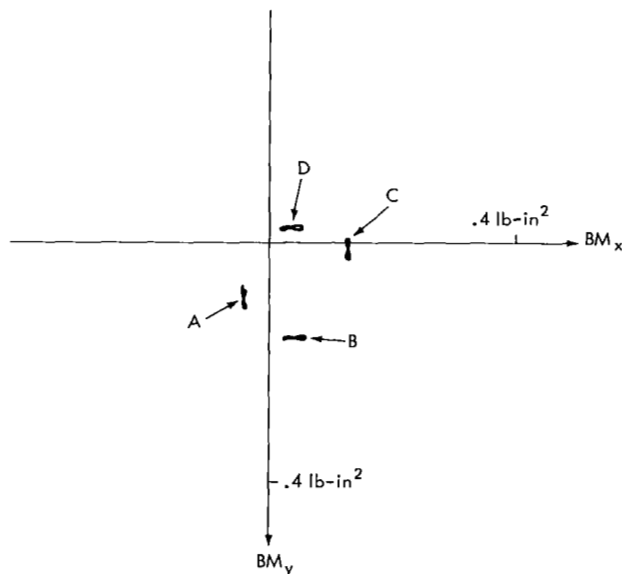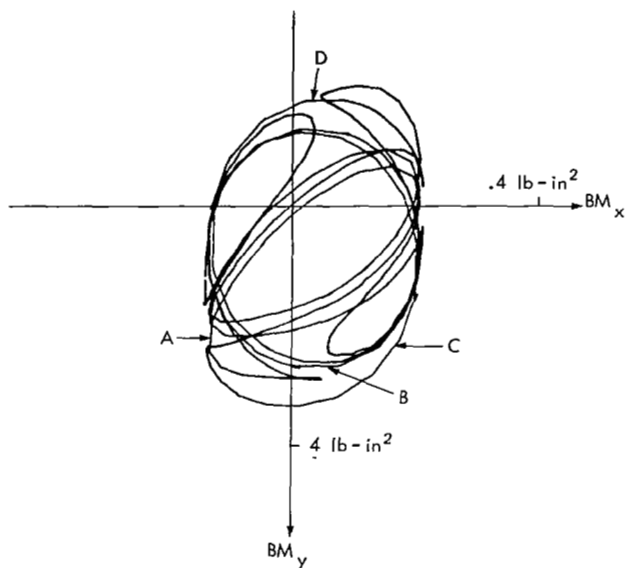Figure 13—Variation in thermal bending moment for oscillating sun cases.

Table 2

Figure #	ω^* (rad/sec)	ψ^* (rad)
6	.05	$\pi/4$
7	.50	$\pi/4$
8	5.00	$\pi/4$
9	.05	$\pi/2$
10	.50	$\pi/2$
11	5.00	$\pi/2$
12	.05	π
13	.50	π
14	5.00	π

A. $\psi(z,t) = \pi \sin(5t - 0)$
B. $\psi(z,t) = \pi \sin(5t - \pi/2)$
C. $\psi(z,t) = \pi \sin(5t - \pi)$
D. $\psi(z,t) = \pi \sin(5t - 3\pi/2)$

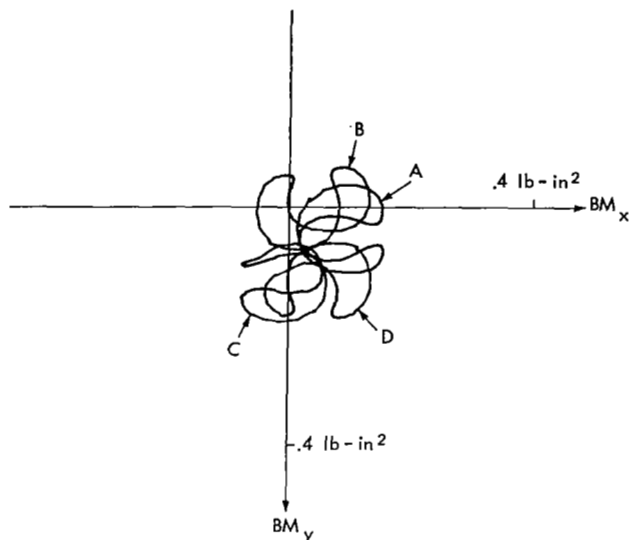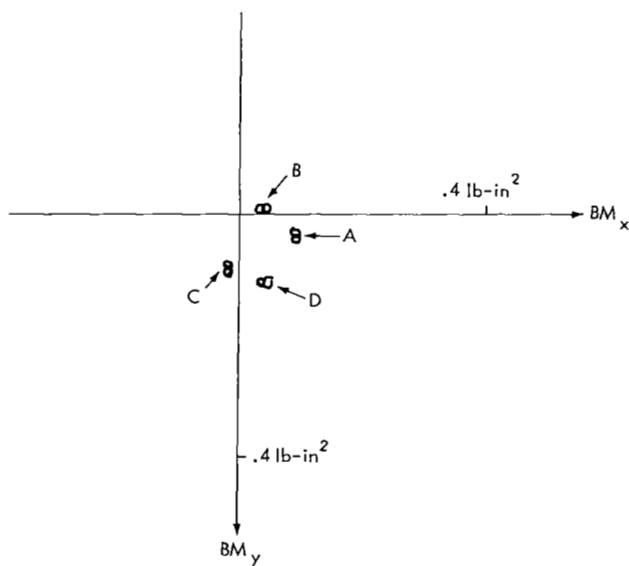Figure 14—Variation in thermal bending moment for oscillating sun cases.

The values of ω^* listed bracket the frequency range in which nearly all booms of interest will respond torsionally. It is interesting to note that outside of this frequency range a much simpler thermal model could probably be justified.

To intuitively justify the results shown, one must determine the magnitude of the thermal time constants τ_n. For the parameters listed in Table 1 these values are

$$\tau_0 = 330.38 \text{ sec},$$

$$\tau_1 = 9.236 \text{ sec},$$

$$\tau_2 = 2.359 \text{ sec},$$

$$\tau_3 = 1.052 \text{ sec},$$

$$\tau_4 = .593 \text{ sec}.$$

A few general statements can be made concerning these figures.

1. The effect of thermal time constants cannot be neglected in any analysis for which vibrational response periods and thermal time constants are of the same order of magnitude.

2. In any particular case of a torsionally vibrating cylinder of open section, the amplitude of vibration will vary from station to station along the length. By comparing Figures 6, 9, 12, Figures 7, 10, 13, and Figures 8, 11, 14, it is evident that the thermal loading can be quite different at different places along the length. A sufficient number of thermal stations along the length will therefore have to be used to describe the thermal loading accurately.

Figures 5 through 14 deal exclusively with the effective thermal bending moment components $BM_x(z, t)$ and $BM_y(z, t)$. Figures 15 through 24 deal exclusively with thermal torque. To do so, we
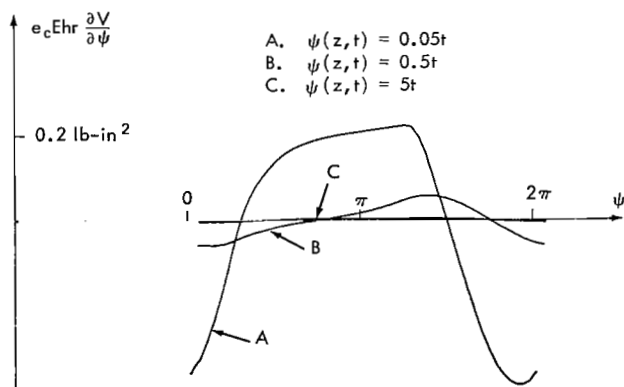

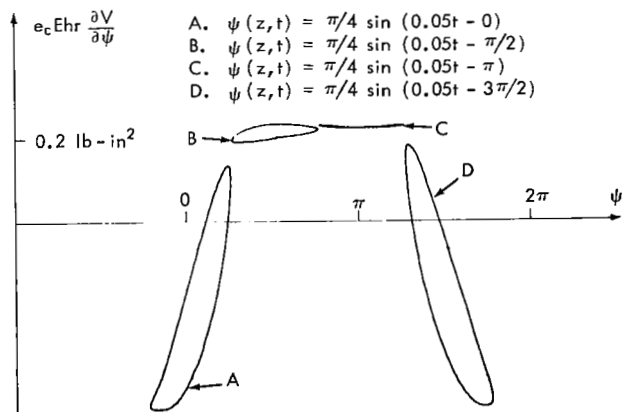Figure 15—Variation in thermal torque coefficient for spinning sun cases.

Figure 16—Variation in thermal torque coefficient for oscillating sun cases.
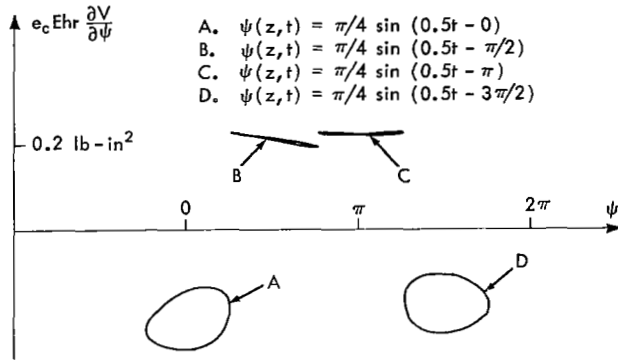
Figure 17—Variation in thermal torque coefficient for oscillating sun cases.

$e_c Ehr \frac{\partial V}{\partial \psi}$

A. $\psi(z,t) = \pi/4 \sin (0.5t - 0)$
B. $\psi(z,t) = \pi/4 \sin (0.5t - \pi/2)$
C. $\psi(z,t) = \pi/4 \sin (0.5t - \pi)$
D. $\psi(z,t) = \pi/4 \sin (0.5t - 3\pi/2)$
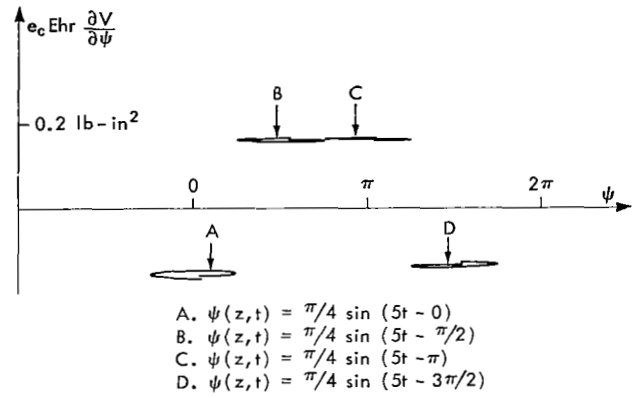
Figure 18—Variation in thermal torque coefficient for oscillating sun cases.

$e_c Ehr \frac{\partial V}{\partial \psi}$

A. $\psi(z,t) = \pi/4 \sin (5t - 0)$
B. $\psi(z,t) = \pi/4 \sin (5t - \pi/2)$
C. $\psi(z,t) = \pi/4 \sin (5t - \pi)$
D. $\psi(z,t) = \pi/4 \sin (5t - 3\pi/2)$
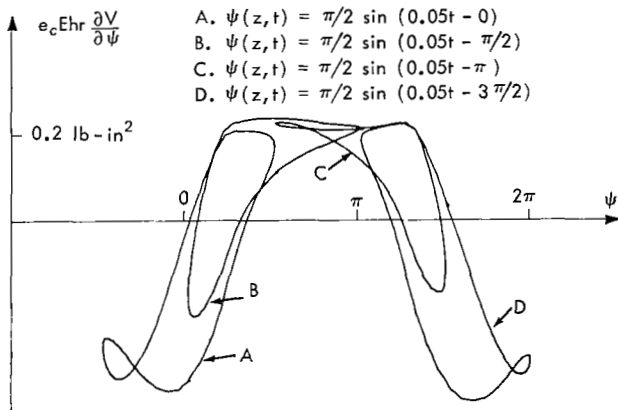
Figure 19—Variation in thermal torque coefficient for oscillating sun cases.

$e_c Ehr \frac{\partial V}{\partial \psi}$

A. $\psi(z,t) = \pi/2 \sin (0.05t - 0)$
B. $\psi(z,t) = \pi/2 \sin (0.05t - \pi/2)$
C. $\psi(z,t) = \pi/2 \sin (0.05t - \pi)$
D. $\psi(z,t) = \pi/2 \sin (0.05t - 3\pi/2)$
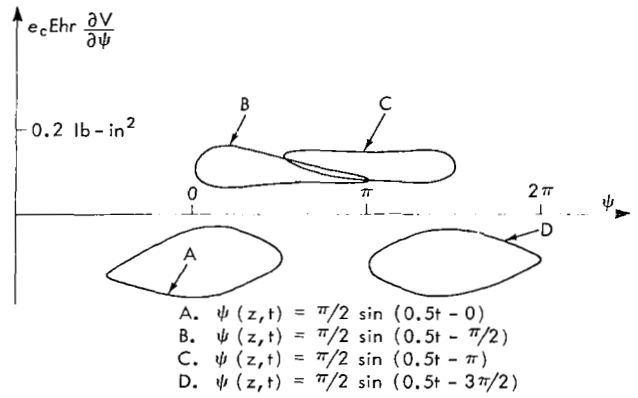
Figure 20—Variation in thermal torque coefficient for oscillating sun cases.

$e_c Ehr \frac{\partial V}{\partial \psi}$

A. $\psi(z,t) = \pi/2 \sin (0.5t - 0)$
B. $\psi(z,t) = \pi/2 \sin (0.5t - \pi/2)$
C. $\psi(z,t) = \pi/2 \sin (0.5t - \pi)$
D. $\psi(z,t) = \pi/2 \sin (0.5t - 3\pi/2)$
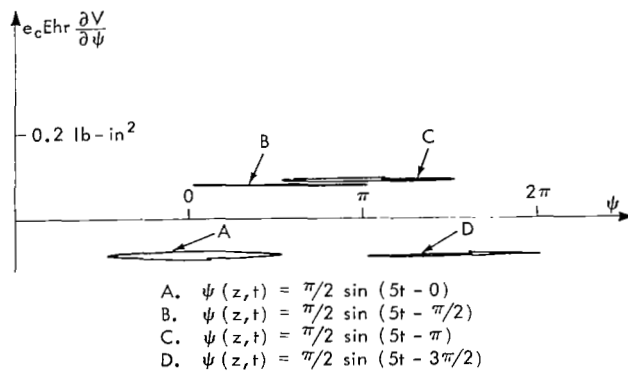
Figure 21—Variation in thermal torque coefficient for oscillating sun cases.

$e_c Ehr \frac{\partial V}{\partial \psi}$

A. $\psi(z,t) = \pi/2 \sin (5t - 0)$
B. $\psi(z,t) = \pi/2 \sin (5t - \pi/2)$
C. $\psi(z,t) = \pi/2 \sin (5t - \pi)$
D. $\psi(z,t) = \pi/2 \sin (5t - 3\pi/2)$
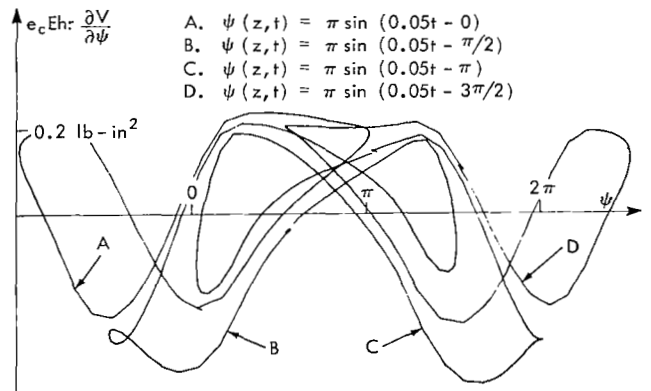
Figure 22—Variation in thermal torque coefficient for oscillating sun cases.

$e_c Eh r \frac{\partial V}{\partial \psi}$

A. $\psi(z,t) = \pi \sin (0.05t - 0)$
B. $\psi(z,t) = \pi \sin (0.05t - \pi/2)$
C. $\psi(z,t) = \pi \sin (0.05t - \pi)$
D. $\psi(z,t) = \pi \sin (0.05t - 3\pi/2)$

A. $\psi(z,t) = \pi \sin(0.5t - 0)$
B. $\psi(z,t) = \pi \sin(0.5t - \pi/2)$
C. $\psi(z,t) = \pi \sin(0.5t - \pi)$
D. $\psi(z,t) = \pi \sin(0.5t - 3\pi/2)$
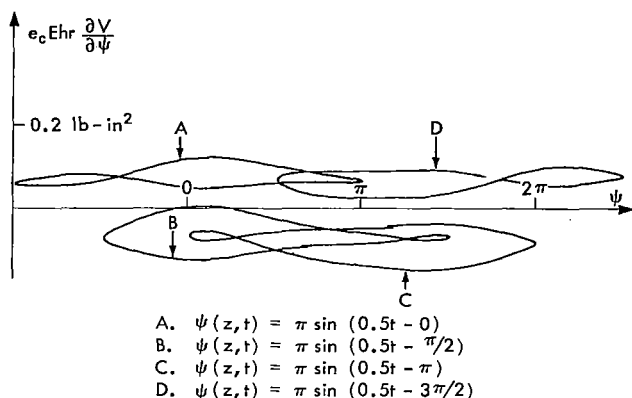
Figure 23—Variation in thermal torque coefficient for oscillating sun cases.

A. $\psi(z,t) = \pi \sin(5t - 0)$
B. $\psi(z,t) = \pi \sin(5t - \pi/2)$
C. $\psi(z,t) = \pi \sin(5t - \pi)$
D. $\psi(z,t) = \pi \sin(5t - 3\pi/2)$
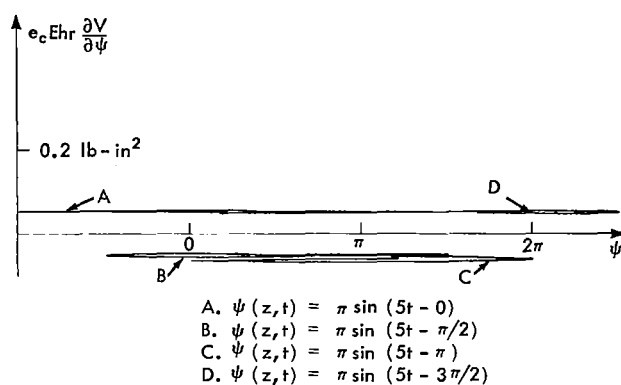
Figure 24—Variation in thermal torque coefficient for oscillating sun cases.

plot the temperature-dependent part of $T_{sc}(z, t)$. That is, in all figures from 15 through 24,

$$e_c \, Ehr \, \frac{\partial V(z, t)}{\partial \psi(z, t)} \quad vs \quad \psi(z, t)$$

is shown for the same respective functions of $\psi(z, t)$ used in Figures 5 through 14.

These figures (15 through 24) are included to provide the reader with a graphic showing of how thermal torque is dependent upon relative sun orientation. These figures will play an important role in the determination of whether or not a thermally-induced torsional instability can be excited for a particular sun orientation.

The same general statements made previously concerning Figures 5 through 14 can be applied here in discussing Figures 15 through 24. Again the reader is directed to Reference 1 for additional work pertaining to the static analysis of thermal bending and twist.

Preliminary test data obtained by R. Predmore and C. Staugaitis at NASA/GSFC indicate that the thermal model used herein does tend to yield results which are consistent with experimentally observed bending and torsion. More testing is necessary, however, before any direct comparison between experiment and theory can be made.

EQUATIONS OF BENDING AND TORSION

In order for the results of this work to have practical significance, a certain amount of generality must be reatined in developing them so that they may be applied to cylinders of open, closed, and zippered cross-section with only minor adjustments of the torsional stiffness parameters and the thermal model. Since the actual booms used in flight are not mathematically perfect, any attempt to describe analytically the non-uniformities in such parameters as bending stiffness, cross-sectional diameter, shear center offset, initial curvature frictional damping, etc., leads to equations which are

and specialized to a particular experimentally studied boom. The inclusion of these details tends to mask the basic mechanism producing thermally-induced vibrations behind a veil of second-order perturbations. It is argued that, if the simplified model can be shown to be strongly unstable, it would be virtually impossible to show that the inclusion of second-order terms could reverse the situation and analytically stabilize the system.

Accordingly, the boom is modeled as a beam clamped in both two-axis bending and torsion at its root. The tip is free to translate and rotate, and has attached to it a tip weight which has both translational and rotational inertia. The tip weight is fixed to the boom tip in a way which allows it to be free to warp. For the long booms of interest, it is assumed that the effect of the shear center axis being displaced from the centroidal axis is negligible and that the bending stiffness about any axis passing through the centroid of the cross-section is constant.

The determination of deflection under thermal loading is performed under the assumption that the longitudinal thermal strain in any fiber passing through an arbitrary cross-section along the length of the rod is a linear function of the distance from the fiber to the neutral axis of the cross-section.

Furthermore, the stress couples that produce pure bending are proportional to local curvature, and the stress couple that produces pure torsion is a function of the resistance of the cylinder to both torsion and warping. By varying the magnitudes of the torsional stiffness parameters, it is possible to show how the response of the boom changes as the torsional stiffness is increased from the case of an open-section cylinder to that of a closed-section cylinder. This transition region in effect simulates the torsional stiffness characteristics of zippered-section cylinders.

As indicated in the Introduction, the small-angle assumptions made are valid over any short segment of the boom; however, when extended over very long lengths they do not completely define the situation. It is thus desirable to develop the equations of elastic equilibrium from elementary considerations.

This is done by using vector techniques to derive the equations of elastic equilibrium relative to a coordinate system which slides along the longitudinal axis of the boom with uniform constant rate, relative to an inertially fixed system.

The body forces associated with the translational and rotational acceleration of mass elements along the boom, the dissipative forces associated with viscoelastic damping, and the thermal loading induced by the thermal environment can also be expressed in vector form relative to either the sliding or the fixed coordinate system.

These equations can, by means of the transformation matrix, be expressed in a common coordinate system and reduced to a manageable form by the deletion of terms that are of second order in displacement.

Basic Equations of Elastic Equilibrium in Vector Form

The derivation of the equations herein is based upon the work presented by A. E. H. Love in Reference 6 and Landau and Lifshitz in Reference 5. Where possible, the notation used will follow that used by Love.

Consider two adjacent cross-sections along the length of an elastically deformed beam that are a distance dz apart, as shown in Figure 25. Suppose also that the beam is deformed by forces that are applied along the length of the beam. The resultant effect that these forces have on the beam is estimated from:

1. $\vec{F}$ their resultant force distribution measured per unit length along the longitudinal axis of the beam, and

2. $\vec{K}$ their resultant couple distribution measured per unit length along the longitudinal axis of the beam.

For the element shown in Figure 25 to be in elastic equilibrium, an internal stress distribution must be set up which will have the resultant effect of exactly counterbalancing the applied resultant force and couple distributions.

Figure 26 isolates this element from the rest of the beam. Shown in this figure are:

$\vec{V}$ = resultant of the internal stress distribution on the cross-section at O'

$\vec{V} + d\vec{V}$ = resultant of the internal stress distribution on the cross-section at O.

These are the shear forces at O' and O respectively; similarly,

$\vec{M}$ = moment of the internal stress distribution on the cross-section at O' and about the point O',

$\vec{M} + d\vec{M}$ = moment of the internal stress distribution on the cross-section at O and about the point O.

These are the moments at O' and O respectively.

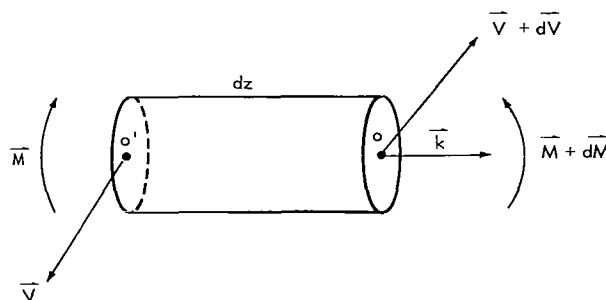For the element to be in equilibrium, the vector sum of the internal and applied force
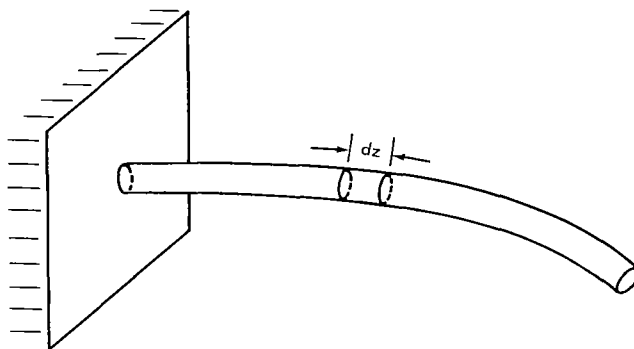
Figure 25—Clamped free beam.

Figure 26—Beam element.

resultants must be equal to zero. Thus

$$- \vec{V} + \vec{V} + d\vec{V} + \vec{F}\,dz \;=\; 0\,,\tag{67}$$

or

$$\frac{d\vec{V}}{dz} + \vec{F} \;=\; 0\,,\tag{68}$$

where dz is the distance between O' and O measured along the longitudinal axis of the beam.

In addition to the above condition, the vector sum of the internal and applied couple or moment resultants must be equal to zero. Then

$$- \vec{M} + \vec{M} + d\vec{M} + (-dz\,\vec{k}) \times (-\vec{V}) + \vec{K}\,dz \;=\; 0\,,\tag{69}$$

or

$$\frac{d\vec{M}}{dz} + \vec{k} \times \vec{V} + \vec{K} \;=\; 0\,,\tag{70}$$

where

$\vec{k}$ = unit vector normal to the cross-section at O, and the moment due to the applied force resultant $\vec{F}$ about O is a second-order effect which can be neglected (see Love, Reference 6).

The vector equations that define the elastic equilibrium condition for any element along the beam are thus given by

$$\frac{d\vec{V}}{dz} + \vec{F} \;=\; 0\,,\tag{68}$$

$$\frac{d\vec{M}}{dz} + \vec{k} \times \vec{V} + \vec{K} \;=\; 0\,.\tag{70}$$

For the equations to be effectively used in solving the problem of thermally-induced vibration, coordinate systems must be defined in which deflection can be measured and in which the applied forces associated with kinetic motion, damping, and the thermal environment can be defined.
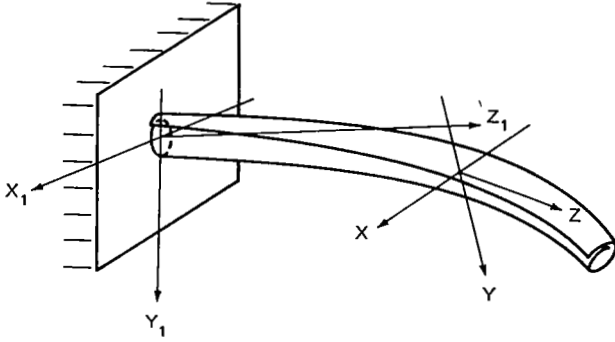
Figure 27—Clamped free thin-walled cylinder of open section.

Figure 28—Boom cross-section at station z.

Coordinate Systems

Two coordinate systems are defined and are related to each other through an Euler angle transformation matrix. These systems are identical to those used in Reference 1. Consider the triads shown in Figures 27 and 28.

Let:

$[X_1, Y_1, Z_1]$ be the inertially fixed triad defined at the centroid of the clamped root

$[X, Y, Z]$ be the local, or body, triad. This triad slides with constant velocity along the centroidal axis of the boom, maintaining a fixed orientation with respect to the local cross-sectional principal axis of inertia (directions shown in Figure 28)

z be the coordinate used to measure arc length along the centroidal axis of the boom, measured positive from the clamped root. At $z = 0$, the inertial and local triads are coincident.

$[\vec{i}_1, \vec{j}_1, \vec{k}_1]$ be a basis of three orthonormal vectors fixed in the inertial triad at $z = 0$ and parallel with the X_1, Y_1, and Z_1, axes respectively, with their origin at the centroid of the cross-section

$[\vec{i}, \vec{j}, \vec{k}]$ be a basis of three orthonormal vectors parallel respectively to the X, Y, and Z triad at the point z, with their origin at the centroid of the cross-section at $z = 0.$

The two sets of basis vectors are continually related to each other by means of an Euler angle transformation matrix. This transformation matrix is given below, and the rotation sequence is shown in Figure 29.
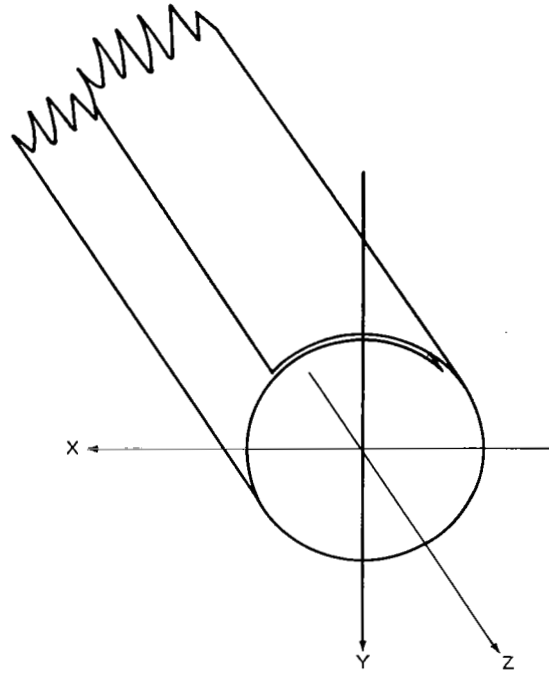
$$\begin{Bmatrix} \vec{i}_1 \\ \vec{j}_1 \\ \vec{k}_1 \end{Bmatrix} = \begin{bmatrix} 1 & 0 & 0 \\ 0 & \cos\theta_1 & -\sin\theta_1 \\ 0 & \sin\theta_1 & \cos\theta_1 \end{bmatrix} \begin{bmatrix} \cos\theta_2 & 0 & \sin\theta_2 \\ 0 & 1 & 0 \\ -\sin\theta_2 & 0 & \cos\theta_2 \end{bmatrix} \begin{bmatrix} \cos\varphi & -\sin\varphi & 0 \\ \sin\varphi & \cos\varphi & 0 \\ 0 & 0 & 1 \end{bmatrix} \begin{Bmatrix} \vec{i} \\ \vec{j} \\ \vec{k} \end{Bmatrix}$$

$$= \begin{bmatrix} \cos\theta_2 \cos\varphi & -\cos\theta_2 \sin\varphi & \sin\theta_2 \\ \sin\theta_1 \sin\theta_2 \cos\varphi + \cos\theta_1 \sin\varphi & -\sin\theta_1 \sin\theta_2 \sin\varphi + \cos\theta_1 \cos\varphi & -\sin\theta_1 \cos\theta_2 \\ -\cos\theta_1 \sin\theta_2 \cos\varphi + \sin\theta_1 \sin\varphi & \cos\theta_1 \sin\theta_2 \sin\varphi + \sin\theta_1 \cos\varphi & \cos\theta_1 \cos\theta_2 \end{bmatrix} \begin{Bmatrix} \vec{i} \\ \vec{j} \\ \vec{k} \end{Bmatrix} . \quad (71)$$

At any point z along the beam at time t, the unit vector which is tangent to the centroidal axis is defined by the vector equation
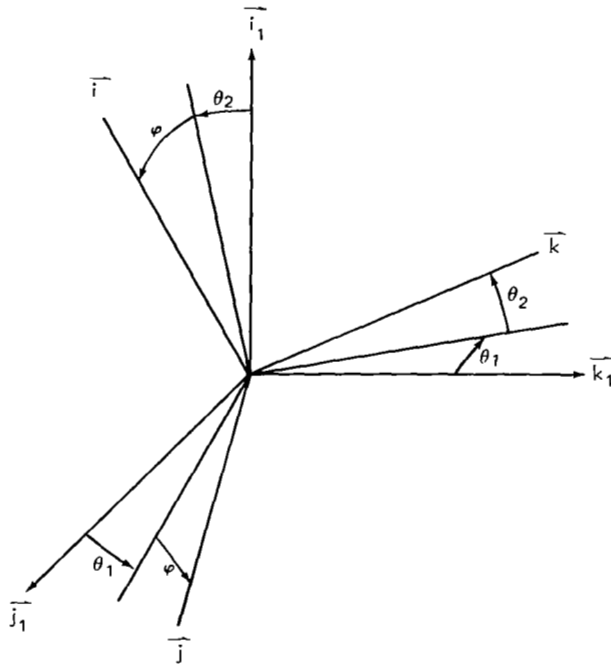
Figure 29—Euler angle rotation sequence.

$$\vec{k}^* = \frac{\partial X(z, t)}{\partial z} \vec{i}_1 + \frac{\partial Y(z, t)}{\partial z} \vec{j}_1 + \frac{\partial Z(z, t)}{\partial z} \vec{k}_1 , \quad (72)$$

where $[X(z, t), Y(z, t), Z(z, t)]$ are the coordinates of the point z along the centroidal axis at time t relative to the $[X_1, Y_1, Z_1]$ axis system. Since $\vec{k}^*$ is equal to $\vec{k}$ by definition and

$$\vec{k} = \sin\theta_2 (z, t) \vec{i}_1 - \sin\theta_1 (z, t) \cos\theta_2 (z, t) \vec{j}_1$$
$$+ \cos\theta_1 (z, t) \cos\theta_2 (z, t) \vec{k}_1 , \quad (73)$$

it follows by equating components that actual deflection can be obtained by solving the equations

$$\frac{\partial X(z, t)}{\partial z} = \sin\theta_2 (z, t) , \quad (74)$$

$$\frac{\partial Y(z, t)}{\partial z} = -\sin\theta_1 (z, t) \cos\theta_2 (z, t) , \quad (75)$$

$$\frac{\partial Z(z, t)}{\partial z} = \cos\theta_1 (z, t) \cos\theta_2 (z, t) . \quad (76)$$

Suppose that the body triad $[X, Y, Z]$ slides along the centroidal axis of the boom with unit velocity. The angular velocity $\vec{\Omega}$ with which the body triad rotates can be expressed in terms of the $[\vec{i}, \vec{j}, \vec{k}]$ set of basis vectors which maintains the same rotational orientation as $[X, Y, Z]$ relative to the inertial fixed-axis system. The angular velocity vector $\vec{\Omega}$ can be written as

$$\vec{\Omega} = \kappa \vec{i} + \kappa' \vec{j} + \tau \vec{k} , \quad (77)$$

where it can be shown that

$$\kappa = \frac{d\theta_1}{dz} \cos \theta_2 \cos \varphi + \frac{d\theta_2}{dz} \sin \varphi , \qquad (78)$$

$$\kappa' = -\frac{d\theta_1}{dz} \cos \theta_2 \sin \varphi + \frac{d\theta_2}{dz} \cos \varphi , \qquad (79)$$

$$\tau = \frac{d\varphi}{dz} + \frac{d\theta_1}{dz} \sin \theta_2 . \qquad (80)$$

κ and κ' are simply the components of the curvature of the centroidal axis at the point z and time t, and τ is the twist at the same point and time. The vector $\vec{\Omega}$ will be needed in the subsequent analysis whenever the derivatives of $\vec{i}$, $\vec{j}$, and $\vec{k}$ with respect to the coordinate z are needed.

Simplified Equations of Elastic Equilibrium

The vector equations of elastic equilibrium as derived earlier are:

$$\frac{d\vec{V}}{dz} + \vec{F} = 0 , \qquad (68)$$

$$\frac{d\vec{M}}{dz} + \vec{k} \times \vec{V} + \vec{K} = 0 . \qquad (70)$$

In order to solve these equations, they must first be reduced to component form, be simplified by taking into account the constraints of the problem, and have the forcing functions defined.

Using the notation and terminology of Love (Reference 6), we let:

$$V = N\vec{i} + N'\vec{j} + T\vec{k} , \qquad (81)$$

where N and N' are the "shearing forces," and the force T is the "tension";

$$\vec{M} = G\vec{i} + G'\vec{j} + H\vec{k} , \qquad (82)$$

where G and G' are the "flexural couples," and the couple H is the "torsional couple." The forces N, N', T are called the "stress resultants," and the couples G, G', H the "stress couples." Furthermore, the applied resultant force distribution is written as

$$\vec{F} = F_1 \vec{i} + F_2 \vec{j} + F_3 \vec{k} , \qquad (83)$$

and the applied resultant couple distribution is written as

$$\vec{K} = K\vec{i} + K'\vec{j} + \Theta\vec{k} .$$ (84)

By applying the principle that the change in a vector due to an infinitesimal rotation is equal to the vector product of the rotation vector and the vector itself, one is led to

$$\frac{d\vec{i}}{dz} = \vec{\Omega} \times \vec{i} = \tau\vec{j} - \kappa'\vec{k} ,$$ (85)

$$\frac{d\vec{j}}{dz} = \vec{\Omega} \times \vec{j} = -\tau\vec{i} + \kappa\vec{k} ,$$ (86)

$$\frac{d\vec{k}}{dz} = \vec{\Omega} \times \vec{k} = \kappa'\vec{i} - \kappa\vec{j} .$$ (87)

The obvious substitutions can be made into Equations 68 and 70, the necessary vector operations performed, and the resulting expressions derived:

$$\left[\frac{dN}{dz} - N'\tau + T\kappa' + F_1\right]\vec{i} + \left[\frac{dN'}{dz} - T\kappa + N\tau + F_2\right]\vec{j} + \left[\frac{dT}{dz} - N\kappa' + N'\kappa + F_3\right]\vec{k} = 0 ,$$ (88)

$$\left[\frac{dG}{dz} - G'\tau + H\kappa' - N' + K\right]\vec{i} + \left[\frac{dG'}{dz} - H\kappa + G\tau + N + K'\right]\vec{j} + \left[\frac{dH}{dz} - G\kappa' + G'\kappa + \Theta\right]\vec{k} = 0 .$$ (89)

Small-displacement theory can be applied and the equations of equilibrium simplified if displacements from the unstrained state are assumed small. This assumption reduces the equations to a tractable form. The stability of the response of the system can now be analyzed; however, predicted steady state amplitudes of vibration must be interpreted with the assumptions of small-displacement theory in mind.

By omission of terms that are second order in displacement, the equilibrium Equations 88 and 89 become

$$\left[\frac{dN}{dz} + F_1\right]\vec{i} + \left[\frac{dN'}{dz} + F_2\right]\vec{j} + \left[\frac{dT}{dz} + F_3\right]\vec{k} = 0 .$$ (90)

and

$$\left[\frac{dG}{dz} - N' + K\right]\vec{i} + \left[\frac{dG'}{dz} + N + K'\right]\vec{j} + \left[\frac{dH}{dz} + \Theta\right]\vec{k} = 0 .$$ (91)

From Timoshenko's theory of members of open section, the flexural and torsional couples are related to the components of curvature and twist by the following:

$$G \;=\; EI\kappa \; , \tag{92}$$

$$G' \;=\; EI\kappa' \; , \tag{93}$$

$$H \;=\; -\,C_W \frac{\partial^2 \tau}{\partial z^2} + C_T \tau \; , \tag{94}$$

where

EI = average bending stiffness,

C_T = torsional rigidity,

C_W = warping rigidity.

If there is an initial pretwist in the rod defined by

$$\tau_0 \;=\; \frac{d\varphi_0\,(z,\,0)}{dz} \; , \tag{94a}$$

then the stress couple H is related to twist by

$$H \;=\; -\,C_W \frac{\partial^2 \,(\tau - \tau_0)}{\partial z^2} + C_T\,(\tau - \tau_0) \; . \tag{94b}$$

It can be found in various texts, in particular Reference 1, that for a thin-walled cylinder of open cross-section

$$EI \;=\; \frac{E}{2}\left[I_x + I_y\right] \; , \tag{95}$$

$$C_T \;=\; \frac{1}{3}\,Ph^3\,G_s \; , \tag{96}$$

$$C_W \;=\; \frac{2}{3}\,hEr^5 \left\{ \left(\pi + \frac{\phi}{2}\right)^3 - \frac{6\left[\sin\frac{\phi}{2} - \left(\pi + \frac{\phi}{2}\right)\cos\frac{\phi}{2}\right]^2}{\pi + \frac{\phi}{2} - \sin\phi} \right\} \; , \tag{97}$$

where

$$I_x \;=\; hr^3\left[\left(\pi + \frac{\phi}{2}\right) + \frac{1}{2}\,\sin\phi\right] - (2\pi + \phi)\,hr\delta_c^{\,2} \; , \tag{98}$$

37

$$I_y = hr^3 \left[\left(\pi + \frac{\phi}{2} \right) - \frac{1}{2} \sin \phi \right], \tag{99}$$

$$\delta_c = \frac{r \sin \frac{\phi}{2}}{\pi + \frac{\phi}{2}}, \tag{100}$$

G_s = shear modulus of elasticity,

E = Young's modulus of elasticity.

Since small-displacement assumptions have been introduced into the equilibrium equations, they may be introduced also into the transformation matrix (71) to obtain

$$\begin{Bmatrix} \vec{i} \\ \vec{j} \\ \vec{k} \end{Bmatrix} = \begin{bmatrix} \cos \varphi & \sin \varphi & -\theta_2 \cos \varphi + \theta_1 \sin \varphi \\ -\sin \varphi & \cos \varphi & \theta_2 \sin \varphi + \theta_1 \cos \varphi \\ \theta_2 & -\theta_1 & 1 \end{bmatrix} \begin{Bmatrix} \vec{i}_1 \\ \vec{j}_1 \\ \vec{k}_1 \end{Bmatrix} \tag{101}$$

into Equations 78, 79, and 80 (for curvature components and twist) to obtain

$$\kappa = \frac{d\theta_1}{dz} \cos \varphi + \frac{d\theta_2}{dz} \sin \varphi, \tag{102}$$

$$\kappa' = -\frac{d\theta_1}{dz} \sin \varphi + \frac{d\theta_2}{dz} \cos \varphi, \tag{103}$$

$$\tau = \frac{d\varphi}{dz}, \tag{104}$$

and into the displacement Equations (74, 75, and 76) to obtain

$$\theta_2 = \frac{\partial X(z, t)}{\partial z}, \tag{105}$$

$$\theta_1 = -\frac{\partial Y(z, t)}{\partial z}, \tag{106}$$

$$z = Z(z, t). \tag{107}$$

The force equilibrium Equation (90) can be resolved into the inertial coordinate system, and the effect of tension deleted from the analysis. Equation 90 can then be rewritten as

$$\left[\left(\frac{dN}{dz} + F_1 \right) \cos \varphi - \left(\frac{dN'}{dz} + F_2 \right) \sin \varphi \right] \vec{i}_1 + \left[\left(\frac{dN}{dz} + F_1 \right) \sin \varphi + \left(\frac{dN'}{dz} + F_2 \right) \cos \varphi \right] \vec{j}_1 = 0. \tag{108}$$

38

Since the vector equation defining the sum of all moments (Equation 91) equals zero, each component must equal zero and hence

$$\frac{dG}{dz} - N' + K = 0 , \tag{109}$$

$$\frac{dG'}{dz} + N + K' = 0 , \tag{110}$$

$$\frac{dH}{dz} + \Theta = 0 . \tag{111}$$

Substituting Equations 109 and 110 into Equation 108 yields

$$\left[\left(-\frac{d^2 G'}{dz^2} - \frac{dK'}{dz} + F_1\right)\cos\varphi - \left(\frac{d^2 G}{dz^2} + \frac{dK}{dz} + F_2\right)\sin\varphi\right]\vec{i}_1$$
$$+ \left[\left(-\frac{d^2 G'}{dz^2} - \frac{dK'}{dz} + F_1\right)\sin\varphi + \left(\frac{d^2 G}{dz^2} + \frac{dK}{dz} + F_2\right)\cos\varphi\right]\vec{j}_1 = 0 , \tag{112}$$

By using the relation between G, G' and κ, κ' given by Equations 92 and 93, and by noting that products of small-displacement terms are of second order, we may express the derivatives of G and G' as

$$\frac{d^2 G}{dz^2} = EI\left[\frac{d^3 \theta_1}{dz^3}\cos\varphi + \frac{d^3 \theta_2}{dz^3}\sin\varphi\right] , \tag{113}$$

$$\frac{d^2 G'}{dz^2} = EI\left[-\frac{d^3 \theta_1}{dz^3}\sin\varphi + \frac{d^3 \theta_2}{dz^3}\cos\varphi\right] . \tag{114}$$

Setting the components of Equation 112 equal to zero and substituting 113 and 114 yield

$$- EI\frac{d^3 \theta_2}{dz^3} - \left(\frac{dK'}{dz} - F_1\right)\cos\varphi - \left(\frac{dK}{dz} + F_2\right)\sin\varphi = 0 , \tag{115}$$

$$EI\frac{d^3 \theta_1}{dz^3} - \left(\frac{dK'}{dz} - F_1\right)\sin\varphi + \left(\frac{dK}{dz} + F_2\right)\cos\varphi = 0 . \tag{116}$$

From the relationships defined in Equations 94, 104, 105, 106, and 111, the equations of elastic equilibrium reduce to

$$EI\frac{\partial^4 X(z, t)}{\partial z^4} + \left(\frac{dK'}{dz} - F_1\right)\cos\varphi + \left(\frac{dK}{dz} + F_2\right)\sin\varphi = 0 , \tag{117}$$

$$EI \frac{\partial^4 Y(z, t)}{\partial z^4} + \left(\frac{dK'}{dz} - F_1\right) \sin\varphi - \left(\frac{dK}{dz} + F_2\right) \cos\varphi = 0 , \qquad (118)$$

$$- C_W \frac{\partial^4 \varphi(z, t)}{\partial z^4} + C_T \frac{\partial^2 \varphi(z, t)}{\partial z^2} + \Theta = 0 . \qquad (119)$$

If pretwist τ_0 is considered and if it and the amount of twist τ about it can be assumed small-angle, then the torsion Equation (119) can be rewritten as

$$- C_W \frac{\partial^4 \left[\varphi(z, t) - \varphi_0(z, 0)\right]}{\partial z^4} + C_T \frac{\partial^2 \left[\varphi(z, t) - \varphi_0(z, 0)\right]}{\partial z^2} + \Theta = 0 . \qquad (120)$$

These are the equations of equilibrium which will be solved after the resultant force and couple distributions defined by $\vec{F}$ and $\vec{K}$ have been derived.

DISTURBANCE FORCES AND THE EQUATIONS OF THERMALLY-INDUCED VIBRATION

The only disturbance forces which will be of interest in this paper are:

1. The body forces associated with the translational and rotational acceleration of all mass elements along the length of the boom.

2. The dissipative forces associated with viscoelastic damping of transverse and torsional motion.

3. The thermal loading associated with the presence of the boom in direct sunlight.

In addition to these forcing functions, the boom attached to an orbiting satellite will be disturbed by such effects as: solar pressure, aerodynamic drag, gravity gradient, satellite body motion, etc. When accounted for, each of these effects will perturb the actual motion slightly. By excluding these effects completely from the analysis, one can clearly show that thermally-induced vibration is possible and is a prime first-order effect not to be overlooked.

The disturbance forces which are distributed along the length of the boom can be expressed as an equivalent resultant force and couple distribution. The equations of two-axis transverse bending and torsional vibration are the same as the derived equations of equilibrium under the action of the equivalent resultant force and couple distributions.

The body forces associated with the reversed kinetic reactions of all accelerating mass elements along the entire length must be obtained using vector techniques. The expression is not merely stated, but is derived from elementary considerations; since the standard small-angle assumptions break down when long, torsionally weak booms are studied.

The actual description of the dissipative forces is extremely complicated, and has not yet been completely defined experimentally. It is known (see Reference 10) that frictional contact in the overlap region is a strong contributor to the damping of large-amplitude transverse and torsion motion. It is also known that small-amplitude motion is damped by a viscoelastic-type damping mechanism. Experimental work done in a cold vacuum leads to results which give damping ratios for small-angle motion of anywhere from 1.0% to .01% of critical. No work, however, has been done to measure damping in a thermal environment or after extensive wear and/or thermal cycling.

Since there are so many unknowns in the description of damping, it is assumed that by defining two viscous damping ratios, one associated with transverse motion and one associated with torsional motion, an estimation of the effect of transverse and torsional damping can be obtained. These two ratios are distinct from each other; no attempt is made to determine how or whether they are related to each other through friction. They are simply used as independent parameters which can be varied independently of each other to determine their influence on the resultant motion of the boom.

The thermal loading is dependent upon the boom's torsional response. By defining a sufficient number of thermal stations at which the torsional motion is recorded, and solving the thermodynamic equation at each station simultaneously with the vibration equations, a broken linear description of the temperature profile and hence the thermal loading is obtainable. By using higher-order interpolation techniques between stations, an accurate description of the thermal loading can be derived in terms of a thermal bending moment and torque defined at every point along the length.

Each of the three disturbance forces can be described completely in terms of a resultant couple distribution and a zero resultant force distribution. This is done in the following three subsections. In the fourth subsection, the results are combined and the actual equations of thermally-induced vibration to be solved are written.

Body Forces Associated With Kinetic Reaction of Mass Elements

The body forces associated with the reverse kinetic reactions can be derived from elementary considerations. At any particular instant of time, the vibrating boom will be in some deflected state, as shown in Figure 30.

Let $z = 0$ define the clamped root of the boom, $z = L$ define the free tip, z be an arbitrary point along the length, and z' be the location of any mass element between z and L. The mass element at z' is assumed to have mass $\rho^* dz'$ and rotational inertia $I_s dz'$, where

$\rho^* = \rho hP$ = mass per unit length of boom,

$I_s = \rho^* \left[r^2 + e_s^2 + 2e_s \delta_c \right]$ = rotational inertia per unit length about the shear center axis of the boom.

If the mass element at z' is separated from z by a finite amount and is accelerating in the transverse direction, it will produce a moment about the point z.

Figure 30—Instantaneous deflected position of boom.

Let $\Delta\vec{R}(z', z, t)$ define the vector connecting the points z and z'. From the coordinate systems defined,

$$\Delta\vec{R}(z', z, t) = \left[X(z', t) - X(z, t)\right] \vec{i}_1$$

$$+ \left[Y(z', t) - Y(z, t)\right] \vec{j}_1 + (z' - z) \vec{k}_1 . \quad (121)$$
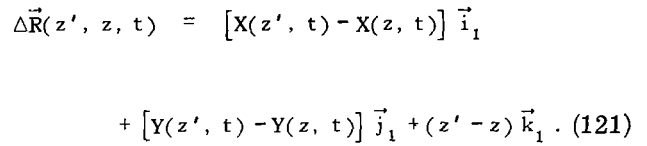
Furthermore, let $\rho^* \ddot{\vec{R}}(z', t) \, dz'$ be the force associated with the transversely accelerating mass element at z', where

$$\rho^* \ddot{\vec{R}}(z', t) \, dz' = \rho^* \frac{\partial^2 X(z', t)}{\partial t^2} \, dz' \vec{i}_1 + \rho^* \frac{\partial^2 Y(z', t)}{\partial t^2} \, dz' \vec{j}_1 . \quad (122)$$

The moment at z due to the accelerating mass element is

$$\Delta\vec{R}(z', z, t) \times \rho^* \ddot{\vec{R}}(z', t) \, dz' , \quad (123)$$

and the equivalent couple distribution due to the reversed kinetic reactions associated with the transverse acceleration of all mass elements along the boom is $\vec{K}_B$, where

$$\vec{K}_B = -\frac{d}{dz} \int_L^z \Delta\vec{R}(z', z, t) \times \rho^* \ddot{\vec{R}}(z', t) \, dz' . \quad (124)$$

Relative to the inertial coordinate system, $\vec{K}_B$ can be written as

$$\vec{K}_B = -\frac{d}{dz} \int_L^z \left(-\rho^* (z' - z) \frac{\partial^2 Y(z', t)}{\partial t^2} \vec{i}_1 \right.$$

$$+ \rho^* (z' - z) \frac{\partial^2 X(z', t)}{\partial t^2} \vec{j}_1$$

$$+ \rho^* \left\{ \left[X(z', t) - X(z, t)\right] \frac{\partial^2 Y(z', t)}{\partial t^2} - \left[Y(z', t) - Y(z, t)\right] \frac{\partial^2 X(z', t)}{\partial t^2} \right\} \vec{k}_1 \right) dz' , \quad (125)$$

and by the transformation matrix (101) it can be expressed in the desired form relative to the local $[\vec{i}, \vec{j}, \vec{k}]$ coordinate system as

$$\vec{K}_B = -\int_L^z \rho^* \left\{ \left[\frac{\partial^2 Y(z', t)}{\partial t^2} \cos\varphi(z, t) - \frac{\partial^2 X(z', t)}{\partial t^2} \sin\varphi(z, t) \right] \vec{i} - \left[\frac{\partial^2 Y(z', t)}{\partial t^2} \sin\varphi(z, t) \right. \right.$$

$$\left. \left. + \frac{\partial^2 X(z', t)}{\partial t^2} \cos\varphi(z, t) \right] \vec{j} + \left[-(z' - z) \frac{\partial^2 X(z, t)}{\partial z^2} \frac{\partial^2 Y(z', t)}{\partial t^2} + (z' - z) \frac{\partial^2 Y(z, t)}{\partial z^2} \frac{\partial^2 X(z', t)}{\partial t^2} \right] \vec{k} \right\} dz', \quad (126)$$

where the differentiation has been carried out and second-order term deleted.

Consider the kinetic reaction at z associated with the rotational acceleration of the mass element at z'. The torque at z due to this element is

$$I_s \frac{\partial^2 \varphi(z', t)}{\partial t^2} \vec{k}(z') \, dz', \quad (127)$$

where

$\vec{k}(z')$ = unit vector tangent to the boom at z'.

The equivalent couple distribution due to the reversed kinetic reaction associated with the torsional acceleration of all mass elements along the boom is $\vec{K}_w$, where

$$\vec{K}_w = -\frac{d}{dz} \int_L^z I_s \frac{\partial^2 \varphi(z', t)}{\partial t^2} \vec{k}(z') \, dz'. \quad (128)$$

To write $\vec{K}_w$ relative to the body axes $[\vec{i}, \vec{j}, \vec{k}]$, it must first be written relative to the inertial axis system $[\vec{i}_1, \vec{j}_1, \vec{k}_1]$. Since

$$\vec{k}(z') = [\vec{k}(z') \cdot \vec{i}_1] \vec{i}_1 + [\vec{k}(z') \cdot \vec{j}_1] \vec{j}_1 + [\vec{k}(z') \cdot \vec{k}_1] \vec{k}_1, \quad (129)$$

it can be seen from the transformation matrix (101) that

$$\vec{K}_w = -I_s \frac{\partial^2 \varphi(z, t)}{\partial t^2} \left[\frac{\partial X(z, t)}{\partial z} \vec{i}_1 + \frac{\partial Y(z, t)}{\partial z} \vec{j}_1 + \vec{k}_1 \right]. \quad (130)$$

In terms of body axes, this becomes

$$\vec{K}_w = -I_s \frac{\partial^2 \varphi(z, t)}{\partial t^2} \left\{ \left[\frac{\partial X(z, t)}{\partial z} \cos\varphi(z, t) + \frac{\partial Y(z, t)}{\partial z} \sin\varphi(z, t) \right] \vec{i} \right.$$

$$\left. + \left[-\frac{\partial X(z, t)}{\partial z} \sin\varphi(z, t) + \frac{\partial Y(z, t)}{\partial z} \cos\varphi(z, t) \right] \vec{j} + \vec{k} \right\}. \quad (131)$$

43

By combining $\vec{K}_B$ and $\vec{K}_W$, the total couple distribution which describes the reversed kinetic reactions of all accelerating mass elements can be written as $\vec{K}_C$, where

$$\vec{K}_C = \vec{K}_B + \vec{K}_W$$

$$= K_C \vec{i} + K_C' \vec{j} + \Theta_C \vec{k} \tag{132}$$

and

$$K_C = -\int_L^z \rho^* \left[\frac{\partial^2 Y(z', t)}{\partial t^2} \cos \varphi(z, t) - \frac{\partial^2 X(z', t)}{\partial t^2} \sin \varphi(z, t) \right] dz'$$

$$- I_s \frac{\partial^2 \varphi(z, t)}{\partial t^2} \left[\frac{\partial X(z, t)}{\partial z} \cos \varphi(z, t) + \frac{\partial Y(z, t)}{\partial z} \sin \varphi(z, t) \right] , \tag{133}$$

$$K_C' = \int_L^z \rho^* \left[\frac{\partial^2 Y(z', t)}{\partial t^2} \sin \varphi(z, t) + \frac{\partial^2 X(z', t)}{\partial t^2} \cos \varphi(z, t) \right] dz'$$

$$- I_s \frac{\partial^2 \varphi(z, t)}{\partial t^2} \left[-\frac{\partial X(z, t)}{\partial z} \sin \varphi(z, t) + \frac{\partial Y(z, t)}{\partial z} \cos \varphi(z, t) \right] , \tag{134}$$

$$\Theta_C = +\int_L^z \rho^* (z' - z) \left[\frac{\partial^2 X(z, t)}{\partial z^2} \frac{\partial^2 Y(z', t)}{\partial t^2} - \frac{\partial^2 Y(z, t)}{\partial z^2} \frac{\partial^2 X(z', t)}{\partial t^2} \right] dz' - I_s \frac{\partial^2 \varphi(z, t)}{\partial t^2} . \tag{135}$$

Dissipative Forces Associated With Viscoelastic Damping

As previously discussed, experimental evidence shows that the dissipative forces are not precisely definable for any arbitrary boom. It can be seen from Reference 10 that so-called identical booms may have damping characteristics which vary by as much as two orders of magnitude. In accordance with these findings, only viscous-type damping is included. It is argued that, by varying the damping parameters, the effect of frictional damping can be estimated via an equivalent viscous damping term.

Let $\beta_x \vec{R}(z', t) \, dz'$ be the dissipative force associated with the transverse motion, where

$$\beta_x \vec{R}(z', t) \, dz' = \beta_x \frac{\partial X(z', t)}{\partial t} dz' \vec{i}_1 + \beta_x \frac{\partial Y(z', t)}{\partial t} dz' \vec{j}_1 , \tag{136}$$

44

and let

$$\beta_\varphi \frac{\partial \varphi(z', t)}{\partial t} dz' \vec{k}_1 \tag{137}$$

be the dissipative torque associated with the torsional motion.

The equivalent couple distribution at z due to the dissipative force and torque associated with all moving mass elements along the boom is taken to be

$$\vec{K}_D = -\frac{d}{dz} \int_L^z \left[(z' - z) \vec{k}_1 \times \beta_x \vec{R}(z', t) + \beta_\varphi \frac{\partial \varphi(z', t)}{\partial t} \vec{k}_1 \right] dz'$$

$$= \int_L^z \left[-\beta_x \frac{\partial Y(z', t)}{\partial t} \vec{i}_1 + \beta_x \frac{\partial X(z', t)}{\partial t} \vec{j}_1 \right] dz' - \beta_\varphi \frac{\partial \varphi(z, t)}{\partial t} \vec{k}_1 . \tag{138}$$

By the transformation matrix (101), $\vec{K}_D$ can be rewritten as

$$\vec{K}_D = K_D \vec{i} + K_D' \vec{j} + \Theta_D \vec{k} , \tag{139}$$

where, upon elimination of second-order terms,

$$K_D = -\beta_x \int_L^z \left[\frac{\partial Y(z', t)}{\partial t} \cos \varphi(z, t) - \frac{\partial X(z', t)}{\partial t} \sin \varphi(z, t) \right] dz' , \tag{140}$$

$$K_D' = \beta_x \int_L^z \left[\frac{\partial Y(z', t)}{\partial t} \sin \varphi(z, t) + \frac{\partial X(z', t)}{\partial t} \cos \varphi(z, t) \right] dz' , \tag{141}$$

$$\Theta_D = -\beta_\varphi \frac{\partial \varphi(z, t)}{\partial t} . \tag{142}$$

Resultant Thermal Forces Associated With Thermal Loading

In an earlier subsection, "Thermal Loading Associated with Non-Uniform Temperature Distribution," expressions are derived which define the resultant thermal bending moment and thermal torque at any particular thermal station z. If one assumes a sufficient number of thermal stations at which the thermodynamic equation is solved simultaneously with the vibration equations, then by interpolation techniques the resultant thermal loading can be accurately defined at every point along the length.

From the work previously done, the thermal loading at position z at time t can be defined by the thermal loading vector $\overrightarrow{BM}(z, t)$, where

$$\overrightarrow{BM}(z, t) = BM_x(z, t)\vec{i} + BM_y(z, t)\vec{j} + T_{sc}(z, t)\vec{k}. \tag{143}$$

From Equations 64, 65, and 66,

$$BM_x(z, t) = 2\sqrt{2}\, e_c\, Ehr^2 P^2 \sin\frac{\phi}{2} \sum_{\substack{n=2 \\ n\ \text{even}}}^{\infty} \frac{q_n(z, t)}{(n\pi r)^2 - P^2}, \tag{144}$$

$$BM_y(z, t) = -2\sqrt{2}\, e_c\, Ehr^2 P^2 \cos\frac{\phi}{2} \sum_{\substack{n=1 \\ n\ \text{odd}}}^{\infty} \frac{q_n(z, t)}{(n\pi r)^2 - P^2}, \tag{145}$$

$$T_{sc}(z, t) = 2\sqrt{2}\, e_c\, EhrP \left\{ \sum_{\substack{n=1 \\ n\ \text{odd}}}^{\infty} \frac{1}{n\pi} \left[\frac{n\pi Pre_s \cos\frac{\phi}{2}}{P^2 - (n\pi r)^2} - \frac{P}{n\pi} \right] \cdot \frac{\partial q_n(z, t)}{\partial \psi(z, t)} \right\} \frac{\partial \psi(z, t)}{\partial \varphi(z, t)} \frac{d\varphi(z, t)}{dz}. \tag{146}$$

To obtain the equivalent couple distribution

$$\vec{K}_H = K_H\vec{i} + K_H'\vec{j} + \Theta_H\vec{k}$$

due to the thermal loading, Equation 143 may be differentiated with respect to z to obtain the reversed thermal reactions

$$K_H = -\frac{\partial BM_x(z, t)}{\partial z},$$

$$K_H' = -\frac{\partial BM_y(z, t)}{\partial z},$$

$$\Theta_H = -\frac{\partial T_{sc}(z, t)}{\partial z},$$

where the derivatives of $\vec{i}, \vec{j}, \vec{k}$ are considered of second-order smallness.

It must be noted that neither $BM(z, t)$ nor

$$\frac{\partial BM(z, t)}{\partial z}$$

46

is necessarily equal to zero at the tip of the boom, $z = L$. This fact implies that the thermal loading introduces a time-dependent set of boundary conditions which must be satisfied for all time t.

Thermoelastic Equations of Thermally-Induced Vibration

Near the conclusion of an earlier subsection, "Simplified Equations of Elastic Equilibrium," it was found that the equations of equilibrium were

$$EI \frac{\partial^4 X(z, t)}{\partial z^4} + \left(\frac{dK'}{dz} - F_1\right) \cos \varphi + \left(\frac{dK}{dz} + F_2\right) \sin \varphi = 0, \tag{117}$$

$$EI \frac{\partial^4 Y(z, t)}{\partial z^4} + \left(\frac{dK'}{dz} - F_1\right) \sin \varphi - \left(\frac{dK}{dz} + F_2\right) \cos \varphi = 0, \tag{118}$$

$$- C_W \frac{\partial^4 \varphi(z, t)}{\partial z^4} + C_T \frac{\partial^2 \varphi(z, t)}{\partial z^2} + \Theta = 0; \tag{119}$$

and near the beginning of the same subsection it was found that the resultant force and couple distributions $\vec{F}$ and $\vec{K}$ are given by

$$\vec{F} = F_1 \vec{i} + F_2 \vec{j} + F_3 \vec{k}, \tag{83}$$

$$\vec{K} = K\vec{i} + K' \vec{j} + \Theta\vec{k}. \tag{84}$$

For the three disturbance forces of interest, it was found that each could be described by a zero resultant force distribution and a particular resultant couple distribution. By vector addition, the total resultant couple and force distributions are

$$\vec{F} = F_1 \vec{i} + F_2 \vec{j} + F_3 \vec{k} = 0, \tag{147}$$

$$\vec{K} = \vec{K}_C + \vec{K}_D + \vec{K}_H$$

$$= \left(K_C + K_D + K_H\right) \vec{i} + \left(K_C' + K_D' + K_H'\right)\vec{j} + \left(\Theta_C + \Theta_D + \Theta_H\right) \vec{k}$$

$$= K\vec{i} + K' \vec{j} + \Theta\vec{k}. \tag{148}$$

Upon substitution into the equations of equilibrium, it follows that

$$EI \frac{\partial^4 X(z, t)}{\partial z^4} + \frac{d}{dz} \left(K_C' + K_D' + K_H'\right) \cos \varphi + \frac{d}{dz} \left(K_C + K_D + K_H\right) \sin \varphi = 0, \tag{149}$$

$$EI \frac{\partial^4 Y(z, t)}{\partial z^4} + \frac{d}{dz} \left(K_C' + K_D' + K_H' \right) \sin \varphi - \frac{d}{dz} \left(K_C + K_D + K_H \right) \cos \varphi = 0 , \tag{150}$$

$$- C_W \frac{\partial^4 \varphi(z, t)}{\partial z^4} + C_T \frac{\partial^2 \varphi(z, t)}{\partial z^2} + \Theta_C + \Theta_D + \Theta_H = 0 , \tag{151}$$

where, if pretwist is considered, $\varphi(z, t)$ in the torsion Equation (151) is replaced by $\big[\varphi(z, t)$ $-\varphi_0(z, 0)\big]$. By further substitution of the equations developed in the preceding three subsections and deletion of second-order terms, one obtains:

$$EI \frac{\partial^4 X(z, t)}{\partial z^4} + \rho^* \frac{\partial^2 X(z, t)}{\partial t^2} + \beta_x \frac{\partial X(z, t)}{\partial t}$$

$$= \frac{\partial^2 BM_y(z, t)}{\partial z^2} \cos \varphi(z, t) + \frac{\partial^2 BM_x(z, t)}{\partial z^2} \sin \varphi(z, t)$$

$$+ I_s \left[\frac{\partial^2 \varphi(z, t)}{\partial t^2} \frac{\partial^2 Y(z, t)}{\partial z^2} + \frac{\partial^3 \varphi(z, t)}{\partial z \partial t^2} \frac{\partial Y(z, t)}{\partial z} \right] , \tag{152}$$

$$EI \frac{\partial^4 Y(z, t)}{\partial z^4} + \rho^* \frac{\partial^2 Y(z, t)}{\partial t^2} + \beta_x \frac{\partial Y(z, t)}{\partial t}$$

$$= \frac{\partial^2 BM_y(z, t)}{\partial z^2} \sin \varphi(z, t) - \frac{\partial^2 BM_x(z, t)}{\partial z^2} \cos \varphi(z, t)$$

$$- I_s \left[\frac{\partial^2 \varphi(z, t)}{\partial t^2} \frac{\partial^2 X(z, t)}{\partial z^2} + \frac{\partial^3 \varphi(z, t)}{\partial z \partial t^2} \frac{\partial X(z, t)}{\partial z} \right] , \tag{153}$$

$$C_W \frac{\partial^4 \varphi(z, t)}{\partial z^4} - C_T \frac{\partial^2 \varphi(z, t)}{\partial z^2} + I_s \frac{\partial^2 \varphi(z, t)}{\partial t^2} + \beta_\phi \frac{\partial \varphi(z, t)}{\partial t}$$

$$= - \frac{\partial T_{sc}(z, t)}{\partial z} + \int_L^z \rho^*(z' - z) \left[\frac{\partial^2 X(z, t)}{\partial z^2} \frac{\partial^2 Y(z', t)}{\partial t^2} - \frac{\partial^2 Y(z, t)}{\partial z^2} \frac{\partial^2 X(z', t)}{\partial t^2} \right] dz' . \tag{154}$$

These are the equations of thermally-induced vibration which will be solved simultaneously with the thermodynamic equation defined at each thermal station.

SOLUTION TO EQUATIONS OF THERMALLY-INDUCED VIBRATIONS

Equations 152, 153, and 154 define the response of a thin-walled cylinder in a solar thermal field. These equations may have their solution expressed in terms of the orthogonal functions which define the undamped-unforced normal modes of vibration for the system.

The boundary conditions that define the undamped-unforced system are time-independent. They define a boom that is clamped at the root, $z = 0$, in both two-axis bending and torsion. The tip, $z = L$, is free both to translate and to rotate, but has a tip weight attached to it which has both translational and rotational inertia. The method of attachment of the tip weight is such that the tip remains free to warp. This condition is consistent with the end conditions for OGO IV, OGO V, and ATS D.

When the system is in a thermal field, there are certain time-dependent boundary conditions that must be satisfied and that are a function of the thermal loading.

To solve a set of equations having time-dependent boundary conditions, the techniques developed by Mindlin and Goodman (Reference 11), and applied by Boley (Reference 2) to solve a different thermally-induced vibration problem, are used.

The resulting equations can be given a physical interpretation. They imply that the elastic-restoring force, which tends to drive the cylinder toward equilibrium, is measured not from its undeflected position but from a time-varying position of static thermal equilibrium. The frequency content of the moving position of thermal equilibrium is therefore important, since if it has a strong component at the first natural bending frequency a resonant condition can be excited.

To determine the motion of the position of thermal equilibrium, both the thermodynamic and the vibration equations must be solved simultaneously.

Time-Dependent Boundary Conditions

As previously discussed, the cylinder is assumed to be clamped in both two-axis bending and torsion at the root. Hence

$$X(z, t)\big|_{z=0} = Y(z, t)\big|_{z=0} = \varphi(z, t)\big|_{z=0} = 0, \qquad \text{(155a, b, c)}$$

$$\frac{\partial X(z, t)}{\partial z}\bigg|_{z=0} = \frac{\partial Y(z, t)}{\partial z}\bigg|_{z=0} = \frac{\partial \varphi(z, t)}{\partial z}\bigg|_{z=0} = 0. \qquad \text{(156a, b, c)}$$

In actual practice these root conditions are functions of the satellite body motion. For a gravity gradient satellite, the situation is further complicated by the fact that roll, pitch, and yaw motion are coupled. Breakwell and Pringle* show that, for an undamped rigid body in circular orbit, low frequency (near orbital) non-linear resonances affecting gravity gradient stabilization can exist. This is another phenomenom not yet fully understood which can impair the performance of a flexible gravity gradient satellite. It is, however, not related to the relatively high frequency thermally induced oscillation problem discussed herein.

At the tip warping is not restrained. Hence

$$\frac{\partial^2 \varphi(z, t)}{\partial z^2}\bigg|_{z=L} = 0. \qquad \text{(157c)}$$

If pretwist is to be considered, the boundary conditions on the torsion equation are obtained by simply replacing $\varphi(z, t)$ by $[\varphi(z, t) - \varphi_0(z, 0)]$ in the above and subsequent torsional boundary condition equations.

*Breakwell, J.V., and Pringle, R. Jr., "Nonlinear Resonance Affecting Gravity-Gradient Stability," Astrodynamics (ed. Michal Lunc), Proc. XVI International Nautical Congress, Athens, 1965, Gauthier-Villair, Paris, pp. 305-325, 1966.

Attached to the tip is a tip weight which has both translational and rotational inertia. Let

W_T = tip weight, lbs,

I_T = rotational inertia of tip weight, lbs sec^2 in.,

g = acceleration of gravity, in./sec^2,

and assume that the tip is free to translate and rotate in the thermal environment. At the tip there is zero bending moment attributable to the tip weight; but the thermal loading does impose a condition that must be satisfied. Hence

$$EI \left. \frac{\partial^2 X(z, t)}{\partial z^2} \right|_{z=L} = \left[BM_y (z, t) \cos \varphi(z, t) + BM_x (z, t) \sin \varphi(z, t) \right] \Big|_{z=L} , \qquad (157a)$$

$$EI \left. \frac{\partial^2 Y(z, t)}{\partial z^2} \right|_{z=L} = \left[BM_y (z, t) \sin \varphi(z, t) - BM_x (z, t) \cos \varphi(z, t) \right] \Big|_{z=L} . \qquad (157b)$$

The translational and rotational acceleration of the tip weight gives rise to a shear force, and the thermal loading gives rise to what might be termed a "thermal shear." Both must be balanced at the tip by the internal stresses. Hence

$$EI \left. \frac{\partial^3 X(z, t)}{\partial z^3} \right|_{z=L} = \left\{ \frac{W_T}{g} \frac{\partial^2 X(z, t)}{\partial t^2} + \frac{\partial}{\partial z} \left[BM_y (z, t) \cos \varphi(z, t) \right. \right.$$
$$\left. \left. + BM_x (z, t) \sin \varphi(z, t) \right] \right\} \Bigg|_{z=L} , \qquad (158a)$$

$$EI \left. \frac{\partial^3 Y(z, t)}{\partial z^3} \right|_{z=L} = \left\{ \frac{W_T}{g} \frac{\partial^2 Y(z, t)}{\partial t^2} + \frac{\partial}{\partial z} \left[BM_y (z, t) \sin \varphi(z, t) \right. \right.$$
$$\left. \left. - BM_x (z, t) \cos \varphi(z, t) \right] \right\} \Bigg|_{z=L} , \qquad (158b)$$

$$+ C_W \left. \frac{\partial^3 \varphi(z, t)}{\partial z^3} - C_T \frac{\partial \varphi(z, t)}{\partial z} \right|_{z=L} = - \left[I_T \frac{\partial^2 \varphi(z, t)}{\partial t^2} + T_{sc} (z, t) \right] \Bigg|_{z=L} . \qquad (158c)$$

These stated boundary conditions are consistent with the thermostress analysis of Boley and Weiner (Reference 2). Recent work by P. Jordan (Reference 12) shows that, when warping deformation due to thermal strain is accounted for, the warping condition at the free end (Equation 157c) is non-zero. However, for a boom of practical interest (long length) this quantity is small and its effect approaches that of other deleted second-order terms.

Instantaneous Position of Thermal Equilibrium

In order to solve the equations of thermally-induced vibration and satisfy the time-dependent boundary conditions, the concept of an instantaneous position of thermal equilibrium must be introduced. It is defined as the position that the boom would instantaneously assume if it had zero mass. From this definition, Equations 152, 153, 154, and the boundary conditions defined in the preceding subsection, it follows that the instantaneous thermal equilibrium shape of the boom is defined by the solution of the equations

$$EI \frac{\partial^4 X_s(z, t)}{\partial z^4} = \frac{\partial^2}{\partial z^2} \left[BM_y(z, t) \cos \varphi(z, t) + BM_x(z, t) \sin \varphi(z, t) \right] , \tag{159}$$

$$EI \frac{\partial^4 Y_s(z, t)}{\partial z^4} = \frac{\partial^2}{\partial z^2} \left[BM_y(z, t) \sin \varphi(z, t) - BM_x(z, t) \cos \varphi(z, t) \right] , \tag{160}$$

$$C_W \frac{\partial^4 \varphi_s(z, t)}{\partial z^4} - C_T \frac{\partial^2 \varphi_s(z, t)}{\partial z^2} = - \frac{\partial T_{sc}(z, t)}{\partial z} , \tag{161}$$

and the boundary conditions

$$X_s(z, t)\big|_{z=0} = Y_s(z, t)\big|_{z=0} = \varphi_s(z, t)\big|_{z=0} = 0 , \tag{162a, b, c}$$

$$\frac{\partial X_s(z, t)}{\partial z}\bigg|_{z=0} = \frac{\partial Y_s(z, t)}{\partial z}\bigg|_{z=0} = \frac{\partial \varphi_s(z, t)}{\partial z}\bigg|_{z=0} = 0 , \tag{163a, b, c}$$

$$EI \frac{\partial^2 X_s(z, t)}{\partial z^2}\bigg|_{z=L} = \left[BM_y(z, t) \cos \varphi(z, t) + BM_x(z, t) \sin \varphi(z, t) \right]\bigg|_{z=L} , \tag{164a}$$

$$EI \frac{\partial^2 Y_s(z, t)}{\partial z^2}\bigg|_{z=L} = \left[BM_y(z, t) \sin \varphi(z, t) - BM_x(z, t) \cos \varphi(z, t) \right]\bigg|_{z=L} , \tag{164b}$$

$$\frac{\partial^2 \varphi_s(z, t)}{\partial z^2}\bigg|_{z=L} = 0 , \tag{164c}$$

$$EI \frac{\partial^3 X_s(z, t)}{\partial z^3}\bigg|_{z=L} = \frac{\partial}{\partial z}\left[BM_y(z, t) \cos \varphi(z, t) + BM_x(z, t) \sin \varphi(z, t) \right]\bigg|_{z=L} , \tag{165a}$$

$$EI \frac{\partial^3 Y_s(z, t)}{\partial z^3}\bigg|_{z=L} = \frac{\partial}{\partial z}\left[BM_y(z, t) \sin \varphi(z, t) - BM_x(z, t) \cos \varphi(z, t) \right]\bigg|_{z=L} , \tag{165b}$$

$$C_W \frac{\partial^3 \varphi_s(z, t)}{\partial z^3} - C_T \frac{\partial \varphi_s(z, t)}{\partial z}\bigg|_{z=L} = - T_{sc}(z, t)\bigg|_{z=L} . \tag{165c}$$

Integrate both sides of Equations 159 and 160 twice with respect to z, integrate both sides of Equation 161 once with respect to z, apply the boundary conditions 164a through 165c, and find that:

$$EI \frac{\partial^2 X_s(z, t)}{\partial z^2} = BM_y(z, t) \cos \varphi(z, t) + BM_x(z, t) \sin \varphi(z, t) , \tag{166}$$

$$EI \frac{\partial^2 Y_s(z, t)}{\partial z^2} = BM_y(z, t) \sin \varphi(z, t) - BM_x(z, t) \cos \varphi(z, t) , \tag{167}$$

$$C_W \frac{\partial^3 \varphi_s(z, t)}{\partial z^3} - C_T \frac{\partial \varphi_s(z, t)}{\partial z} = - T_{sc}(z, t) , \tag{168}$$

and

$$X_s(z, t)\big|_{z=0} = Y_s(z, t)\big|_{z=0} = \varphi_s(z, t)\big|_{z=0} = 0 , \tag{169a, b, c}$$

$$\frac{\partial X_s(z, t)}{\partial z}\bigg|_{z=0} = \frac{\partial Y_s(z, t)}{\partial z}\bigg|_{z=0} = \frac{\partial \varphi_s(z, t)}{\partial z}\bigg|_{z=0} = 0 , \tag{170a, b, c}$$

$$\frac{\partial^2 \varphi_s(z, t)}{\partial z^2}\bigg|_{z=L} = 0 . \tag{171c}$$

where it will be recalled from an earlier section that

$$BM_x(z, t) = 2\sqrt{2} e_c Ehr^2 P^2 \sin \frac{\phi}{2} \sum_{\substack{n=2 \\ n \text{ even}}}^{\infty} \frac{q_n(z, t)}{(n\pi r)^2 - P^2} , \tag{64}$$

$$BM_y(z, t) = -2\sqrt{2} e_c Ehr^2 P^2 \cos \frac{\phi}{2} \sum_{\substack{n=1 \\ n \text{ odd}}}^{\infty} \frac{q_n(z, t)}{(n\pi r)^2 - P^2} , \tag{65}$$

$$T_{sc}(z, t) = 2\sqrt{2} e_c EhrP \left\{ \sum_{\substack{n=1 \\ n \text{ odd}}}^{\infty} \frac{1}{n\pi} \left[\frac{n\pi Pre_s \cos \frac{\phi}{2}}{P^2 - (n\pi r)^2} \right. \right.$$

$$\left. \left. - \frac{P}{n\pi} \right] \frac{\partial q_n(z, t)}{\partial \psi(z, t)} \right\} \frac{\partial \psi(z, t)}{\partial \varphi(z, t)} \frac{d\varphi(z, t)}{dz} . \tag{66}$$

52

Since the sun line $\overrightarrow{SL}(z, t)$ is always assumed to be normal to the longitudinal axis of the boom, and $\varphi(z, t)$ measures positive rotation of the cross-section about the axis,

$$\psi(z, t) = \psi_0 + \varphi(z, t), \tag{172}$$

where

$$\psi_0 = \psi(z, t)\big|_{z=0}.$$

Having defined a sufficient number of thermal stations at which the generalized thermal co-ordinate equations are solved, we have a good approximation to $BM_x(z, t)$, $BM_y(z, t)$, and $T_{sc}(z, t)$ at hand. Equations 166 and 167 are initial-value problems and are readily integrated using any standard higher-order numerical integration technique. Equation 168 along with 169c, 170c, and 171c defines a boundary value problem which is not as easily solved. It is, however, a linear differential equation with constant coefficients.

To solve Equation 168, let $\varphi_P(z, t)$ be the particular solution of the initial-value problem defined by

$$C_W \frac{\partial^3 \varphi_P(z, t)}{\partial z^3} - C_T \frac{\partial \varphi_P(z, t)}{\partial z} = -T_{sc}(z, t), \tag{173}$$

where

$$\varphi_P(z, t)\big|_{z=0} = \frac{\partial \varphi_P(z, t)}{\partial z}\bigg|_{z=0} = \frac{\partial^2 \varphi_P(z, t)}{\partial z^2}\bigg|_{z=0} = 0 \tag{174}$$

(this problem is readily solvable by numerical techniques). Making use of $\varphi_P(z, t)$, it is then easily shown that the equation

$$\varphi_s(z, t) = \left[\frac{1 - \cosh \eta z}{\eta^2 \cosh \eta L}\right] \frac{d^2 \varphi_P(L, t)}{dz^2} + \varphi_P(z, t), \tag{175}$$

where

$$\eta^2 = \frac{C_T}{C_W}, \tag{176}$$

satisfies Equation 168 and its respective boundary conditions.

Thus the instantaneous thermal equilibrium position defined by the coordinates

$$\left[X_s (z, t), Y_s (z, t), \varphi_s (z, t) \right]$$

can be obtained by numerically integrating the generalized thermal coordinate along the length of the boom at each instant of time.

If pretwist is considered, $\varphi_s (z, t)$ as it appears in the preceding equations is replaced by $\left[\varphi_s (z, t) - \varphi_0 (z, 0) \right]$. The instantaneous position of thermal equilibrium is then defined by the coordinates $\left[X_s (z, t), Y_s (z, t), \varphi_s (z, t) - \varphi_0 (z, 0) \right]$.

Equations of Undamped-Uncoupled Thermally-Induced Vibration

The solution to the equations of thermally-induced vibration (152, 153, and 154) can be expressed in terms of the solutions to the eigenvalue problem defined by the equations of undamped-uncoupled thermally-induced vibration; that is,

$$EI \frac{\partial^4 X(z, t)}{\partial z^4} + \rho^* \frac{\partial^2 X(z, t)}{\partial t^2} = \frac{\partial^2}{\partial z^2} \left[BM_y (z, t) \cos \varphi(z, t) + BM_x (z, t) \sin \varphi(z, t) \right] , \qquad (177)$$

$$EI \frac{\partial^4 Y(z, t)}{\partial z^4} + \rho^* \frac{\partial^2 Y(z, t)}{\partial t^2} = \frac{\partial^2}{\partial z^2} \left[BM_y (z, t) \sin \varphi(z, t) - BM_x (z, t) \cos \varphi(z, t) \right] , \qquad (178)$$

$$C_w \frac{\partial^4 \varphi(z, t)}{\partial z^4} - C_T \frac{\partial^2 \varphi(z, t)}{\partial z^2} + I_s \frac{\partial^2 \varphi(z, t)}{\partial t^2} = - \frac{\partial T_{sc} (z, t)}{\partial z} , \qquad (179)$$

and the boundary conditions given by Equations 155a through 158c. Assume solutions of the form

$$X(z, t) = X_s (z, t) + e^{i \omega_x t} x(z) , \qquad (180)$$

$$Y(z, t) = Y_s (z, t) + e^{i \omega_x t} y(z) , \qquad (181)$$

$$\varphi(z, t) = \varphi_s (z, t) + e^{i \omega_\varphi t} \varphi(z) , \qquad (182)$$

and directly substitute into Equations 177, 178, 179 and the boundary condition Equations (155a through 158c), using the relations developed in the preceding subsection. One is immediately led to the following set of eigenvalue problems:

$$EI \frac{d^4 x(z)}{dz^4} - \rho^* \omega_x^2 x(z) = 0 , \qquad (183)$$

54

$$EI \frac{d^4 y(z)}{dz^4} - \rho^* \omega_x^2 y(z) = 0 , \tag{184}$$

$$C_W \frac{d^4 \varphi(z)}{dz^4} - C_T \frac{d^2 \varphi(z)}{dz^2} - I_s \omega_\varphi^2 \varphi(z) = 0 , \tag{185}$$

where

$$x(z)\big|_{z=0} = y(z)\big|_{z=0} = \varphi(z)\big|_{z=0} = 0 , \tag{186a, b, c}$$

$$\frac{dx(z)}{dz}\bigg|_{z=0} = \frac{dy(z)}{dz}\bigg|_{z=0} = \frac{d\varphi(z)}{dz}\bigg|_{z=0} = 0 , \tag{187a, b, c}$$

$$\frac{d^2 x(z)}{dz^2}\bigg|_{z=L} = \frac{d^2 y(z)}{dz^2}\bigg|_{z=L} = \frac{d^2 \varphi(z)}{dz^2}\bigg|_{z=L} = 0 , \tag{188a, b, c}$$

$$EI \frac{d^3 x(z)}{dz^3} + \frac{W_T}{g} \omega_x^2 x(z)\bigg|_{z=L} = 0 , \tag{189a}$$

$$EI \frac{d^3 y(z)}{dz^3} + \frac{W_T}{g} \omega_x^2 y(z)\bigg|_{z=L} = 0 ; \tag{189b}$$

$$C_W \frac{d^3 \varphi(z)}{dz^3} - C_T \frac{d\varphi(z)}{dz} - I_T \omega_\varphi^2 \varphi(z)\bigg|_{z=L} = 0 . \tag{189c}$$

Equations 183 and 184 along with their appropriate boundary conditions are the standard eigenvalue problem which defines the undamped-unforced normal bending modes of vibration of a clamped free beam with tip weight. Similarly Equation 185 along with its appropriate boundary conditions defines the undamped-unforced normal torsional modes of vibration of a thin-walled cylinder of open section without shear center effects, clamped at the root, free to warp at the tip, and having a tip inertia. The solutions to these equations are rather standard, but for completeness are included in Appendix B.

From Appendix B the following is obtained.

ω_{x_n} = nth natural frequency of vibration associated with transverse motion.

$x_n(z) = y_n(z)$ = nth normal-mode of transverse vibration; since bending stiffness EI is constant about all axes, $x_n(z)$ and $y_n(z)$ are equal.

Both $x_n(z)$ and $y_n(z)$ satisfy the orthonormality condition that

$$\int_0^L \rho^*(z) x_n(z) x_m(z) dz = \frac{W_T + W_B}{g} \delta_{m,n} , \tag{190}$$

55

where

$$\rho^*(z) = \begin{cases} \rho^* & 0 < z < L \\ \dfrac{W_T}{g} & z = L \end{cases}, \tag{191}$$

W_B = weight of boom without tip weight

$$W_B = \rho^* Lg, \tag{192}$$

$$\delta_{m,n} = \begin{cases} 1 & \text{if} \quad m = n \\ 0 & \text{if} \quad m \neq n \end{cases}, \tag{193}$$

ω_{φ_n} = nth natural frequency of vibration associated with torsional motion,

$\varphi_n(z)$ = nth normal mode of torsional vibration.

$\varphi_n(z)$ satisfies the orthonormality condition that

$$\int_0^L I_s(z)\,\varphi_n(z)\,\varphi_m(z)\,dz = \left(I_T + I_s L\right)\delta_{m,n}, \tag{194}$$

where

$$I_s(z) = \begin{cases} I_s & 0 < z < L \\ I_T & z = L \end{cases}. \tag{195}$$

If pretwist is considered, $\varphi(z, t)$ and $\varphi_s(z, t)$ are replaced by $\left[\varphi(z, t) - \varphi_0(z, 0)\right]$ and $\left[\varphi_s(z, t) - \varphi_0(z, t)\right]$ respectively in Equations 179 and 182.

Generalized Displacement Coordinates

The results of the two immediately preceding subsections can be used to express the solution to the equations of thermally-induced vibration (152, 153, and 154) in terms of the normal modes of vibration and their corresponding generalized displacement coordinates.

Assume a solution of the form

$$X(z, t) = X_s(z, t) + \sum_{n=1}^{\infty} a_n(t)\,x_n(z), \tag{196}$$

$$Y(z, t) = Y_s(z, t) + \sum_{n=1}^{\infty} b_n(t) y_n(z) , \tag{197}$$

$$\varphi(z, t) = \varphi_s(z, t) + \sum_{n=1}^{\infty} c_n(t) \varphi_n(z) . \tag{198}$$

Since at each instant of time the coordinates of the position of thermal equilibrium are known, they can be expressed as

$$X_s(z, t) = \sum_{n=1}^{\infty} \alpha_n(t) x_n(z) , \tag{199}$$

$$Y_s(z, t) = \sum_{n=1}^{\infty} \beta_n(t) y_n(z) , \tag{200}$$

$$\varphi_s(z, t) = \sum_{n=1}^{\infty} \gamma_n(t) \varphi_n(z) , \tag{201}$$

where

$$\alpha_n(t) = \frac{g}{W_T + W_B} \int_0^L \rho^*(z) X_s(z, t) x_n(z) \, dz , \tag{202}$$

$$\beta_n(t) = \frac{g}{W_T + W_B} \int_0^L \rho^*(z) Y_s(z, t) y_n(z) \, dz , \tag{203}$$

$$\gamma_n(t) = \frac{1}{I_T + I_s L} \int_0^L I_s(z) \varphi_s(z, t) \varphi_n(z) \, dz . \tag{204}$$

Equations 196, 197, and 198 can now be rewritten as

$$X(z, t) = \sum_{n=1}^{\infty} \left[\alpha_n(t) + a_n(t) \right] x_n(z) , \tag{205}$$

$$Y(z, t) = \sum_{n=1}^{\infty} \left[\beta_n(t) + b_n(t) \right] y_n(z) , \tag{206}$$

57

$$\varphi(z, t) \doteq \sum_{n=1}^{\infty} \left[\gamma_n(t) + c_n(t) \right] \varphi_n(z) . \qquad (207)$$

If pretwist is to be induced in the analysis, wherever $\varphi(z, t)$ and $\varphi_s(z, t)$ appear in the above equations the quantities $\left[\varphi(z, t) - \varphi_0(z, 0) \right]$ and $\left[\varphi_s(z, t) - \varphi_0(z, 0) \right]$ should be substituted respectively.

The equations of thermally-induced vibration (152, 153, and 154) are solved by: substituting into them the assumed solutions (205, 206, and 207); making use of the eigenvalue equations (183, 184, and 185), which must be satisfied by all natural modes and frequencies of vibration; and making use of the equations (159, 160, and 161) that define the instantaneous positions of thermal equilibrium. Carrying through the prescribed algebra yields:

$$\sum_{n=1}^{\infty} \left\{ \rho^* \frac{d^2}{dt^2} \left[\alpha_n(t) + a_n(t) \right] + \beta_x \frac{d}{dt} \left[\alpha_n(t) + a_n(t) \right] \right.$$

$$\left. + \rho^* \omega_{x_n}^2 a_n(t) \right\} x_n(z) = I_s \left[\frac{\partial^2 \varphi(z, t)}{\partial t^2} \frac{\partial^2 Y(z, t)}{\partial z^2} + \frac{\partial^3 \varphi(z, t)}{\partial z \partial t^2} \frac{\partial Y(z, t)}{\partial z} \right] , \qquad (208)$$

$$\sum_{n=1}^{\infty} \left\{ \rho^* \frac{d^2}{dt^2} \left[\beta_n(t) + b_n(t) \right] + \beta_x \frac{d}{dt} \left[\beta_n(t) + b_n(t) \right] \right.$$

$$\left. + \rho^* \omega_{x_n}^2 b_n(t) \right\} y_n(z) = -I_s \left[\frac{\partial^2 \varphi(z, t)}{\partial t^2} \frac{\partial^2 X(z, t)}{\partial z^2} + \frac{\partial^3 \varphi(z, t)}{\partial z \partial t^2} \frac{\partial X(z, t)}{\partial z} \right] , \qquad (209)$$

$$\sum_{n=1}^{\infty} \left\{ I_s \frac{d^2}{dt^2} \left[\gamma_n(t) + c_n(t) \right] + \beta_\varphi \frac{d}{dt} \left[\gamma_n(t) + c_n(t) \right] \right.$$

$$\left. + I_s \omega_{\varphi_n}^2 c_n(t) \right\} \varphi_n(z) = \int_L^z \rho^* (z' - z) \left[\frac{\partial^2 X(z, t)}{\partial z^2} \frac{\partial^2 Y(z', t)}{\partial t^2} - \frac{\partial^2 Y(z, t)}{\partial z^2} \frac{\partial X(z', t)}{\partial t^2} \right] dz' . \qquad (210)$$

Equation 210 is unchanged if pretwist is included.

Define the generalized displacement coordinates to be

$$\left[A_n(t), B_n(t), C_n(t) \right] ,$$

where

$$A_n(t) = \alpha_n(t) + a_n(t), \tag{211}$$

$$B_n(t) = \beta_n(t) + b_n(t), \tag{212}$$

$$C_n(t) = \gamma_n(t) + c_n(t). \tag{213}$$

Multiply both sides of Equation 208 by $x_m(z)$, Equation 209 by $y_m(z)$, and Equation 210 by $\varphi_m(z)$. Integrate over the length from $z = 0$ to $z = L$ and apply the orthonormality relations given by Equations 190 and 194 to obtain the ordinary differential equations which define the generalized displacement coordinates:

$$\frac{d^2 A_n(t)}{dt^2} + 2\zeta_{x_n}\omega_{x_n}\frac{dA_n(t)}{dt} + \omega_{x_n}^2\left[A_n(t) - \alpha_n(t)\right] = A_n^*(t), \tag{214}$$

$$\frac{d^2 B_n(t)}{dt^2} + 2\zeta_{x_n}\omega_{x_n}\frac{dB_n(t)}{dt} + \omega_{x_n}^2\left[B_n(t) - \beta_n(t)\right] = B_n^*(t), \tag{215}$$

$$\frac{d^2 C_n(t)}{dt^2} + 2\zeta_{\varphi_n}\omega_{\varphi_n}\frac{dC_n(t)}{dt} + \omega_{\varphi_n}^2\left[C_n(t) - \gamma_n(t)\right] = C_n^*(t), \tag{216}$$

where $A_n^*(t)$, $B_n^*(t)$, and $C_n^*(t)$ are the generalized forces associated with the nth mode of vibration, given by

$$A_n^*(t) = \frac{g}{W_T + W_B}\int_0^L I_s(z)\left[\frac{\partial^2\varphi(z,t)}{\partial t^2}\frac{\partial^2 Y(z,t)}{\partial z^2} + \frac{\partial^3\varphi(z,t)}{\partial z\partial t^2}\frac{\partial Y(z,t)}{\partial z}\right]x_n(z)\,dz, \tag{217}$$

$$B_n^*(t) = -\frac{g}{W_T + W_B}\int_0^L I_s(z)\left[\frac{\partial^2\varphi(z,t)}{\partial t^2}\frac{\partial^2 X(z,t)}{\partial z^2} + \frac{\partial^3\varphi(z,t)}{\partial z\partial t^2}\frac{\partial X(z,t)}{\partial z}\right]y_n(z)\,dz, \tag{218}$$

$$C_n^*(t) = +\frac{1}{I_T + I_s L}\int_0^L\varphi_n(z)\int_L^z\rho^*(z')(z'-z)\left[\frac{\partial^2 X(z,t)}{\partial z^2}\frac{\partial^2 Y(z',t)}{\partial t^2} - \frac{\partial^2 Y(z,t)}{\partial z^2}\frac{\partial^2 X(z',t)}{\partial t^2}\right]dz'dz. \tag{219}$$

and where the damping coefficients β_x and β_φ have been written in terms of their corresponding viscous damping ratios ζ_x and ζ_φ. If there is zero tip weight, they are defined by the expressions

$$\beta_x = 2\rho^*\zeta_x\omega_{x_n}, \tag{220}$$

$$\beta_\varphi = 2I_s\zeta_\varphi\omega_{\varphi_n}, \tag{221}$$

However, if there is a tip weight, since energy cannot be dissipated across it, its effect must be subtracted out. Thereupon it is found that

$$\zeta_{x_n} = \zeta_x \left[1 - \frac{W_T}{W_T + W_B} x_n^2 (L) \right] ,\tag{222}$$

$$\zeta_{\varphi_n} = \zeta_\varphi \left[1 - \frac{I_T}{I_T + I_s L} \varphi_n^2 (L) \right] .\tag{223}$$

Generalized Forces

Equations 217, 218, and 219 define the generalized forces $A_n^*(t)$, $B_n^*(t)$, and $C_n^*(t)$ respectively. These quantities define the dynamic coupling between transverse and torsional motion. It is reasonable to assume that they can be adequately approximated by the first-mode bending and torsional components of the resultant motion. Accordingly, we let

$$X(z, t) \cong A_1(t) x_1(z) ,\tag{224}$$

$$Y(z, t) \cong B_1(t) y_1(z) ,\tag{225}$$

$$\varphi(z, t) \cong C_1(t) \varphi_1(z) ,\tag{226}$$

and substitute into Equations 217, 218, and 219 to obtain

$$A_n^*(t) = \frac{d^2 C_1(t)}{dt^2} B_1(t) T_n ,\tag{227}$$

$$B_n^*(t) = - \frac{d^2 C_1(t)}{dt^2} A_1(t) T_n ,\tag{228}$$

where

$$T_n = \frac{g}{W_T + W_B} \int_0^L I_s(z) \left[\varphi_1(z) \frac{d^2 y_1(z)}{dz^2} + \frac{d\varphi_1(z)}{dz} \frac{dy_1(z)}{dz} \right] x_n(z) \, dz\tag{229}$$

and

$$C_n^*(t) = \left[A_1(t) \frac{d^2 B_1(t)}{dt^2} - B_1(t) \frac{d^2 A_1(t)}{dt^2} \right] P_n ,\tag{230}$$

60

where

$$P_n = \frac{1}{I_T + I_s \, L} \int_0^L \varphi_n(z) \int_L^z \rho^*(z')(z'-z) \frac{d^2 x_1(z)}{dz^2} y_1(z') \, dz' \, dz . \qquad (231)$$

It is noted that

$$x_n(z) = y_n(z) \qquad (232)$$

for all n. Since the equations for the mode shapes $x_n(z)$, $y_n(z)$, and $\varphi_n(z)$ are known and given in Appendix B, the integrals defining T_n and P_n can be obtained by either closed-form or numerical integration.

If numerical integration is used, then T_n can be found by solving the differential equation

$$\frac{dT_n(z)}{dz} = \frac{g}{W_T + W_B} I_s(z) \left[\varphi_1(z) \frac{d^2 y_1(z)}{dz^2} + \frac{d\varphi_1(z)}{dz} \frac{dy_1(z)}{dz} \right] x_n(z) , \qquad (233)$$

where

$$T_n(z)\big|_{z=0} = 0 \qquad (234)$$

and

$$T_n(z)\big|_{z=L} = T_n . \qquad (235)$$

Similarly, P_n can be found by solving the simultaneous differential equations

$$\frac{d\Gamma(z)}{dz} = H(z) , \qquad (236)$$

$$\frac{dH(z)}{dz} = -\rho^*(z) y_1(z) , \qquad (237)$$

$$\frac{dP_n(z)}{dz} = + \frac{1}{I_T + I_s \, L} \varphi_n(z) \frac{d^2 x_1(z)}{dz^2} \Gamma(z) , \qquad (238)$$

where

$$\Gamma(z)\big|_{z=0} = \int_L^0 \rho(z) \, z \, y_1(z) \, dz , \qquad (239)$$

$$H(z)\big|_{z=0} \;=\; -\int_{L}^{0} \rho(z)\,y_1(z)\,dz\,, \tag{240}$$

$$P_n(z)\big|_{z=0} \;=\; 0\,, \tag{241}$$

and

$$P_n(z)\big|_{z=L} \;=\; P_n\,. \tag{242}$$

It must be kept in mind that the generalized force expressions discussed in this section result from the fact that standard small-angle assumptions cannot always be applied in the analysis of extremely long torsionally weak beams. For short and/or torsionally stiff beams, these forces should be negligible.

By comparing the resultant responses obtained for various hypothetical examples with and without these terms included in the analysis, it has been found that:

1. Results obtained either with or without $A_n^*(t)$ and $B_n^*(t)$ included are essentially the same for the class of problems being considered. For beams which are much weaker in bending, however, these terms could be important.

2. Results obtained with and without $C_n^*(t)$ included are radically different for the class of problems being considered. As torsional rigidity is increased or length decreased, the effect of $C_n^*(t)$ on the resultant response is diminished.

For production-type runs these observations are applied to increase the speed of digital computation. That is, $C_n^*(t)$, the coupling of bending into torsion, is left unchanged but all dynamic coupling of torsion into bending, defined by $A_n^*(t)$ and $B_n^*(t)$, is assumed negligible and thus deleted by setting

$$A_n^*(t) \;=\; B_n^*(t) \;=\; 0\,. \tag{243}$$

Summary and Method of Solution

The work presented in the previous subsections shows that the solutions to the equations of thermally-induced vibration can be expressed in the form

$$X(z,\,t) \;=\; \sum_{n=1}^{\infty} A_n(t)\,x_n(z)\,, \tag{244}$$

$$Y(z,\,t) \;=\; \sum_{n=1}^{\infty} B_n(t)\,y_n(z)\,, \tag{245}$$

$$\varphi(z, t) = \varphi_0(z, 0) + \sum_{n=1}^{\infty} C_n(t) \varphi_n(z). \tag{246}$$

The equations that define the generalized displacement coordinates are:

$$\frac{d^2 A_n(t)}{dt^2} + 2\zeta_{x_n} \omega_{x_n} \frac{dA_n(t)}{dt} + \omega_{x_n}^2 \left[A_n(t) - \alpha_n(t) \right] = \frac{d^2 C_1(t)}{dt^2} B_1(t) T_n \cong 0, \tag{247}$$

$$\frac{d^2 B_n(t)}{dt^2} + 2\zeta_{x_n} \omega_{x_n} \frac{dB_n(t)}{dt} + \omega_{x_n}^2 \left[B_n(t) - \beta_n(t) \right] = -\frac{d^2 C_1(t)}{dt^2} A_1(t) T_n \cong 0, \tag{248}$$

$$\frac{d^2 C_n(t)}{dt^2} + 2\zeta_{\varphi_n} \omega_{\varphi_n} \frac{dC_n(t)}{dt} + \omega_{\varphi_n}^2 \left[C_n(t) - \gamma_n(t) \right] = \left[A_1(t) \frac{d^2 B_1(t)}{dt^2} - B_1(t) \frac{d^2 A_1(t)}{dt^2} \right] P_n. \tag{249}$$

Also shown is that the thermal loading defined by the quantities

$$BM_x(z, t), \ BM_y(z, t), \ T_{sc}(z, t)$$

and hence the coordinates of the instantaneous position of thermal equilibrium defined by

$$X_s(z, t) = \sum_{n=1}^{\infty} \alpha_n(t) x_n(z) \tag{199}$$

$$Y_s(z, t) = \sum_{n=1}^{\infty} \beta_n(t) y_n(z) \tag{200}$$

$$\varphi_s(z, t) = \sum_{n=1}^{\infty} \gamma_n(t) \varphi_n(z) \tag{201}$$

can be written in terms of the generalized thermal coordinates $q_n(z, t)$ defined at a sufficient number of thermal stations along the boom.

To solve the generalized thermal coordinate equations

$$\frac{dq_n(z, t)}{dt} + \lambda_n q_n(z, t) = Q_n(z, t), \tag{250}$$

the generalized thermal input $Q_n(z, t)$ must be known as a function of time and position along the boom.

63

$Q_n(z, t)$ has been shown to be an analytic function of the relative sun orientation $\psi(z, t)$. Thus, by simultaneously solving the generalized displacement and thermal coordinate equations, the generalized thermal input $Q_n(z, t)$ can be continually updated from a knowledge of

$$\psi(z, t) = \psi_0 + \varphi_0(z, 0) + \sum_{n=1}^{\infty} C_n(t)\varphi_n(z),$$

and the quantities $\alpha_n(t)$, $\beta_n(t)$, $\gamma_n(t)$ can be updated from a continuous knowledge of $q_n(z, t)$.

The numerical solution of the derived equations thus leads to the description of how a thin-walled cylinder of open section will respond when placed into direct sunlight.

The derived equations given here have been programmed for digital solution on the SDS-9300 computer. The program could use as many as 20 thermal modes, 60 thermal stations, and 9 independent modes of vibration. The results showed that good accuracy was possible using only four thermal modes, excluding that associated with λ_0. The number of thermal stations used for the runs excluding the effect of thermal torque was 20; when thermal torque was included, 50 thermal stations were used. For all runs, transverse motion has been found to be essentially first-mode. Torsional motion, however, was found to have a slight second-mode component, so that two torsional modes of vibration were included in all runs to ensure a good representation of the thermal loading.

Trapezoidal, Heun, Simpson's, and fourth-order fixed-step Runge-Kutta integration techniques were used to solve the generalized displacement coordinate equation and in the integrations needed to define the thermal-equilibrium position. However, for production runs, Runge-Kutta integration proved the most efficient. To circumvent the numerical problems associated with simultaneously solving the thermodynamic and vibration equations when the thermal time constants are much shorter than the natural periods of vibration, an exponential interpolation technique was developed for solving the generalized thermal-coordinate equations. This permitted the use of a reasonable timewise integration step and prevented computational instabilities in solving the thermodynamic equations.

PRESENTATION OF RESULTS

The nominal model for the results presented is the antenna used on OGO IV and other existing satellites. These results should provide a heuristic understanding of the basic mechanism behind thermally-induced vibrations and the effect of changes in various parameters on its magnitude. The parameters studied are those which can be controlled by a manufacturer and used to govern the amplitude and stability of motion. Nominal magnitudes used to describe the geometrical and physical properties of the antenna are shown in Table 3.

For all runs presented, the antenna is assumed to be initially in an unstrained state with a uniform ambient-temperature distribution. The sun is assumed to be turned on at time zero, and its

Table 3

Antenna material	= beryllium copper, silver–plated
Antenna length	$= L = 60$ ft
Perimeter of cross-section	$= P = 2$ in.
Total overlap angle	$= \phi = 90$ deg
Wall thickness	$= h = .002$ in.
Weight density of material	$= \rho = .2714$ lb/in.^{3}
Shear modulus	$= G_s = .6 \times 10^7$ lb/in.^{2}
Young's modulus	$= E = .19 \times 10^8$ lb/in.^{2}
Bending stiffness	$= EI = 16.6$ lb ft^2
Damping ratio for torsion	$= \zeta_\varphi = .2$
Damping ratio for bending	$= \zeta_x = .005$
Torsional rigidity	$= C_T = .05$ lb-in.^{2}
Warping rigidity	$= C_W = 1,700$ lb-in.^{4}
Thermal conductivity	$= K_T = 4.167$ Btu/(hr-in.-°F)
Specific heat	$= c = .1$ Btu/(lb-°F)
Solar radiation intensity	$= J_s = 3.065$ Btu/(hr-in.^{2})
Thermal expansion coefficient	$= e_c = .104 \times 10^{-4}$ in./(in.-°F)
Emissivity	$= \epsilon = .035$
Absorptivity	$= \alpha_s = .13$
Stefan–Boltzmann constant	$= \sigma = .121 \times 10^{-10}$ Btu/(hr-in.^{2})

orientation remains fixed in time, unless otherwise noted, along the inertially fixed negative Y_1 axis. Throughout the ensuing dynamic response, the thermal input at all thermal stations is assumed to be that of one sun normal to the strained longitudinal axis.

It should be further noted that in several examples the predicted amplitudes exceed the limits of small angle deflection theory. However, since numerical results agree with satellite data in a phenomological sense, the effects of including neglected terms would probably change the numerical values of the answers but not the basic characteristics of the motion.

Effect of Thermal Torque

Boley (Reference 2) shows that shear stresses exist in all cases where the temperature varies along the length of the boom. Appendix A derives the shear-stress distribution and resultant thermal torque expression theoretically for the special case of a thin-walled cylinder of open section.

Recent unpublished test data obtained by R. Predmore and C. Staugaitis at NASA/GSFC indicate that torsional response due to thermal torque can be reasonably well predicted by this analysis. More experimental work is needed, however, before a more positive statement can be justified.

In addition to the work of Predmore and Staugaitis at NASA/GSFC, an independent experimental program has been carried out at NASA/Ames by R. M. Beam. The results of Beam's work have been published (Reference 13). Although Beam restricts his study to a boom with zero overlap, he has been the first to conclusively prove experimentally that the theory of thermally-induced vibration as presented herein is physically realizable. In addition to demonstrating thermal flutter, Beam has in his report presented an extensive amount of experimental and theoretical work related to the study of thermal torque. One of his most interesting experimental results is that, for certain sun orientations, thermal torque can excite a torsional instability. This region has been defined both experimentally and theoretically for a short zero-overlap boom. The material to be presented herein is consistent with the experimental findings both of Beam and of Predmore and Staugaitis.

Keeping in mind the possibility of some inadequacy in any representation of thermal torque, we began a qualitative analysis of it by making numerous computer runs to determine the effect of changes in torsional damping, initial sun orientation, pretwist, length, and of the inclusion of the first three torsional modes of vibration.

In order to build confidence in the analytic model, several of these computer runs attempted to duplicate laboratory test data. Actual data obtained by Predmore and Staugaitis at NASA/GSFC will not be presented herein. Simple visual observations concerning basic response characteristics will, however, be stated.

For all booms tested, it was noted that, for some sun orientations relative to the outer seam of the boom, twisting was small; and that, for other sun orientations, twisting was quite large. To accent this effect, a 10-foot black painted standard boom was tested in the laboratory, and simulated with the analytic model. Because of the painting and end conditions, it was felt that damping could be reasonably well simulated by assuming

$$\zeta_x = .05 , \qquad \zeta_\varphi = .75 .$$

Emissivity and absorptivity were measured and found to be

$$\epsilon = .8 , \qquad \alpha_s = .8 .$$

All other parameters were nominal. The effects of pretwist and relative sun orientation were studied. This was done by slowly rotating the sun at $180°/\text{min}$ around the perimeter of the boom. The computed results are summarized in Figure 31.

Tip twist $\varphi(L, t)$ is plotted versus sun orientation $\psi(0, t)$ for varying amounts of pretwist. The curves labeled A, B, C, D, E, and F correspond to linear pretwists of 0, .5, 1.5, 3.0, 4.5, and 6.0 degrees per foot, respectively.
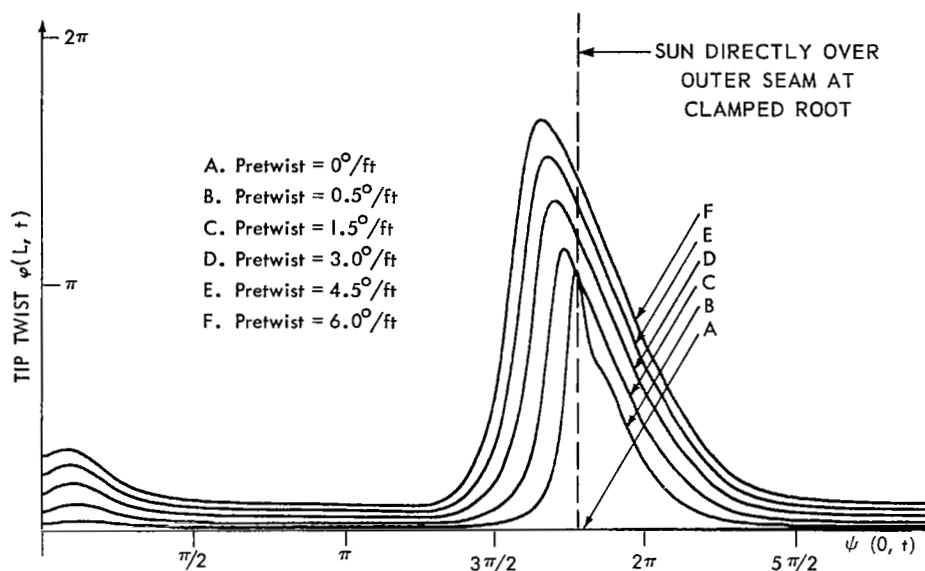
Figure 31—Thermally-induced tip twist vs relative sun orientation for booms having linear pretwist.

Both theory and test data show a significant change in the amount of tip twist when the sun moves across the outer seam of the boom. The magnitude of the twist observed runs approximately the same as that predicted for booms pretwisted 30 to 60 degrees. A significant dependence upon pretwist was not observed in the laboratory. It is suspected that, if shear center offset and the exact boundary conditions for the torsion equation discussed in Reference 12 were accounted for, the torsional response predicted would be less sensitive to changes in pretwist.

In Reference 13 it is stated that if there is sufficient damping in the system all thermally-induced torsional motion will be stable. If damping is small, however, a torsional instability will exist for certain sun orientations. This phenomenon has been observed experimentally both by Predmore and Staugaitis at NASA/GSFC and by Beam at NASA/Ames. Jordan (Reference 12) makes use of earlier work (Reference 1) by Frisch and predicts that the region of instability is where the function e_c Ehr $(\partial V/\partial \psi)$ shown in Figures 15 through 24 is negative.

Beam, in his study of the zero-overlap boom, goes one step further and shows (by a small-angle single-degree-of-freedom analysis) that the instability can be either divergent oscillatory or divergent non-oscillatory.

The results shown in Figures 32 through 37 attempt to illustrate the regions of stability and instability for a particular example. The example chosen is the black painted 10-foot boom used for the results presented in Figure 31. The transverse damping ratio is changed to

$$\zeta_x = .01 ,$$

and a pretwist of 30° is assumed. The sun is turned on at time zero and starts to spin around the perimeter of the boom at a rate of 180°/min in the positive direction starting from a position directly over the axis of symmetry of the clamped root and over the overlap.
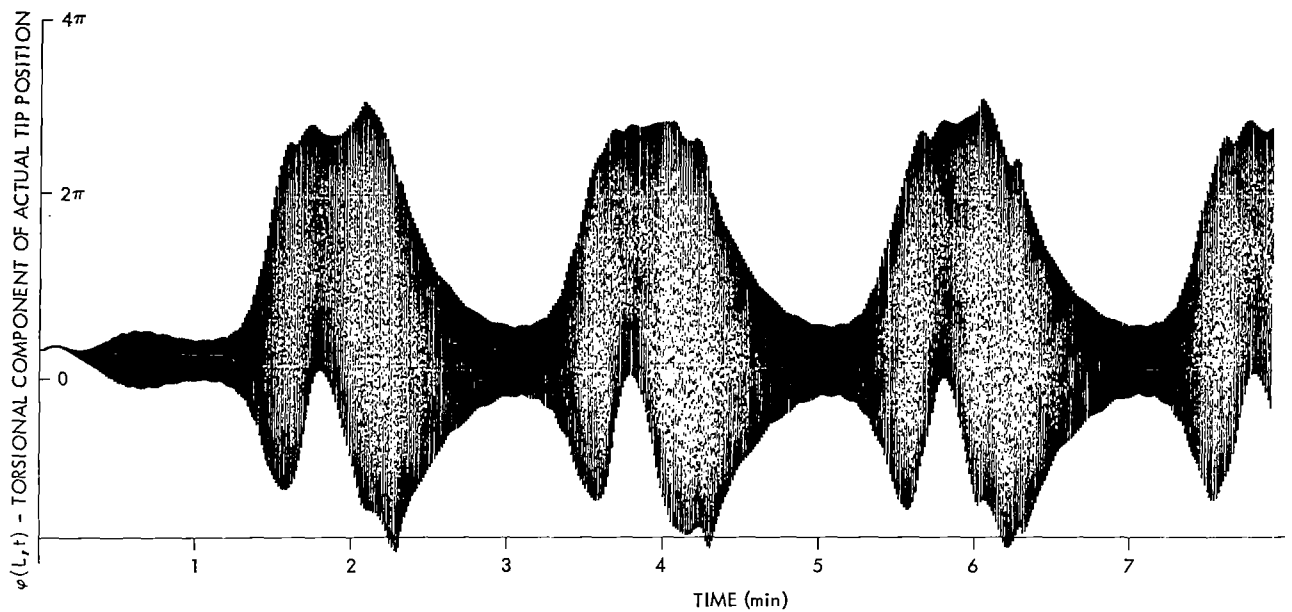
Figure 32—Torsional component for tip of 10' boom, sun spinning at 180°/min, thermal torque included.
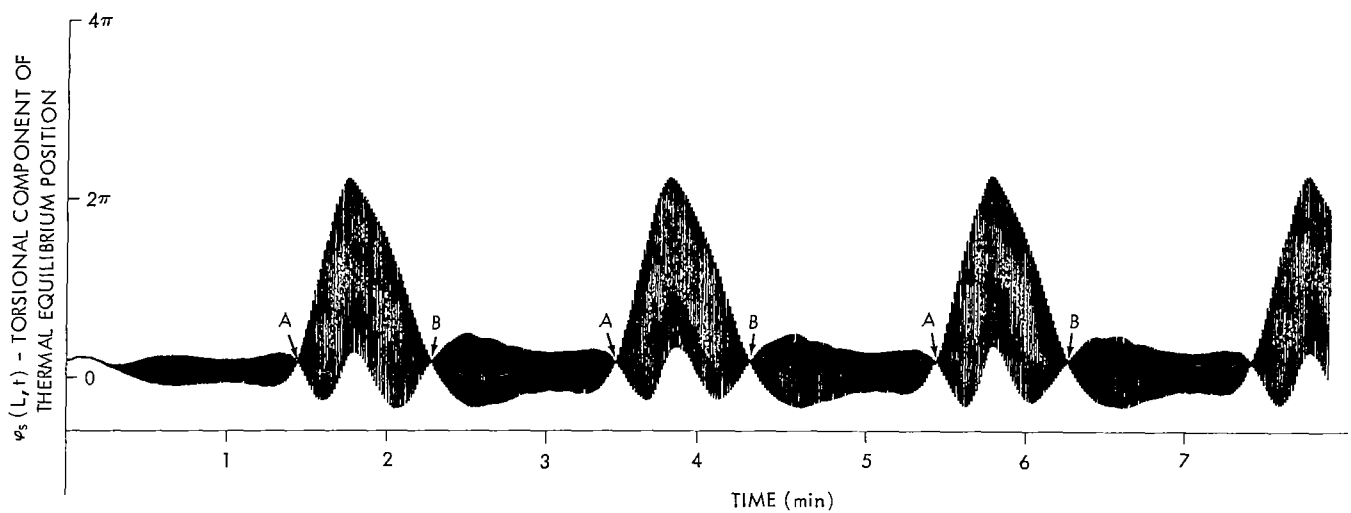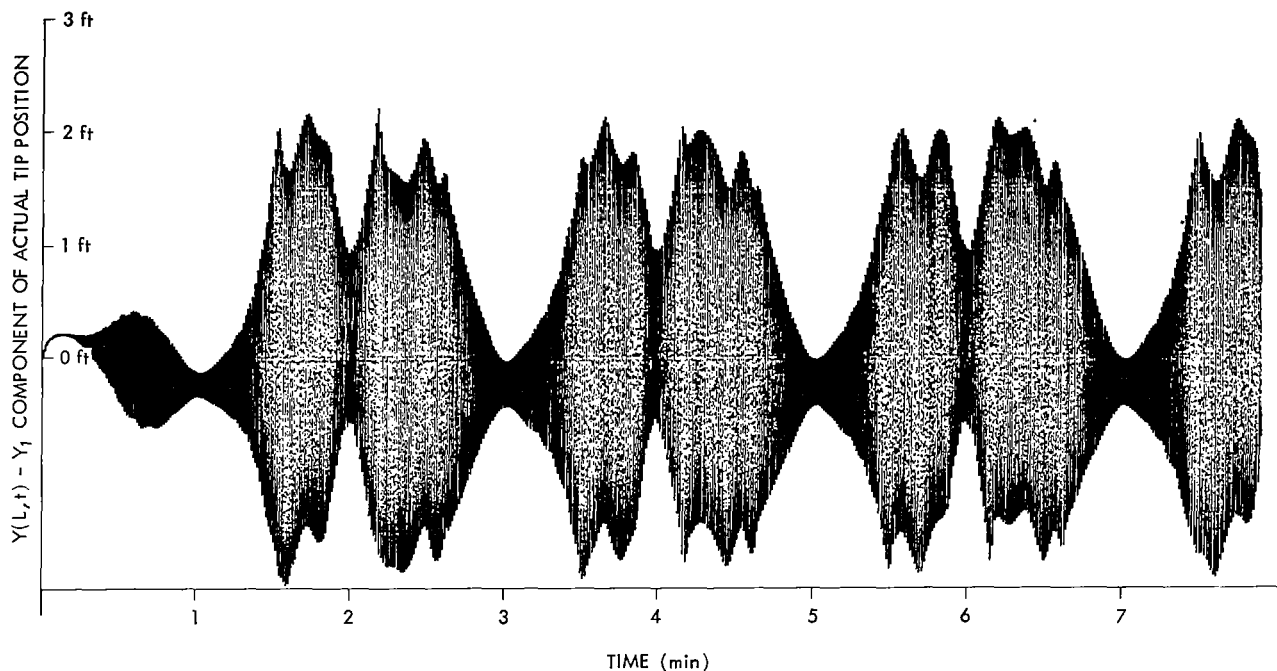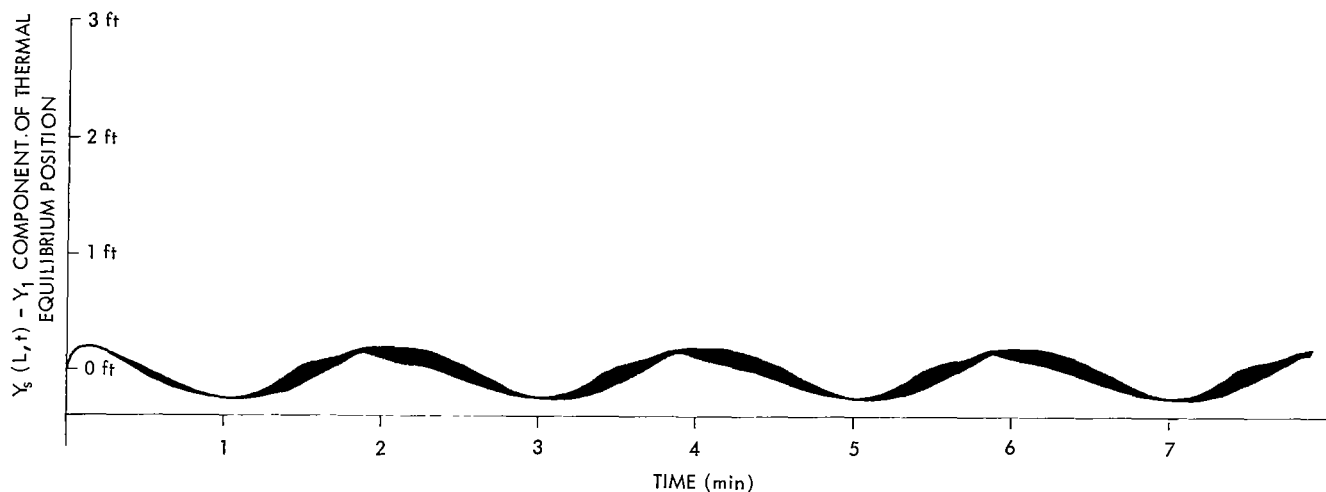

Figure 33—Torsional component of thermal equilibrium position for 10' boom,
sun spinning at 180°/min, thermal torque included.

In Figure 32 the amplitude of the torsional motion of the tip is plotted as a function of time. Relative sun orientation and time are related by the simple linear equation

$$\psi(0, t) = \frac{\pi}{60} t , (radians)$$

where t is time measured in seconds.

68
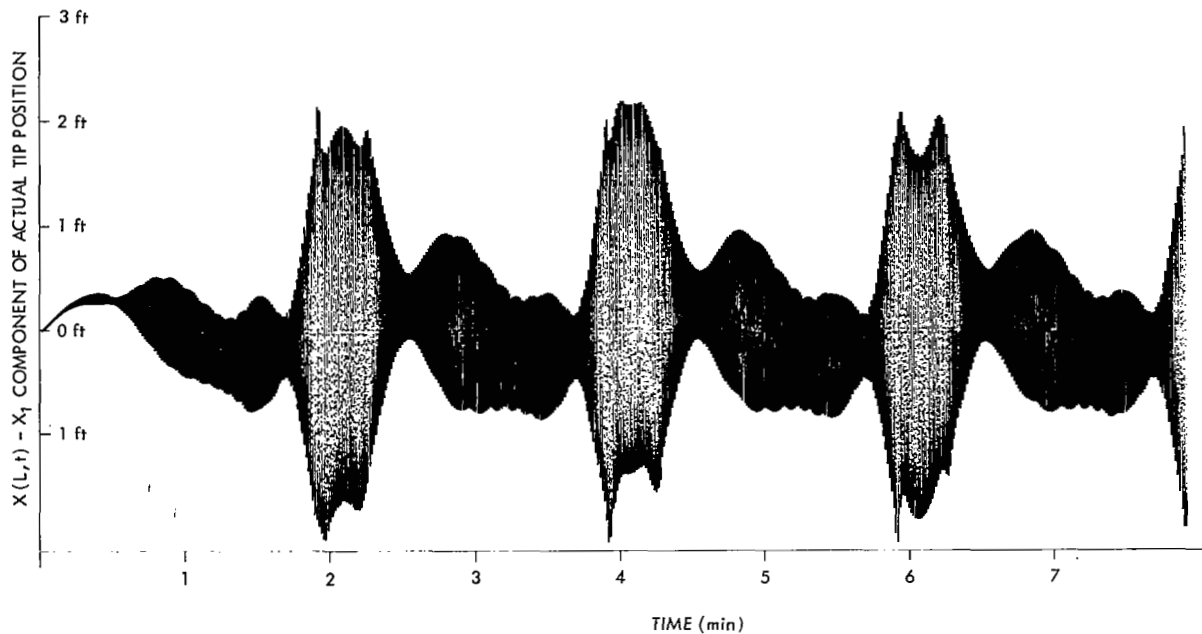
Figure 34—X_1 component for tip of 10' boom, sun spinning at 180°/min, thermal torque included.
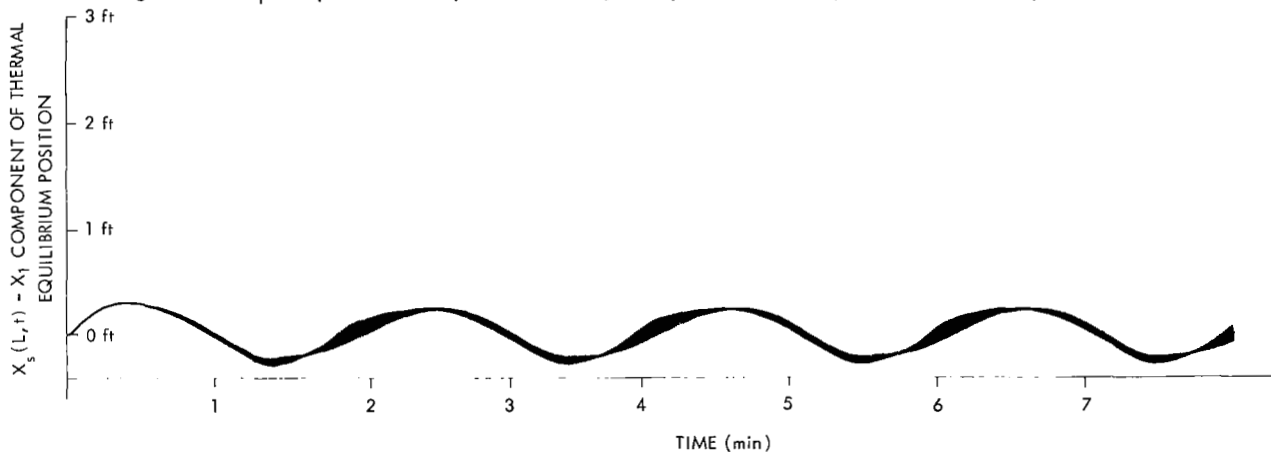
Figure 35—X_1 component of thermal equilibrium position for 10' boom, sun spinning at 180°/min, thermal torque included.

Although the resultant response appears to be quite complex, it is evident that for certain sun orientations the amplitude of the torsional response grows rapidly and for other sun orientations it rapidly decays to an approximate steady state level.

From this single figure it is not possible to pinpoint exactly regions of stability and instability; however, one does see that they exist and that they roughly correspond to those predicted by the small-angle analyses of Jordan (Reference 12) and Beam (Reference 13). That is, where the function e_c Ehr $(\partial V/\partial \psi)$ shown in Figure 15, curve A,* is negative, linear theory applied to a single-degree-of-freedom model predicts a torsional instability.

---

*180°/min = .0524 rad/sec $\cong$ .05 rad/sec.

Figure 36—Y_1 component for tip of 10' boom, sun spinning at 180°/min, thermal torque included.

Figure 37—Y_1 component of thermal equilibrium position for 10' boom,
sun spinning at 180°/min, thermal torque included.

In Figure 33 the torsional component of the position of thermal equilibrium for the tip is plotted as a function of time. For the time span shown it is evident that after the initial thermal transient phase the curve shown repeats itself every two minutes (the time it takes the sun to complete one revolution about the perimeter).

The points labeled Ⓐ and Ⓑ on this curve are the points at which a phase reversal occurs. That is, between these two points the motion of the torsional component of the thermal equilibrium position is such that it acts as a destabilizing negative spring. It has been remarked herein that

70

small-angle theory predicts an instability for relative sun orientations that yield negative e_c Ehr $(\partial V/\partial\psi)$. A direct comparison between Figure 15 (curve A) and Figure 33 shows that the points Ⓐ and Ⓑ in the latter correspond to the points at which e_c Ehr $(\partial V/\partial\psi)$ equals zero in Figure 15 and that for the time spans between Ⓐ and Ⓑ the function is negative.

As previously mentioned, the existence of torsional motion induces changes in the position of thermal equilibrium which in turn can induce transverse vibrational motion. This effect is shown in Figures 34 through 37, in which the X_1 and Y_1 components of the actual position and thermal equilibrium position of the tip are plotted using the same horizontal scale as for Figure 32.

It is evident that a very small motion of the position of thermal equilibrium at the first natural bending frequency of the system can and does induce a significantly strong response. A similar type of response has been observed experimentally.

Although an easily grasped analogy between the phenomenon of thermal torque and some obvious everyday occurrence is not presently apparent, a heuristic discussion of this concept may prove useful for future investigation.

Whenever a non-uniform temperature distribution exists along the boom, the normal thermal stresses that produce pure bending are accompanied by shearing stresses that produce torsion. For most closed-section tubes of practical interest, the shearing stresses are too small to produce any noticeable twisting. For cylinders of open section, however, which are extremely weak in torsion, the effect of these shearing stresses can be quite significant.

Since the mathematically perfect boom has never been made, non-zero shearing stresses will always exist in booms exposed to direct sunlight. The boom attempts to relieve this state of stress not only by bending, but also by twisting, toward a position of thermal equilibrium. In a single-degree-of-freedom analogy of torsion, the net effect of the shearing stresses (or their resultant thermal torque) is to act as a thermal spring whose magnitude and sign are dependent upon sun orientation. For the regions of torsional instability, the thermal spring is negative.

It has been shown here that the inclusion of thermal torque in the analysis is necessary if a detailed description of the torsional response of the boom is desired. If one is interested only in whether or not transverse thermally-induced bending motion is stable, it has been found that the inclusion of thermal torque in the analysis of long booms (greater than 30') is merely a complicating factor that does not affect basic conclusions concerning the stability of transverse motion.

Figures 38 and 39 are included to illustrate this point. The oblique (time) axis is introduced, and the origin of the coordinate system in which tip deflection is measured is allowed to simply translate along the time axis at a constant rate without rotation of the coordinate system. The motion shown is only that of the actual position of the tip; neither the torsional response nor the position of thermal equilibrium toward which the boom is constantly moving is shown.

In Figure 38 the effect of thermal torque is included in the analysis; in Figure 39 the effect is deleted. The boom studied is assumed to be 30' long and to have nominal physical and geometric
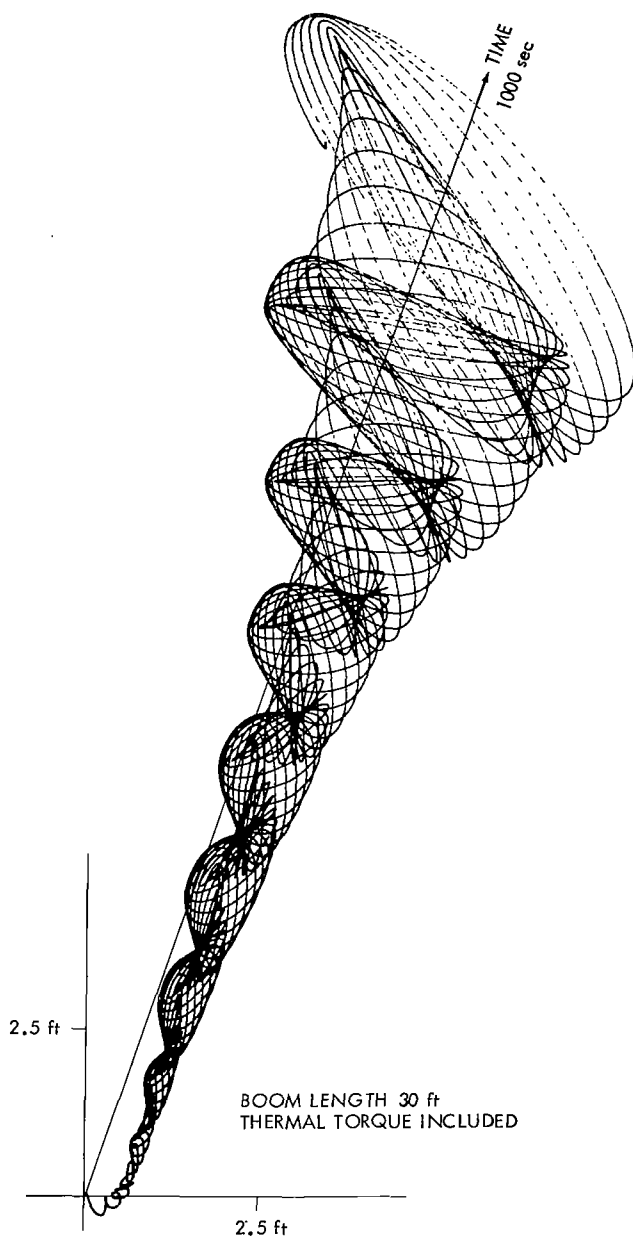
Figure 38—Tip motion of 30' boom for nominal parameters with thermal torque included when placed in direct sunlight at time zero.
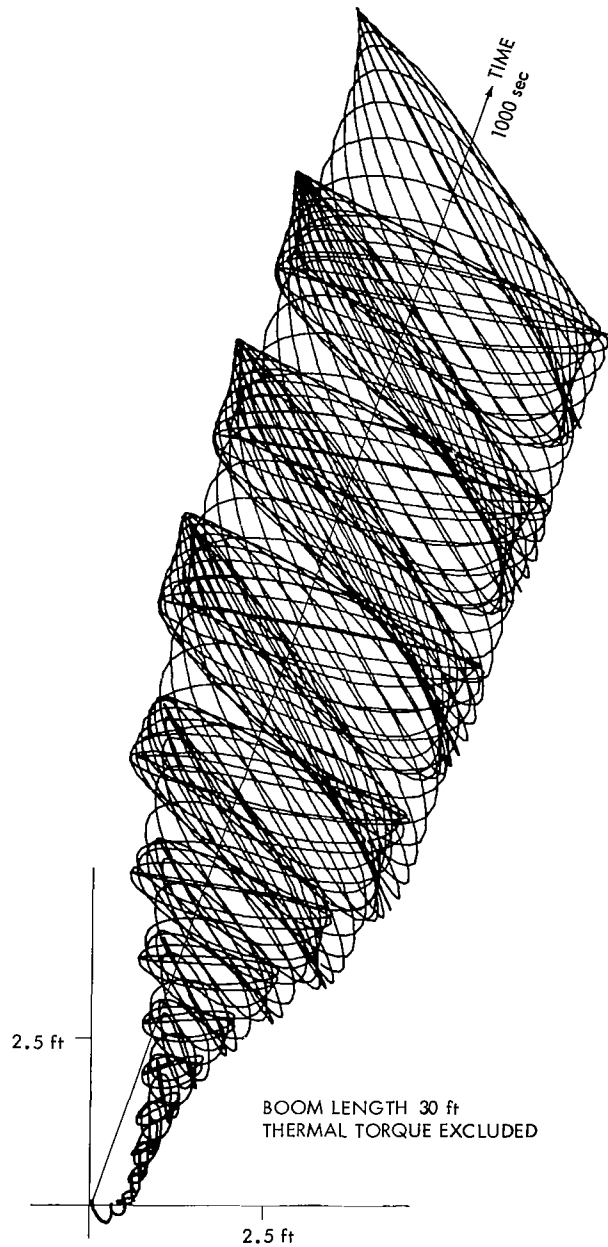

Figure 39—Tip motion of 30' boom for nominal parameters without thermal torque included when placed in direct sunlight at time zero.

characteristics. The sun is assumed to be fixed directly over the cross-sectional axis of symmetry of the clamped root (along the negative Y_1 axis). In both figures the resultant response is seen to be unstable. Although the actual time histories do differ from each other, it can be seen that basic conclusions remain unchanged.

From this example and several other computer runs (not shown) it has been concluded that for *long* booms the effect of thermal torque is simply a complicating factor and that the prime inducer of torsional motion is the dynamic coupling of non-planar bending motion into torsion.

By including only the dynamic coupling terms in the analysis, a practical answer to the stability question can be obtained. This is done in all succeeding runs, which show that with the effect of thermal torque deleted it is still possible to demonstrate that transverse thermally-induced vibrations can occur; and, furthermore, that the predicted amplitudes are reasonably close to those deducible from existing flight data.

Effect of Length

Figures 40, 41, and 42 illustrate the effect of a change in boom length by showing the computed dynamic response of a 60', 45', and 30' nominal boom respectively. For the time span shown, it is seen that each boom exhibits thermally-induced motion. The vibration amplitudes shown in Figures 40 and 42 are consistent with data obtained from the flights of the OGO IV and OGO V satellites: that is, the 60' boom on OGO IV is believed to oscillate with an amplitude of about ±20 feet, and the 30' booms on OGO V are believed to oscillate with an amplitude of about ±2 feet.

Besides showing this correlation between predicted and observed data, these three figures also illustrate the sensitivity of the thermally-induced response to changes in antenna length.

Effect of Transverse Damping

Figures 43, 44, and 45 show the effect of a change in the transverse damping ratio of the antenna. If this parameter could be easily controlled and significantly increased above its nominal value of 0.005, the amplitude of the thermally-induced vibration could be stabilized, or at least limited to an acceptable magnitude.

PEAK VIBRATION AMPLITUDE
±20 ft
BOOM LENGTH 60 ft

10 ft

10 ft
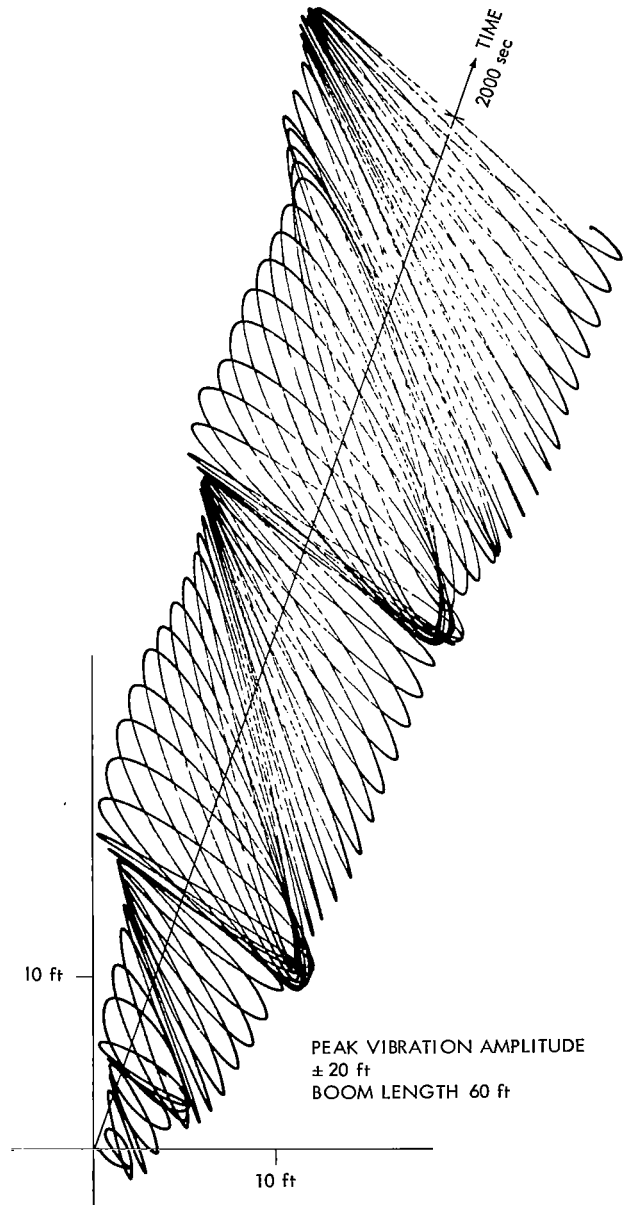
Figure 40—Tip motion of 60' boom on OGO IV when placed in direct sunlight at time zero.
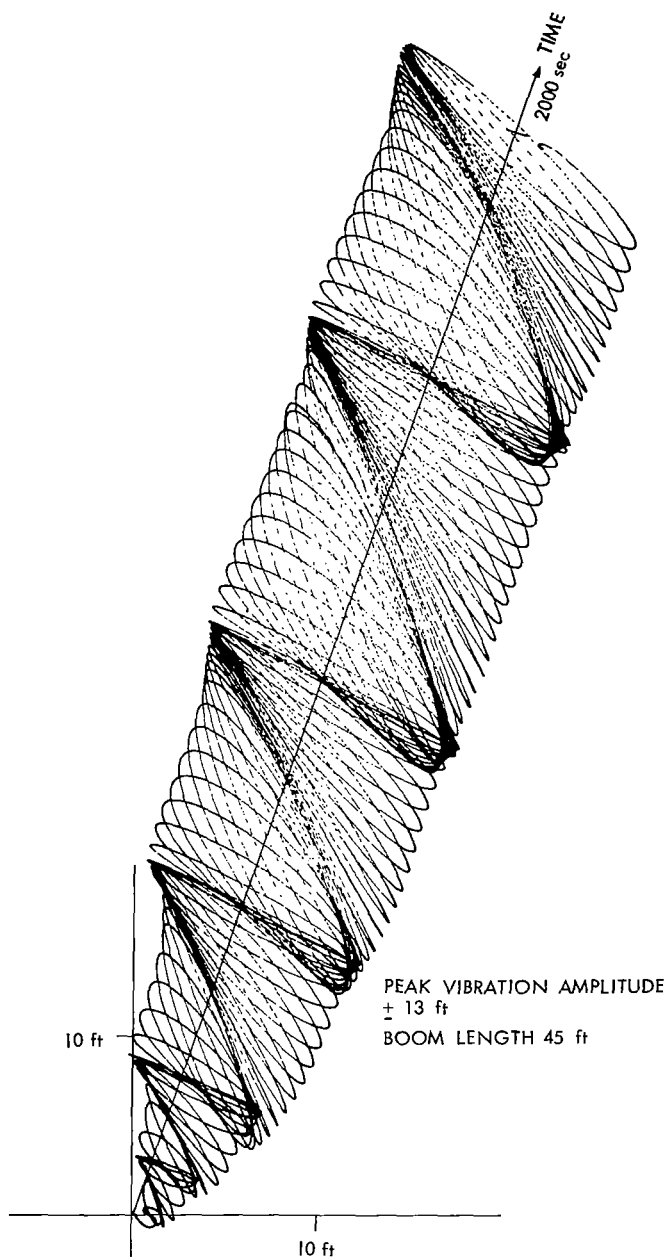
Figure 41—Tip motion of 45' boom for nominal
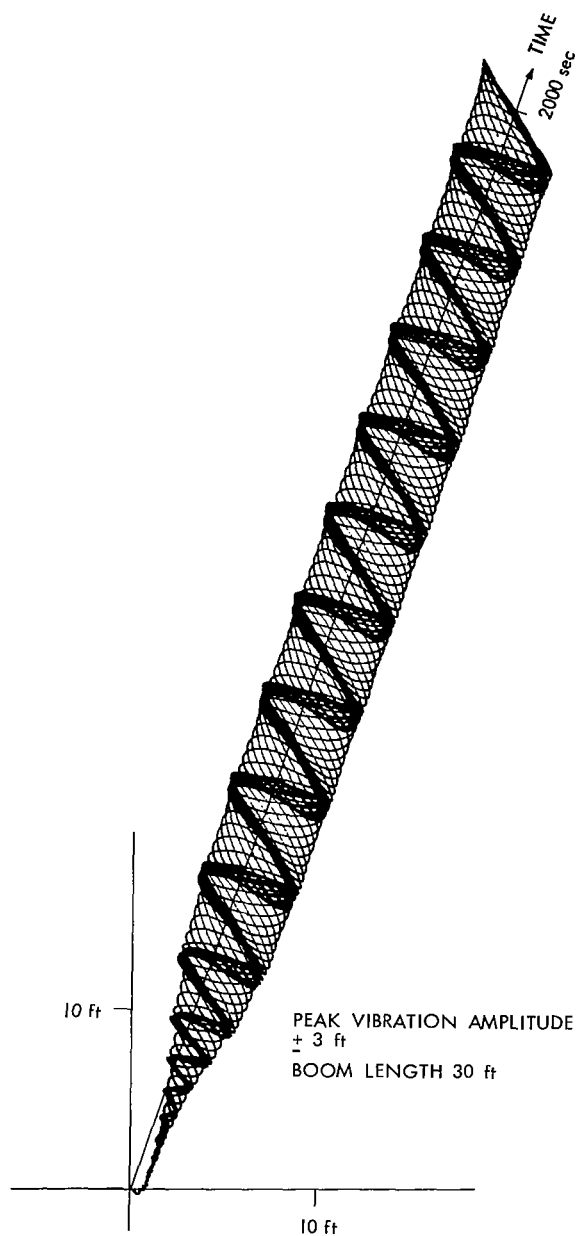parameters when placed in sunlight at time zero.

Figure 42—Tip motion of 30' boom on OGO V
when placed in direct sunlight at time zero.

Attempts have been made to increase the transverse damping characteristics of the antenna by coating the surface with thin viscoelastic laminae; however, the experimental work reported in Reference 10 shows that these attempts have been essentially unsuccessful.
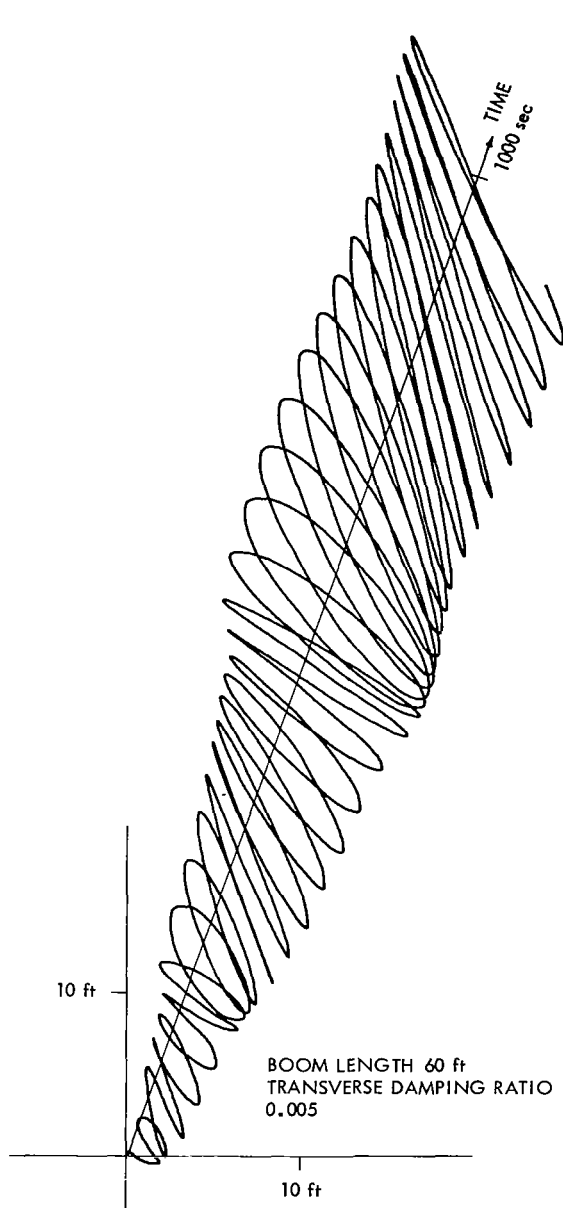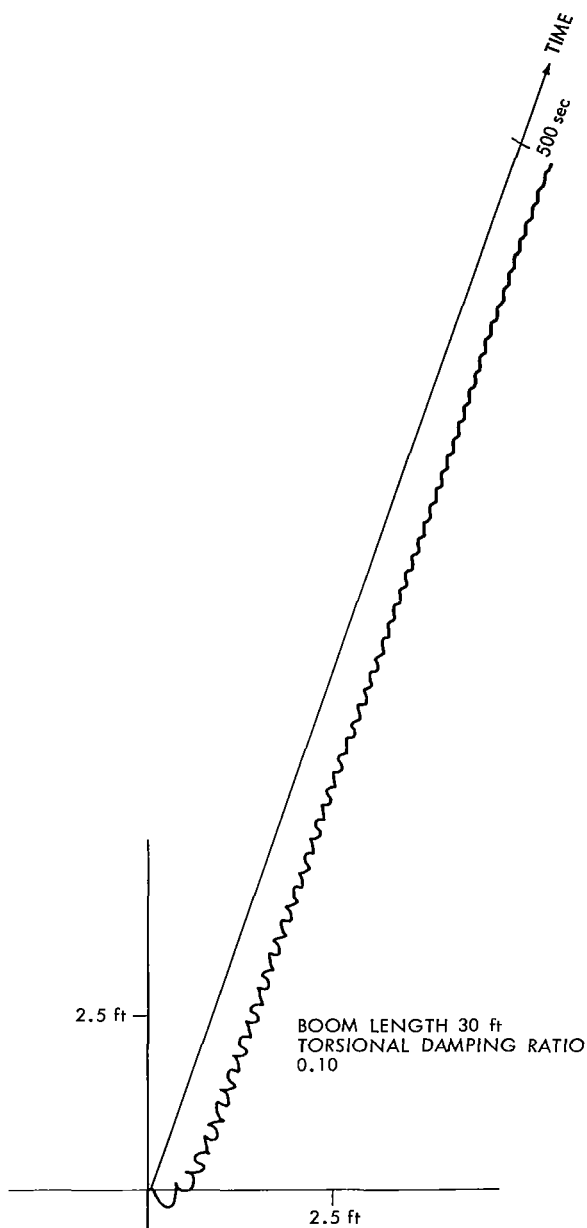
Figure 43—Tip motion of 60' boom for nominal parameters and transverse damping ratio .005 when placed in direct sunlight at time zero.
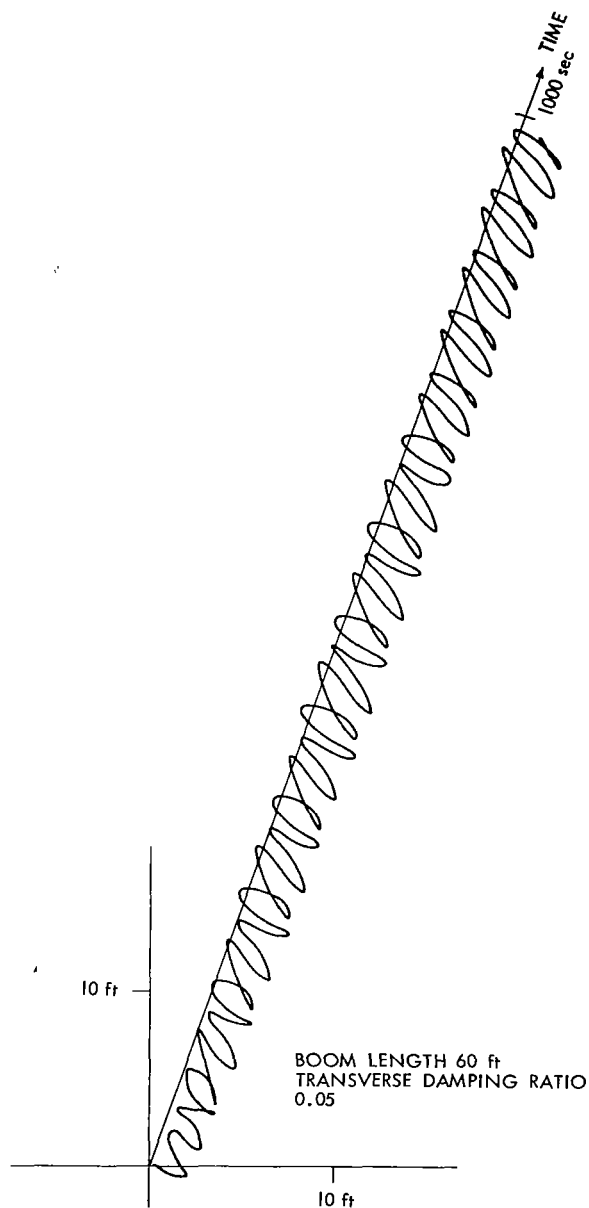
Figure 44—Tip motion of 60' boom for nominal parameters and transverse damping ratio .05 when placed in direct sunlight at time zero.

Effect of Torsional Damping

Figures 46, 47, and 48 illustrate the observation that, for large-amplitude thermally-induced transverse motion to exist, the antenna must respond torsionally at or near the first natural
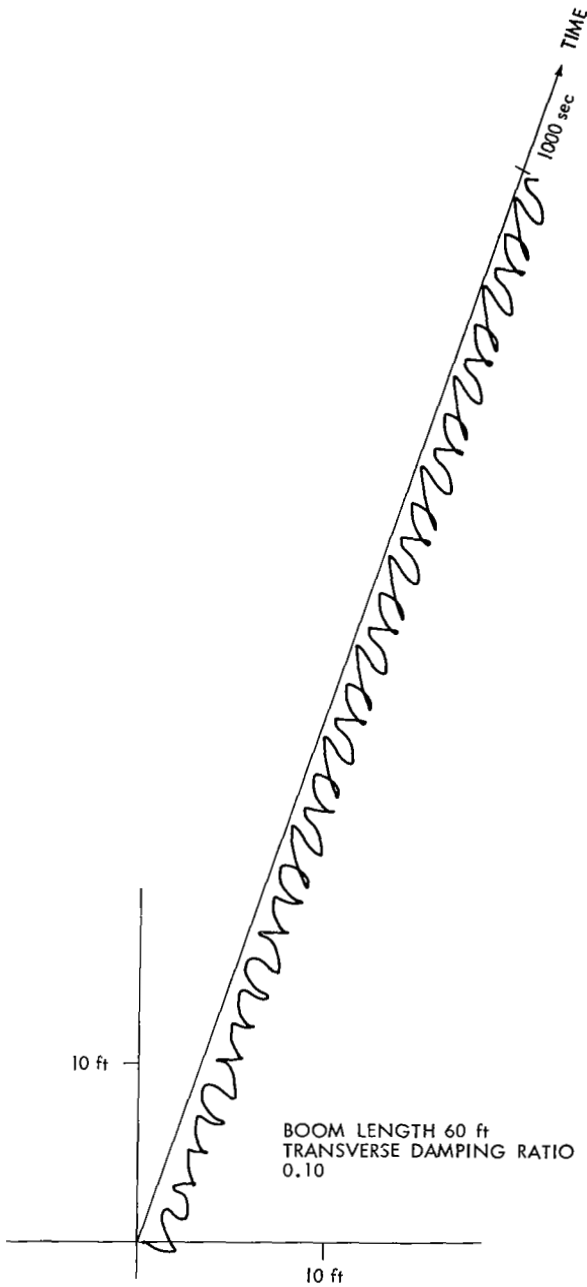
Figure 45—Tip motion of 60' boom for nominal param-
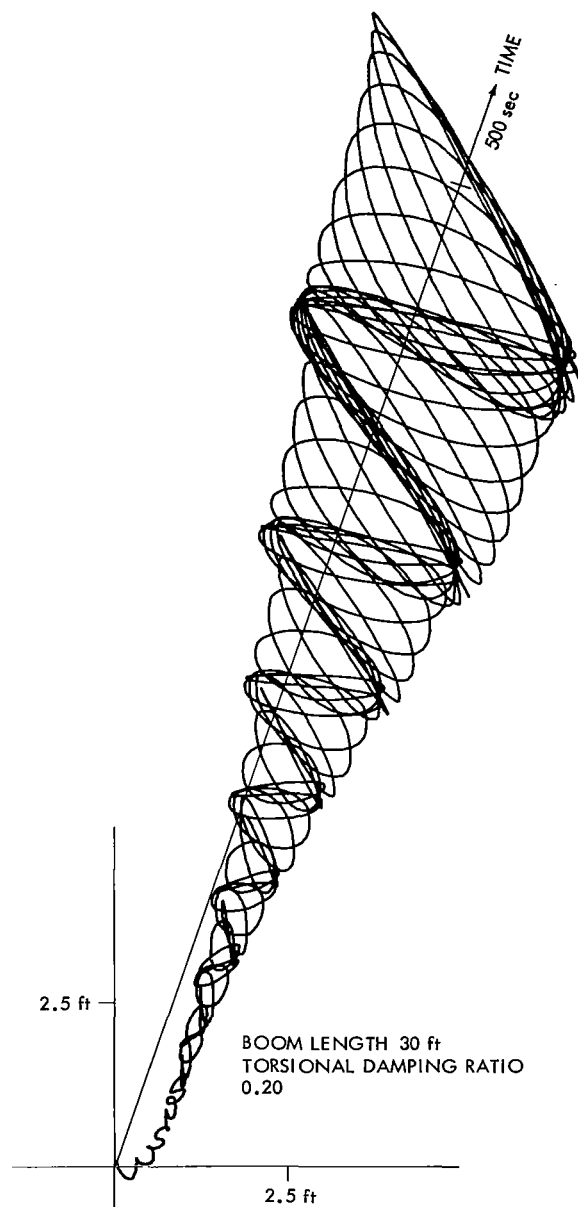eters and transverse damping ratio .10 when placed in
direct sunlight at time zero.
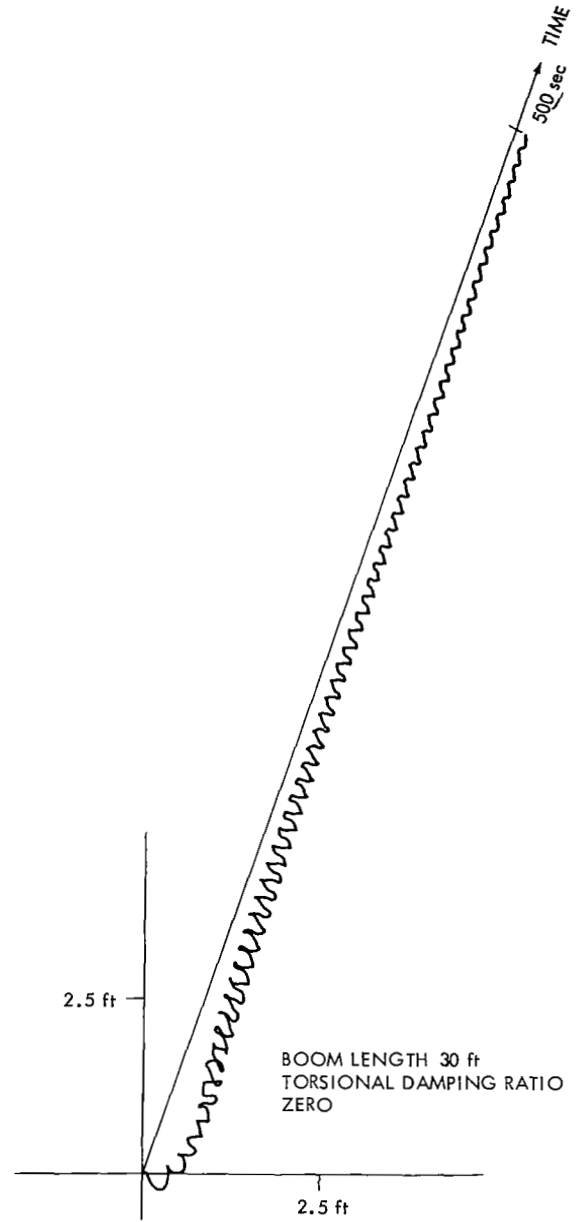
Figure 46—Tip motion of 30' boom for nominal param-
eters and torsional damping ratio zero when placed in
direct sunlight at time zero.

transverse bending frequency ω_{x_1}. This response in effect causes the position of thermal equilibrium to move at ω_{x_1}, and hence to drive the antenna at its resonant frequency.

Equation 216 shows that, with the effect of thermal torque deleted by setting $\gamma_n(t) = 0$, the tor-sional response depends upon the magnitude of the torsional damping ratio ζ_φ and upon the non-linear generalized force $C_n^*(t)$. The fact that $C_n^*(t)$ depends upon the actual position of the antenna and its

Figure 47—Tip motion of 30' boom for nominal param-
eters and torsional damping ratio .10 when placed in
direct sunlight at time zero.

Figure 48—Tip motion of 30' boom for nominal param-
eters and torsional damping ratio .20 when placed in
direct sunlight at time zero.

position of thermal equilibrium leads to results that are extremely complex. The judicious choice
of an example, however, can clearly illustrate the aforementioned observation. Accordingly, Fig-
ures 46, 47, and 48 show how the resultant response of a nominal 30' antenna differs for the tor-
sional damping ratios 0.0, 0.1, and 0.2 respectively.

In Figure 46, torsional damping is taken to be zero. From time zero, the torsional response shown in Figure 49 at the antenna tip gradually builds up at the first torsional frequency ω_{φ_1}. This has the dual effect of causing the position of thermal equilibrium (shown in Figures 50 and 51) to change at about ω_{φ_1} and of causing an averaging of the temperature distribution. Both effects are seen in Figures 50 and 51. Because the position of thermal equilibrium changes at the frequency ω_{φ_1}, the effective thermal loading acts as a high-frequency forcing function. This has only a slight
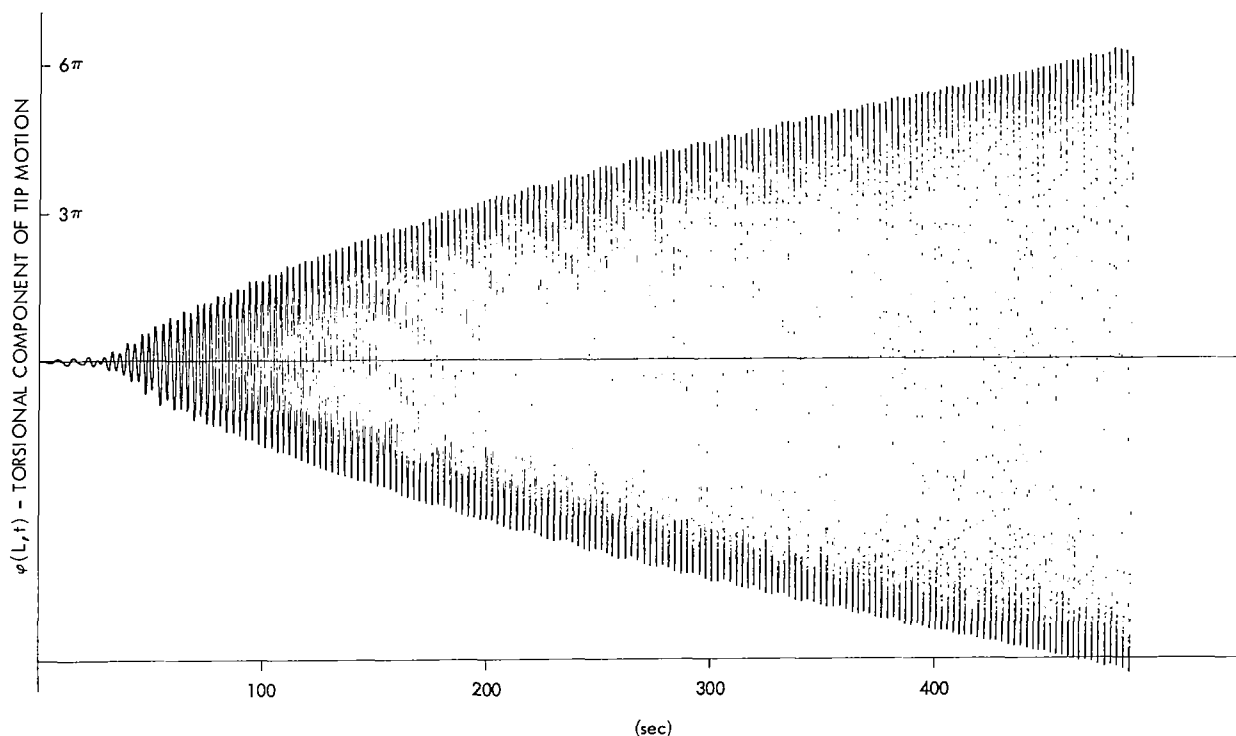
Figure 49—Torsional component of tip motion of the 30' boom studied in Figure 46.
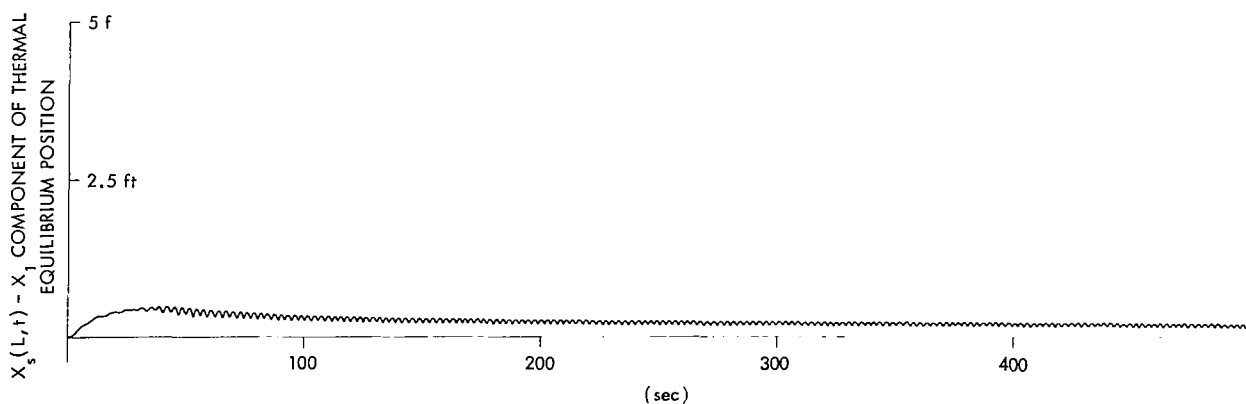
Figure 50—X_1 component of thermal equilibrium position of the 30' boom studied in Figure 46.

effect on the transverse motion, as shown in Figures 52 and 53, and does not excite unstable transverse oscillation. The effect of temperature averaging appears in that the curves shown are closer to the time axis after transient response, rather than during it.

In Figure 47, the torsional damping ratio ζ_φ is 0.1. Here the amplitude of the torsional response achieved during the initial thermal transients, shown in Figure 54, is seen to decay
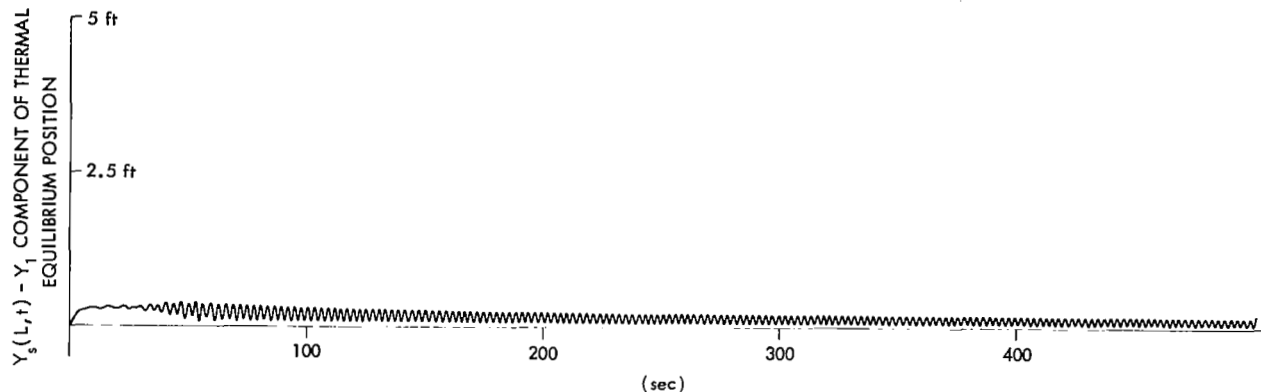

Figure 51—Y_1 component of the thermal equilibrium position of the 30' boom studied in Figure 46.
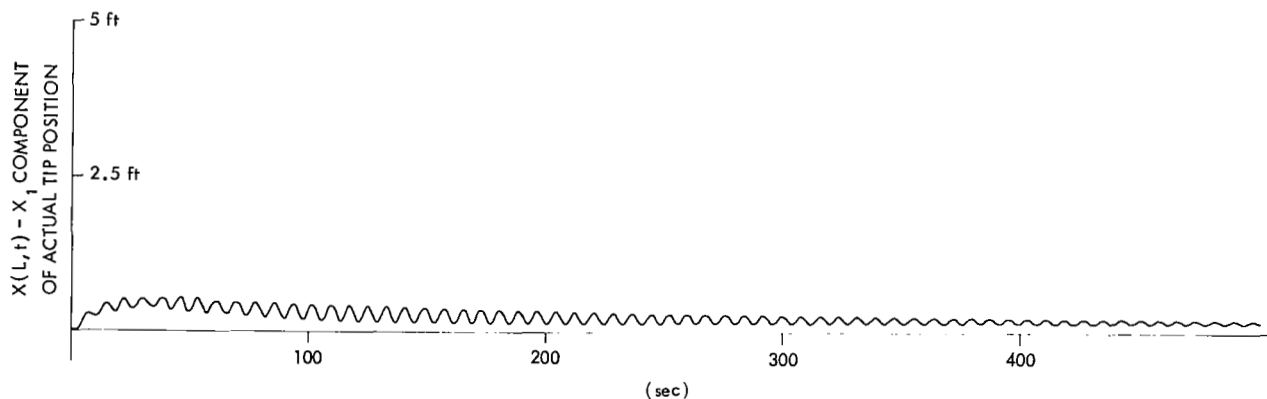

Figure 52—X_1 component of actual tip position of the 30' boom studied in Figure 46.
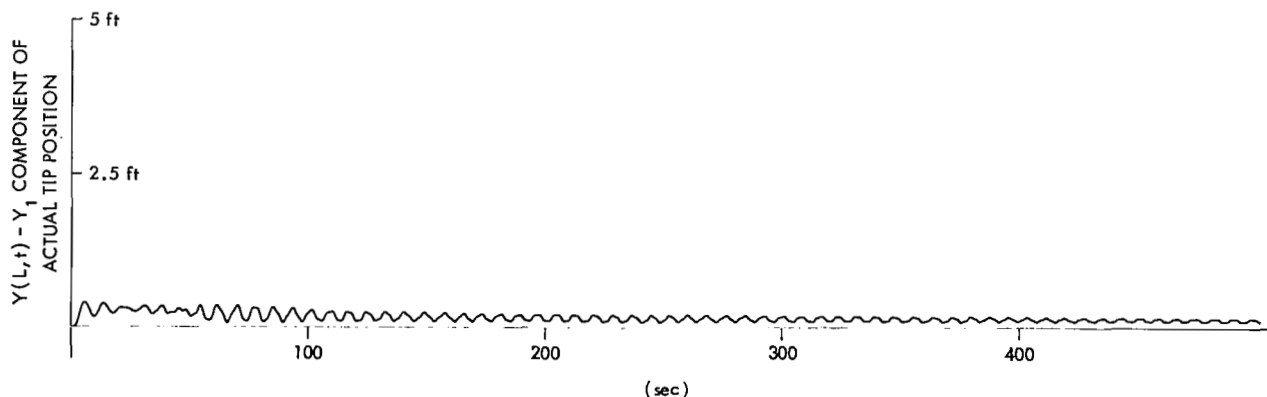

Figure 53—Y_1 component of actual tip position of the 30' boom studied in Figure 46.

79

gradually to zero at a non-resonant frequency. This decay causes the position of thermal equilibrium, shown in Figures 55 and 56, to change at a non-resonant frequency and gradually decay to the position of static thermal equilibrium. This change causes the transverse motion, shown in Figures 57 and 58, also to damp out to the displaced position of static thermal equilibrium.
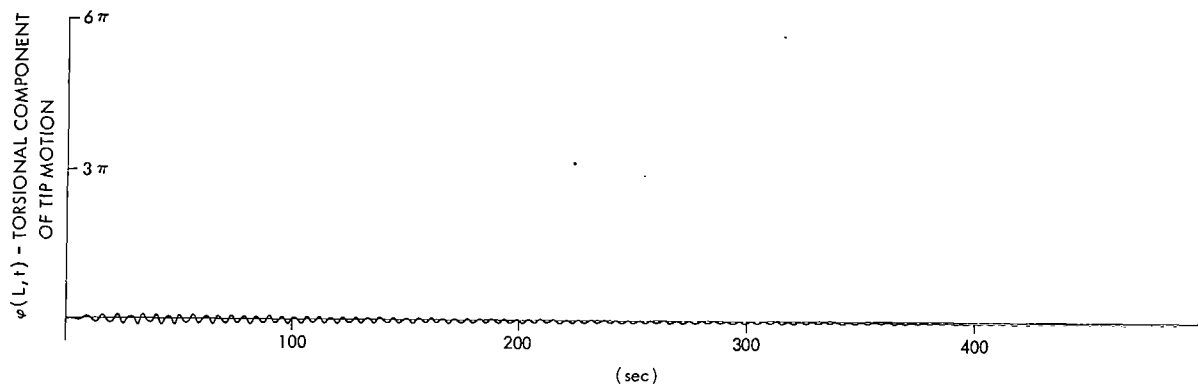
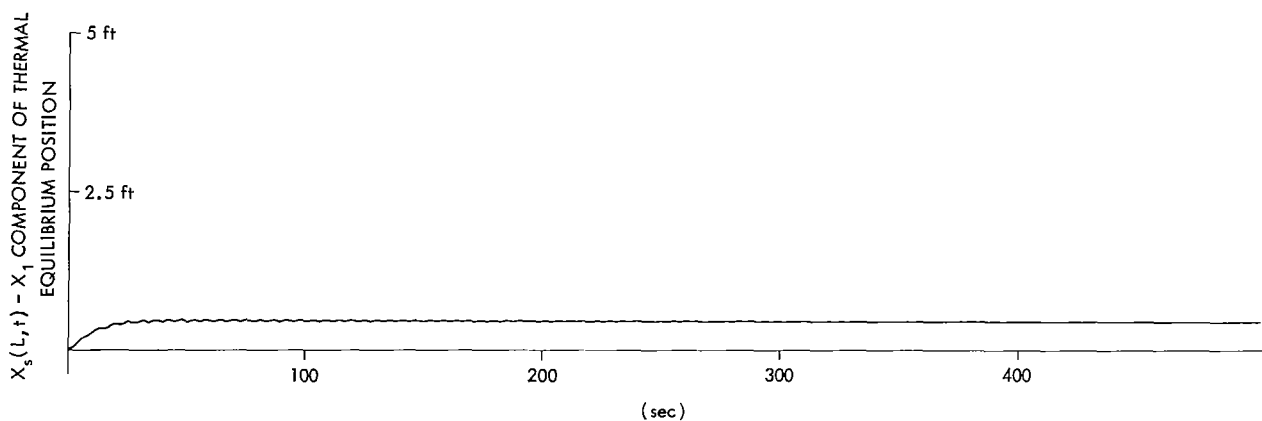Figure 54—Torsional component of tip motion of the 30' boom studied in Figure 47.

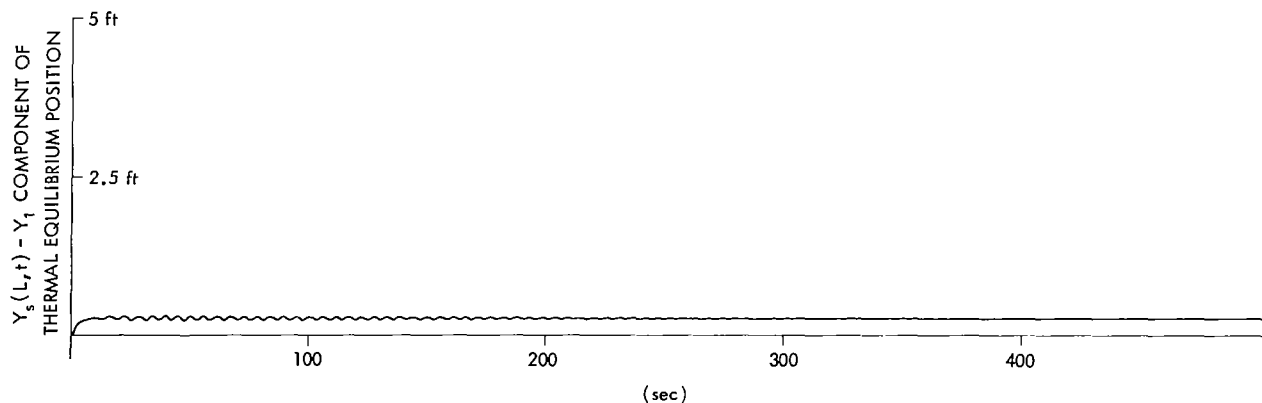Figure 55—X_1 component of thermal equilibrium position of the 30' boom studied in Figure 47.

Figure 56—Y_1 component of thermal equilibrium position of the 30' boom studied in Figure 47.
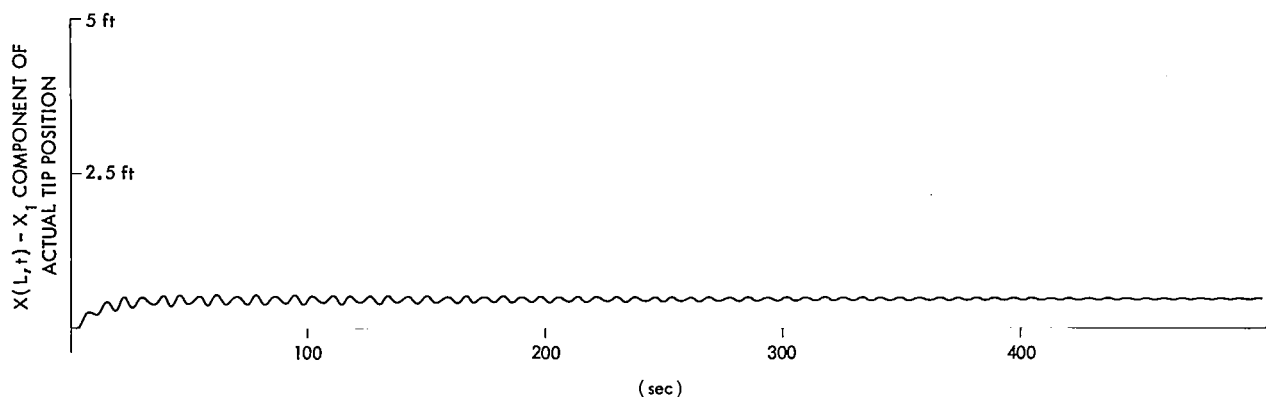
80

Figure 57—X_1 component of actual tip position of the 30' boom studied in Figure 47.
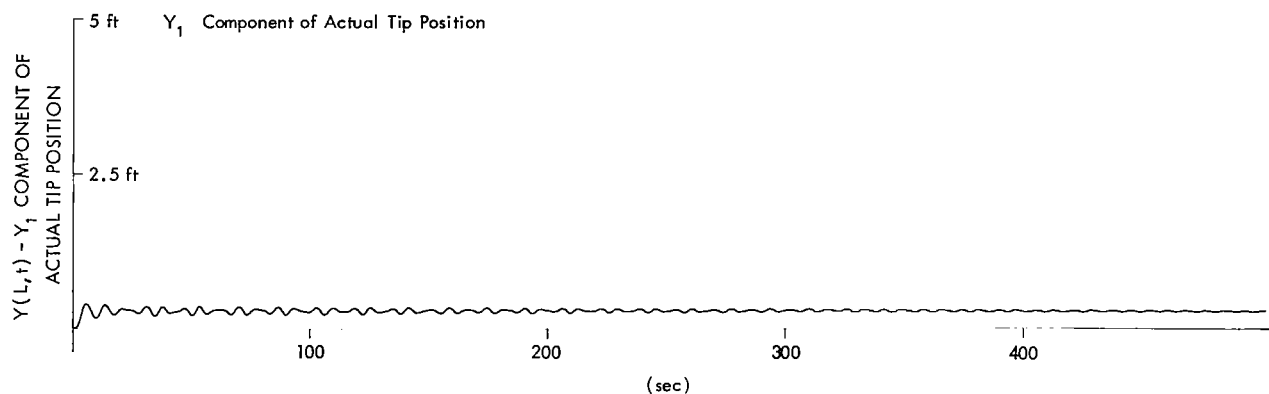

Figure 58—Y_1 component of actual tip position of the 30' boom studied in Figure 47.

In Figure 48, the torsional damping ratio ζ_φ is 0.2. Here the torsional response, shown in Figure 59, is found to increase gradually in amplitude, with a strong component at the first natural bending frequency ω_{x_1}. As the position of thermal equilibrium depends upon the torsional response, it too changes at about ω_{x_1}. This change is seen in Figures 60 and 61. The resultant effect is to drive the system at resonance and hence to excite the large-amplitude thermally-induced transverse motion shown in Figures 62 and 63.

Effect of Torsional Rigidity

Figures 64, 65 and 66 contain curves which indicate a practical means of designing a deployable antenna that will be stable in direct sunlight. The curves show the effect of varying the torsional rigidity of the antenna. Figure 64 shows the response of the nominal 60' antenna, which is obviously unstable; in Figure 65, the torsional rigidity is increased by a factor of 10, to 0.5 lb-in.^{2}. The slight increase in the response amplitude shows that, as the torsional response (not shown) has been reduced by a factor of nearly 10 in amplitude, the effect on temperature averaging of large-angle torsional motion has also been reduced, with a corresponding increase
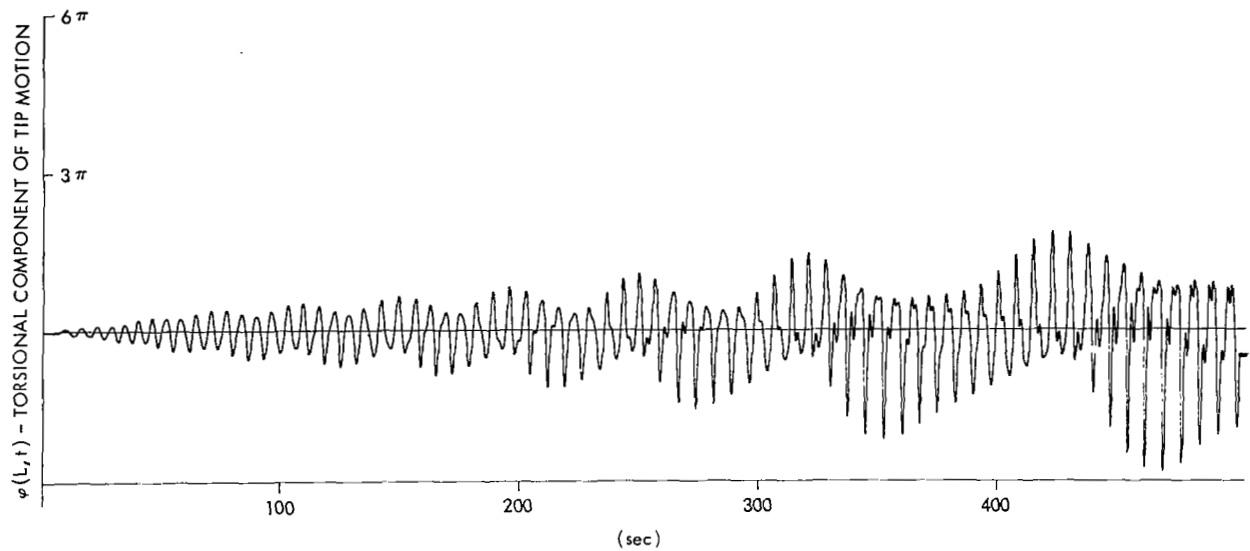
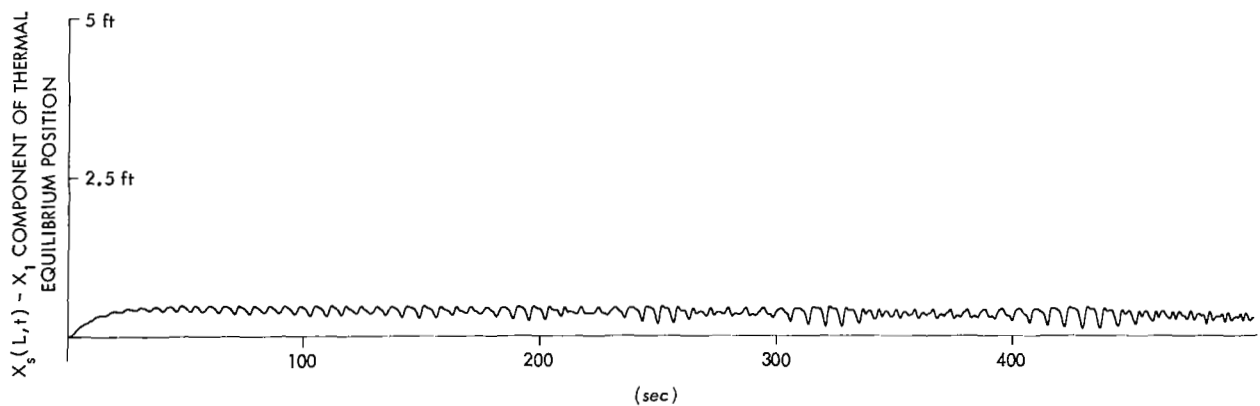Figure 59—Torsional component of tip motion of the 30' boom studied in Figure 48.

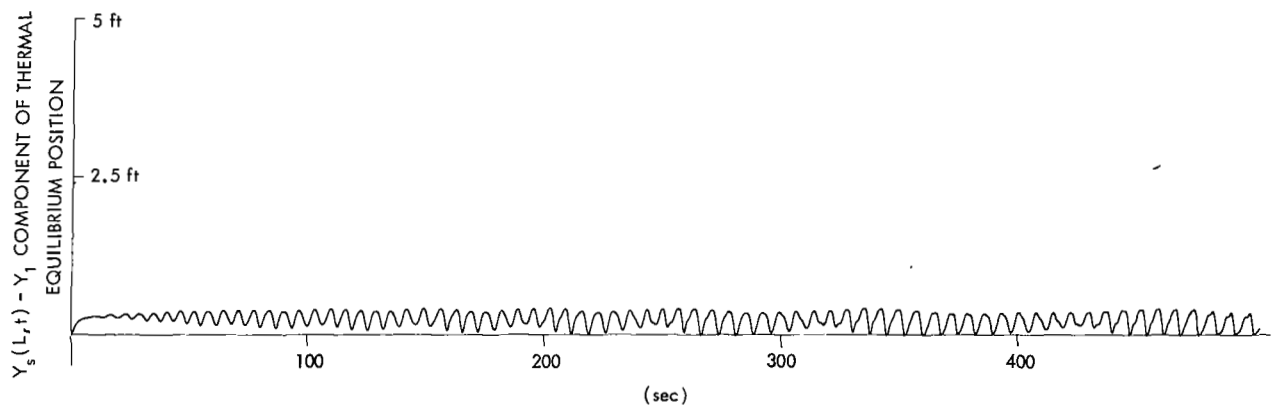Figure 60—X_1 component of thermal equilibrium position of the 30' boom studied in Figure 48.

Figure 61—Y_1 component of thermal equilibrium position of the 30' boom studied in Figure 48.
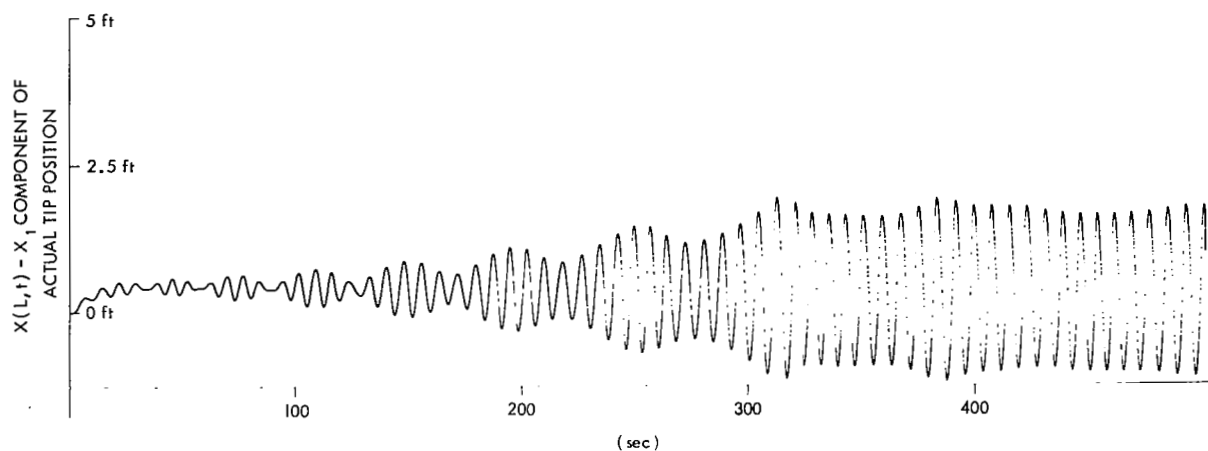
82

Figure 62—X_1 component of thermal equilibrium position of the 30' boom studied in Figure 48.
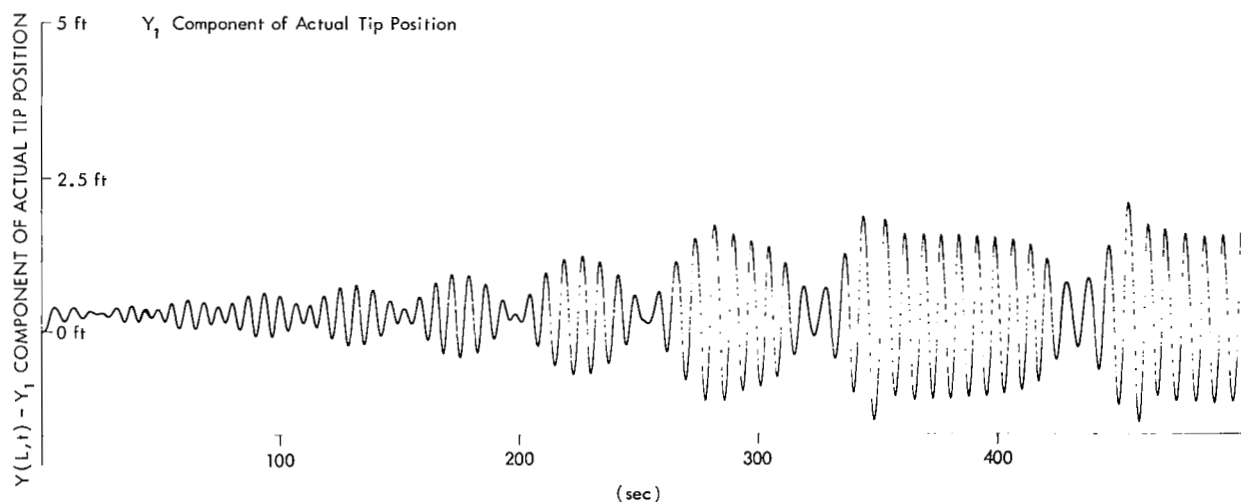
Figure 63—Y_1 component of actual tip position of the 30' boom studied in Figure 48.

in the effective thermal loading. In Figure 66, the torsional rigidity is increased above its nominal value by a factor of 15, to 0.75 lb-in.^{2}. Here the amplitude of the torsional motion has been reduced to the point where it no longer has an effect upon the position of thermal equilibrium. The resulting transverse motion, as shown, is stable.

Various manufacturers have used this idea and have submitted flight-quality antennas to NASA/GSFC for evaluation; all the antennas submitted have the seams of the open-section cylinder zippered in various ways. Each of these designs exhibits a torsional rigidity at least 1,500 times greater than that of the nominal model defined, and about 100 times greater than needed to achieve stability.

Figure 64—Tip motion of 60' boom for nominal parameters and torsional rigidity .05 lb-in.² when placed in direct sunlight at time zero.

Figure 65—Tip motion of 60' boom for nominal parameters and torsional rigidity .5 lb-in.² when placed in direct sunlight at time zero.

Both RAE (Radio Astronomy Explorer), launched September 1968 and OGO-VI (Orbiting Geophysical Observatory), launched June 1969, use the zippered-antenna concept. As predicted the four 750 foot long booms on RAE and the two 30 foot booms on OGO-VI are stable in and out of sunlight.

Applications to Particular Spacecraft

The original design specifications for several large spacecraft such as Nimbus, ATS, FR II, and AAP (Apollo Applications) have called for the use of long, torsionally weak thin-walled cylinders of open section, some with and some without tip weights. The digital program used to derive the figures previously presented has been used to study the thermal response of each of these proposed boom configurations. The results to be presented show that if these configurations were used a thermal instability could exist and seriously degrade the performance of the satellites. On the basis of these results, NASA has initiated a design change that will call for the use of zippered-type booms on each of the aforementioned satellites.

The parameters (listed in Table 3, earlier) that define the boom used on OGO IV can be used to define the proposed booms on FR II, ATS, and AAP except for boom length and tip weight.

For the French satellite, FR II, a 32' boom had been proposed with a tip weight weighing 6 lb and having a moment of inertia of .00258 slug-ft^2. The predicted response is shown in Figure 67. The predicted motion is unstable.

An indication of the effect of introducing a tip weight into the system can be seen by comparing this result with that shown in Figure 42. Both booms are of approximately the same length; however, one has a tip weight, and the other does not. It appears that the addition of a tip weight contributes to the instability of the system.
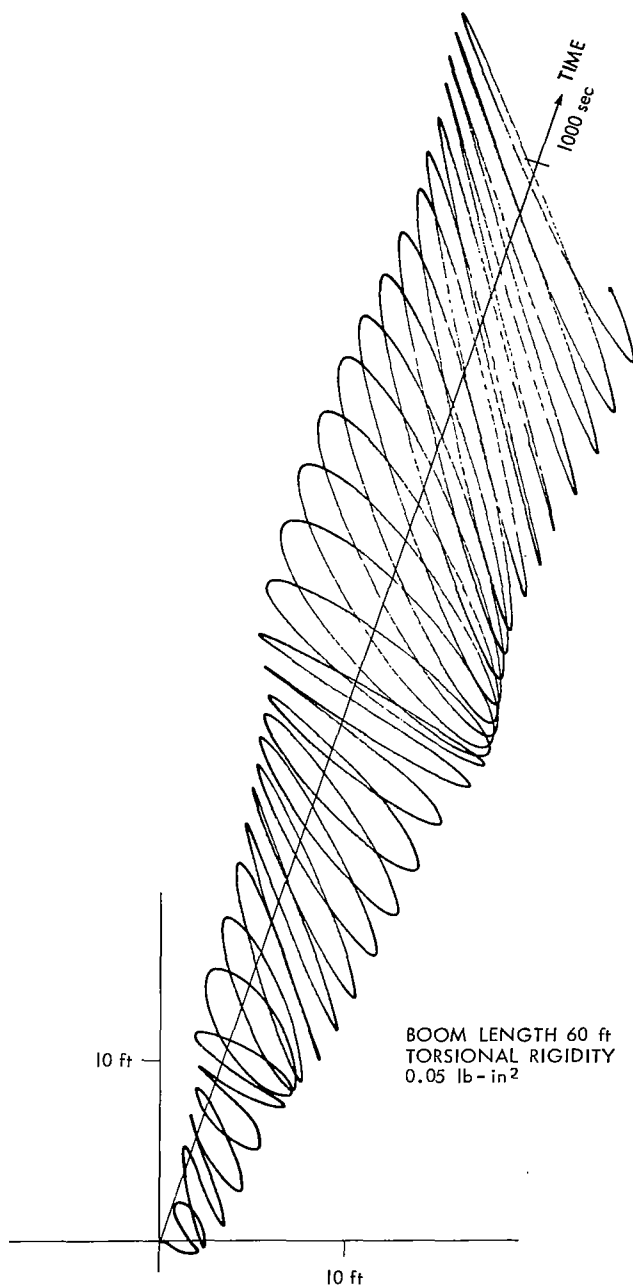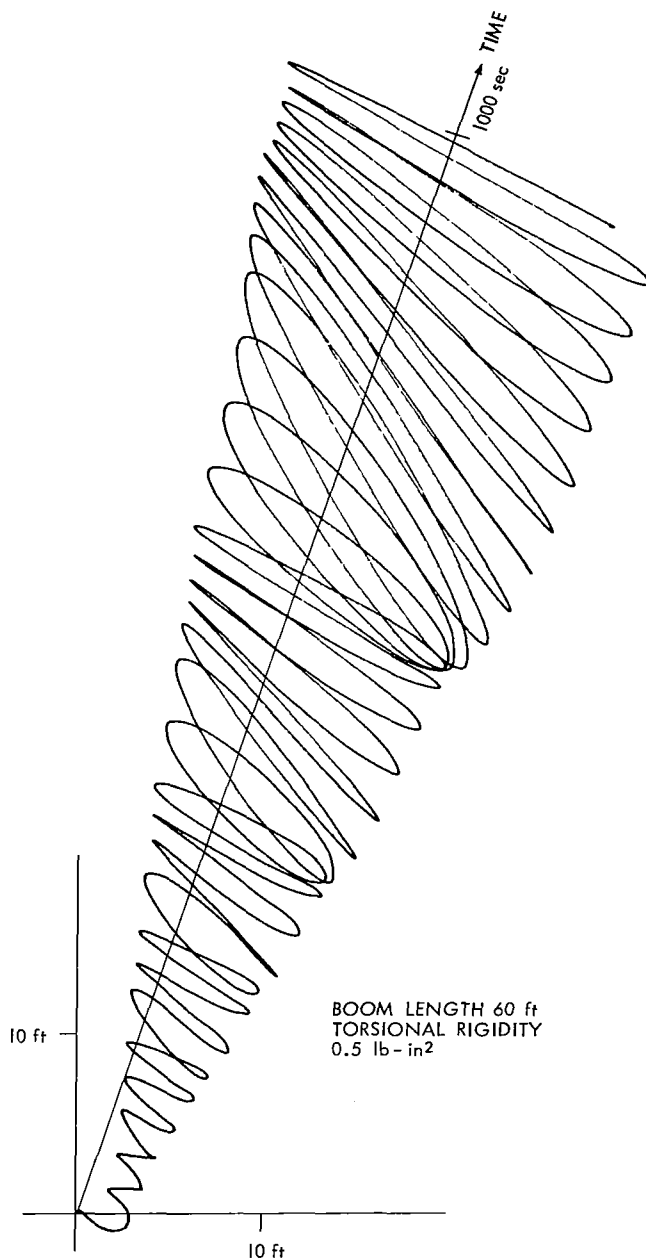

Figure 66—Tip motion of 60' boom for nominal parameters and torsional rigidity .75 lb-in.^{2} when placed in direct sunlight at time zero.

The proposed boom for ATS was 123.5' long and had a tip weight weighing 8 lb with a moment of inertia of about .00266 slug ft^2. The predicted response is shown in Figure 68. The predicted motion is unstable.

The proposed boom for an AAP experiment was 120' without tip weight. Again the predicted motion (shown in Figure 69) is unstable. The influence of tip weight on response characteristics can be seen by comparing Figures 68 and 69.

Figure 67—Tip motion of 32' boom with 6-lb tip weight originally proposed for use on French satellite FR II.
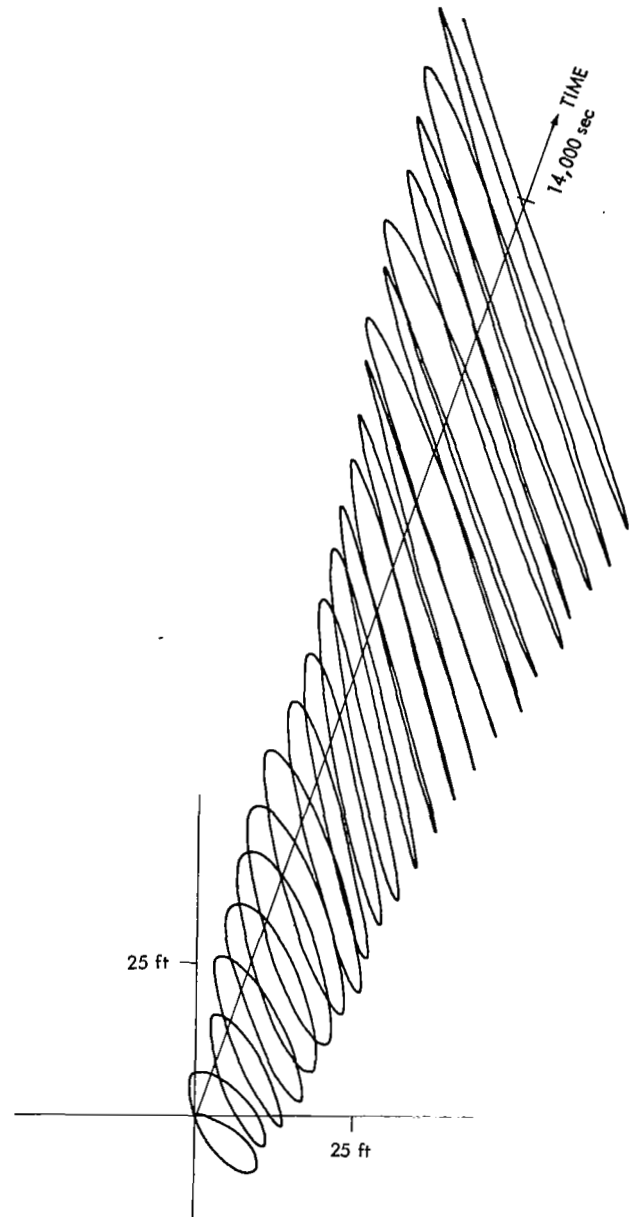
Figure 68—Tip motion of 123.5' boom with 8-lb tip weight originally proposed for use on ATS.

The originally proposed boom for Nimbus differed significantly from that described in Table 3. Its deployment mechanism was designed so that the length of the boom could be changed by ground command. Preliminary studies indicated that lengths of 25', 35', and 45' would be used during flight; the stability of motion at each length was of interest. A list of the nominal parameters used
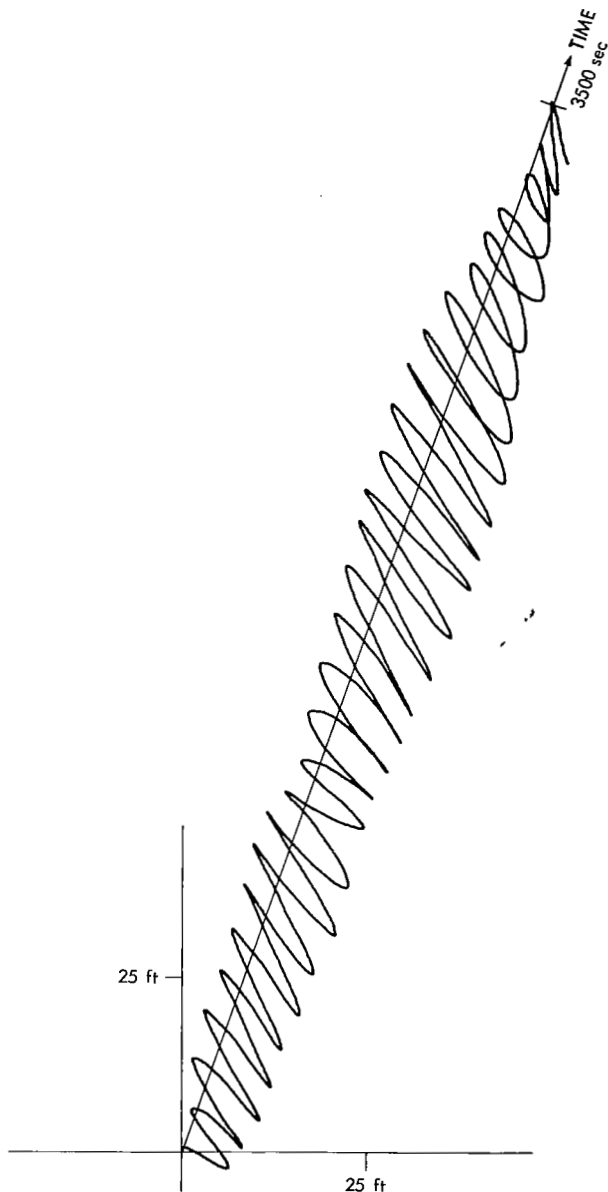
Figure 69—Tip motion of 120' boom with zero tip weight originally proposed for use on an Apollo Applications experiment.

Table 4

Antenna material	= polished beryllium copper
Antenna length	= L = 45, 35, 25 ft
Perimeter of cross-section	= P = 3.5 in.
Total overlap angle	= ϕ = 155 deg
Wall thickness	= h = .004 in.
Weight density of material	= ρ = .2714 lb/in.^{3}
Tip weight	= W_T = 10 lb
Tip inertia	= I_T = .002 slug ft^2
Bending stiffness	= EI = 133.4 lb ft^2
Damping ratio for torsion	= ζ_φ = .1
Damping ratio for bending	= ζ_x = .005
Torsional rigidity	= C_T = .7162 lb-in.^{2}
Warping rigidity	= C_w = 3.546 × 10^4 lb-in.^{4}
Thermal conductivity	= K_T = 4.167 Btu/(hr-in.-°F)
Specific heat	= c = .1 Btu/(lb-°F)
Thermal expansion coefficient	= e_c = .104× 10^{-4} in./(in.-°F)
Emissivity	= ϵ = .06
Absorptivity	= a_s = .35

to define the Nimbus boom is given in Table 4. The resultant response of the 25', 35', and 45' booms is shown in Figures 70, 71, and 72.

From these figures (70 through 72) it is evident that a boom which is significantly different in diameter, thickness, and absorptivity exhibits the same thermally-induced instability. It is recommended, therefore, that any thin-walled cylinder of open section be analyzed before it is used on an actual spacecraft.
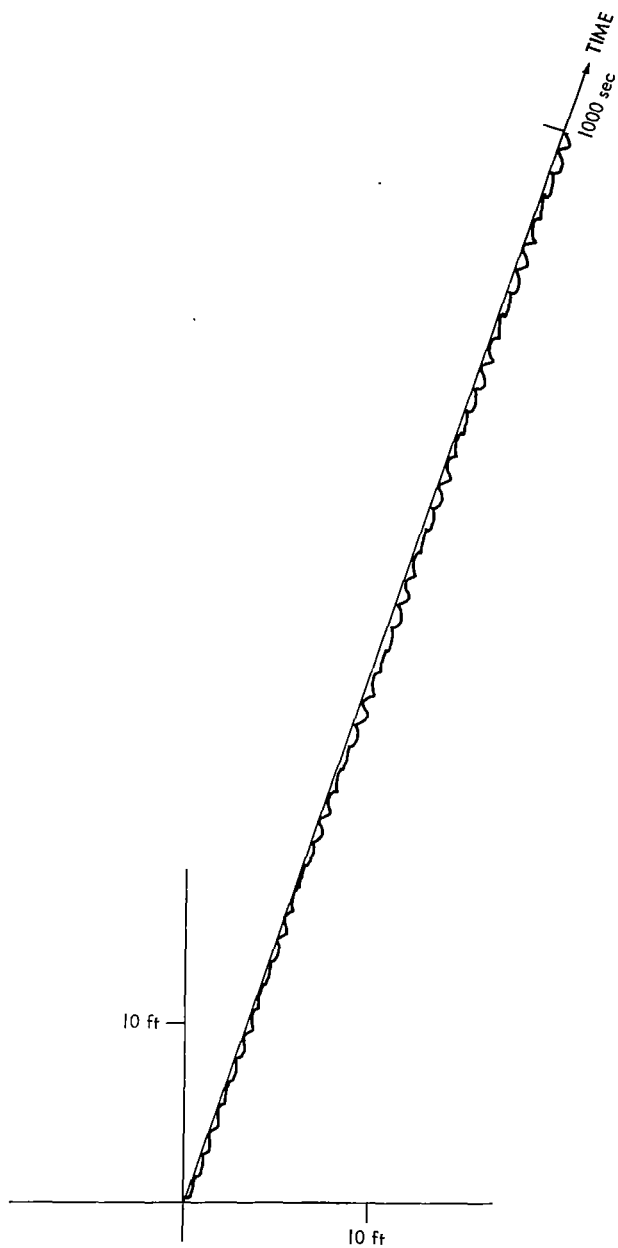
Figure 70—Tip motion of originally proposed 25' Nimbus boom with 10-lb tip weight.
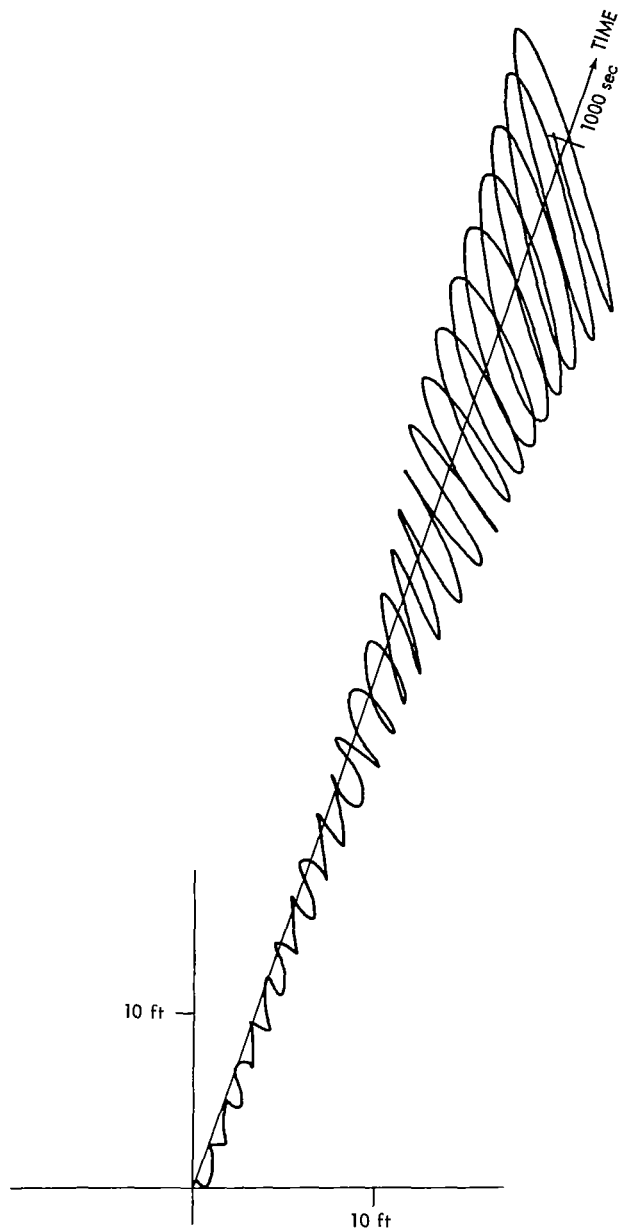
Figure 71—Tip motion of originally proposed 35' Nimbus boom with 10-lb tip weight.

CONCLUSIONS

Most three-axis stabilized satellites deploying long booms have been plagued with varying degrees of anomalous spacecraft body motion. This motion, at times, is solely low frequency (i.e., near orbital), but in several instances, when the booms used are thin walled cylinders of open section, the motion is high frequency (i.e., near the fundamental beam frequency). With regard to the anomalous low frequency motion, there is a growing suspicion that the cause is a nonlinear resonance which allows exchange of energy between roll, pitch, and yaw motion. Since the boom studied in this report is, by definition, rigidly clamped in inertial space, the conclusions reached cannot be directly applied to the low frequency phenomenon. With regard to the high frequency phenomenon, the following conclusions can be drawn:

1. The theory of thermally-induced vibration presented here can be used to explain the anomalous spacecraft-body motion observed on many three-axis-stabilized satellites deploying long, torsionally weak thin-walled cylinders of open section in direct sunlight.

2. The problem of designing a thermally stable deployable antenna can be solved by zippering the seam of the open-section boom so as to increase its torsional rigidity by several orders of magnitude.

3. Any satellite that requires long appendages and geometric stability should not use torsionally weak thin-walled cylinders of open section.

ACKNOWLEDGMENTS
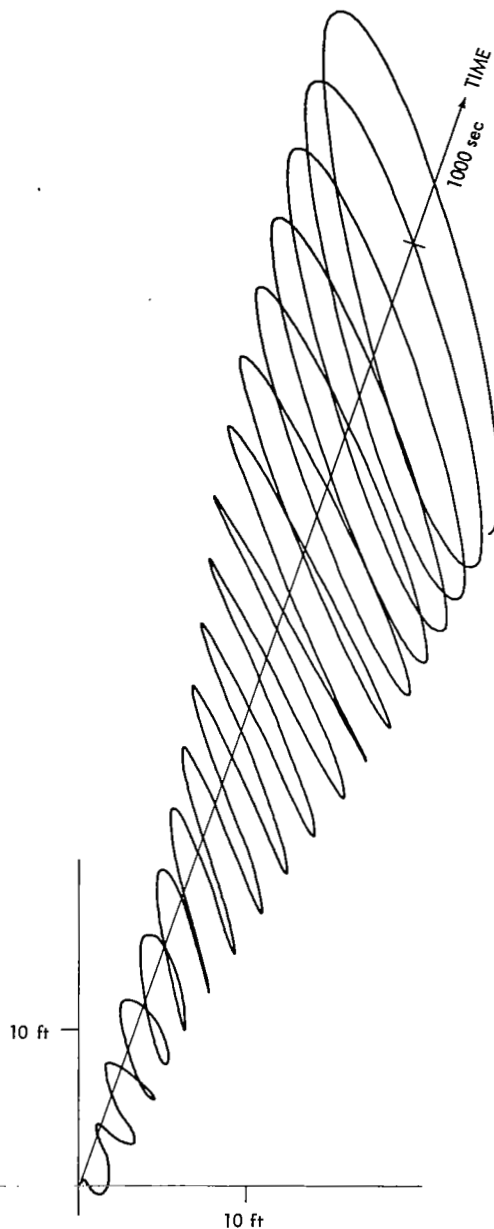
Figure 72—Tip motion of originally proposed 45' Nimbus boom with 10-lb tip weight.

REFERENCES

1. Frisch, H. P., "Thermal Bending Plus Twist of a Thin-Walled Cylinder of Open Section with Application to Gravity Gradient Booms," NASA Technical Note D-4069, August 1967.

2. Boley, B. A., and Weiner, J. H., "Theory of Thermal Stresses," New York: John Wiley and Sons, Inc., 1960.

3. Timoshenko, S. P., "Theory of Bending, Torsion and Buckling of Thin-Walled Members of Open Cross Section, *Journal of the Franklin Institute* 239(3, 4):201-219, 249-268, 1945.

4. Timoshenko, S. P., "Strength of Materials," Third Ed., Part II, Princeton, N. J.: D. Van Nostrand Company, Inc., 1956.

5. Landau, L. D., and Lifshitz, E. M., "Theory of Elasticity," Reading, Mass.: Addison-Wesley Publishing Company, Inc., 1959.

6. Love, A. E. H., "A Treatise on the Mathematical Theory of Elasticity," New York: Dover Publications, 1944.

7. Carslaw, H. S., and Jaeger, J. C., "Conduction of Heat in Solids," Oxford: Clarendon Press, 1959.

8. Florio, F. A., and Hobbs, R. B., Jr., An Analytical Representation of Temperature Distributions in Gravity Gradient Rods," *AIAA Journal* 6(1):99-102, January 1968.

9. Symposium on Gravity Gradient Attitude Control, Aerospace Corporation, El Segundo, Calif., December 3-5, 1968:

   (a) Donohue, J. H., and Frisch, H. P., "Thermoelastic Instability of Open Section Booms."

   (b) Foulke, H., "Effect of Thermal Flutter on Gravity Gradient Stabilized Spacecraft."

   (c) Koval, L. R., Mueller, M. R., and Paroczai, A. J., "Solar Flutter of a Thin-Walled Open Section Boom."

   (d) Raymond, F. W., Wilhelm, P. G., and Beal, R. T., "Gravity Gradient Flight Experience Acquired with the Naval Research Lab Satellites."

10. Predmore, R. E., Staugaitis, C. L., and Jellison, J. E., "Damping Behavior of De Havilland STEM Booms," NASA Technical Note D-3996, June 19, 1967.

11. Mindlin, R. D., and Goodman, L. E., "Beam Vibrations with Time-Dependent Boundary Conditions," *Journal of Applied Mechanics* 17(4):377-380, December 1950.

12. Jordan, P. F., "Observations on the Mechanism of Thermal Torque Instability," ASME/AIAA 10th Structures, Structural Dynamics, and Materials Conference, New Orleans, La., pp. 375-382, April 14-16, 1969.

13. Beam, R. M., "On the Phenomenon of Thermoelastic Instability (Thermal Flutter) of Booms with Open Cross Section," NASA Technical Note D-5222, June 1969.

BIBLIOGRAPHY

Merrick, R. M., "Instability of Slender Thin-Walled Booms Due to Thermally Induced Bending Moments," NASA Technical Note TN D-5774, April 1970.

The above document by Merrick, being published concurrently with this one, contains a linearized dynamic stability analysis of the long slender booms studied in this report. To assess the relative importances of various boom system parameters, Merrick takes a more traditional engineering approach by drastically simplifying the model of the phenomenon to the point where only the most important factors are retained. A stability analysis is then performed on the linearized equations. The conclusions reached by Merrick are in agreement with those presented herein.

Appendix A

Thermal Bending Moment Components and Thermal Torque

The derivations presented in this appendix are a brief summary of those given in more detail in Reference 1.

The thermoelastic equation for longitudinal thermal stress at a point (s, z) at time t on the surface of the boom is

$$\sigma_z(s, z, t) = E\left\{\epsilon_z(s, z, t) - e_c\left[\tilde{T}(s, z, t) - \tilde{T}_A\right]\right\}, \tag{A1}$$

where

$$\sigma_z(s, z, t) = \text{longitudinal thermal stress,}$$
$$\epsilon_z(s, z, t) = \text{longitudinal thermal strain,}$$
$$e_c = \text{thermal expansion coefficient,}$$
$$\tilde{T}(s, z, t) = \text{absolute temperature,}$$
$$\tilde{T}_A = \text{absolute ambient temperature,}$$
$$E = \text{Young's modulus of elasticity.}$$

The longitudinal thermal strain of any fiber passing through an arbitrary cross-section along the boom can be adequately described by

$$\epsilon_z(s, z, t) = f_0(z, t) + x_c(s) f_1(z, t) + y_c(s) f_2(z, t), \tag{A2}$$

where

$$x_c(s) = \text{X-coordinate of point } s \text{ on cross-section,}$$
$$y_c(s) = \text{Y-coordinate of point } s \text{ on cross-section,}$$
$$f_0(z, t), f_1(z, t), f_2(z, t) = \text{functions that are obtainable from the equilibrium conditions.}$$

The equilibrium conditions require that the resultant force and moments about the principal axes of the cross-section vanish; that is,

$$\int_0^P h\sigma_z(s, z, t)\,ds = \int_0^P h\sigma_z(s, z, t)\,y_c(s)\,ds = \int_0^P h\sigma_z(s, z, t)\,x_c(s)\,ds = 0. \tag{A3}$$

It follows from the determination of the three functions $f_0(z, t)$, $f_1(z, t)$, and $f_2(z, t)$ that the longitudinal thermal stress is

$$\sigma_z(s, z, t) = Ee_c\left[\tilde{T}_m(z, t) - \tilde{T}(s, z, t)\right] - \frac{BM_y(z, t)}{I_y} x_c(s) + \frac{BM_x(z, t)}{I_x} y_c(s) . \tag{A4}$$

where

$$I_x = \int_0^P hy_c^2(s)\, ds , \tag{A5}$$

$$I_y = \int_0^P hx_c^2(s)\, ds , \tag{A6}$$

$$\tilde{T}_m(z, t) = \frac{1}{P}\int_0^P \tilde{T}(s, z, t)\, ds , \tag{A7}$$

$$BM_x(z, t) = e_c Eh \int_0^P \tilde{T}(s, z, t)\, y_c(s)\, ds , \tag{A8}$$

$$BM_y(z, t) = -e_c Eh \int_0^P \tilde{T}(s, z, t)\, x_c(s)\, ds . \tag{A9}$$

The quantities $BM_x(z, t)$ and $BM_y(z, t)$ are the thermal bending moment components about the X and Y principal axes of inertia, respectively, of the cross-section at (z, t).

For thin-walled members of open section, the shear stress $\tau(s, z, t)$ is related to the longitudinal stress $\sigma_z(s, z, t)$ by the partial differential equation

$$\frac{\partial h\tau(s, z, t)}{\partial s} = -h \frac{\partial \sigma_z(s, z, t)}{\partial z} . \tag{A10}$$

Substituting Equation A4 along with the geometric identities

$$x_c(s) = -r \sin\left(\frac{s}{r} - \frac{\phi}{2}\right) \tag{A11}$$

$$y_c(s) = -r \cos\left(\frac{s}{r} - \frac{\phi}{2}\right) + \frac{r \sin\frac{\phi}{2}}{\pi + \frac{\phi}{2}} \tag{A12}$$

94

into Equation A10, applying the chain rule of differential calculus to eliminate differentiating the temperature distribution with respect to z, and integrating both sides of the equation from 0 to s yield the expression that defines the shear stress distribution. That is,

$$h\tau(s, z, t) = -h\left\{Ee_c\left[s\frac{\partial\tilde{T}_m(z, t)}{\partial\psi(z, t)} - \int_0^s\frac{\partial\tilde{T}(s, z, t)}{\partial\psi(z, t)}\,ds\right]\right.$$

$$+\frac{r^2}{I_y}\frac{\partial BM_y(z, t)}{\partial\psi(z, t)}\left[-\cos\left(\frac{s}{r} - \frac{\phi}{2}\right) + \cos\frac{\phi}{2}\right]$$

$$-\frac{r^2}{I_x}\frac{\partial BM_x(z, t)}{\partial\psi(z, t)}\left[\sin\left(\frac{s}{r} - \frac{\phi}{2}\right) + \sin\frac{\phi}{2}\right.$$

$$\left.\left.-\frac{s\sin\frac{\phi}{2}}{r\left(\eta + \frac{\phi}{2}\right)}\right]\right\}\frac{\partial\psi(z, t)}{\partial\varphi(z, t)}\frac{d\varphi(z, t)}{dz}\,. \qquad (A13)$$

The element of torque $d\vec{T}_{sc}(z, t)$ due to the shear stress at an element ds of unit longitudinal length on the surface can be obtained from the expression

$$d\vec{T}_{sc}(z, t) = -\vec{e}_{sc} \times h\vec{\tau}(s, z, t)\,ds\,, \qquad (A14)$$

where

$\vec{e}_{sc}$ = vector from the shear center to the surface element ds.

Since $\vec{e}_{sc}$ may be written as

$$\vec{e}_{sc} = \vec{e}_s + \vec{r}\,, \qquad (A15)$$

where

$\vec{e}_s$ = vector from the shear center to the geocenter of the cross-section,

$\vec{r}$ = radius vector to the surface element ds,

it follows from geometry that

$$\left|\vec{e}_s \times h\vec{\tau}(s, z, t)\right| = e_s\,h\tau(s, z, t)\cos\left(\frac{s}{r} - \frac{\phi}{2}\right)\,, \qquad (A16)$$

$$\left|\vec{r} \times h\vec{\tau}(s, z, t)\right| = rh\tau(s, z, t)\,. \qquad (A17)$$

Hence the thermal torque is obtainable from the expression

$$T_{sc}(z, t) = -e_s \int_0^P h\tau(s, z, t) \cos\left(\frac{s}{r} - \frac{\phi}{2}\right) ds - r \int_0^P h\tau(s, z, t) ds , \qquad (A18)$$

where $h\tau(s, z, t)$ is defined by Equation A13. After the appropriate substitutions and integrations have been made, the expression for the thermal torque is found to be

$$T_{sc}(z, t) = hEe_c \ r \ \frac{\partial V(z, t)}{\partial \psi(z, t)} \ \frac{\partial \psi(z, t)}{\partial \varphi(z, t)} \ \frac{d\varphi(z, t)}{dz} , \qquad (A19)$$

where

$$V(z, t) = \left[e_s \sin\frac{\phi}{2} + \frac{P}{2} \right] \int_0^P \widetilde{T}(s, z, t) \, ds$$

$$- \int_0^P \left[\frac{e_s}{r} \cos\left(\frac{s}{r} - \frac{\phi}{2}\right) + 1 \right] \int_0^s \widetilde{T}(\xi, z, t) \, d\xi \, ds \qquad (A20)$$

and

$$e_s = P \left(\frac{\cos\frac{\phi}{2} - \dfrac{\sin\frac{\phi}{2}}{\pi + \frac{\phi}{2}}}{\pi + \frac{\phi}{2} - \frac{1}{2}\sin\phi} \right) . \qquad (A21)$$

Appendix B

Uncoupled Bending and Torsional Modes of Vibration

In the subsection, "Equations of Undamped-Uncoupled Thermally-Induced Vibration," it is shown that, to obtain the solution to the equations of thermally-induced vibration, the uncoupled normal modes of bending and torsional vibration must be determined. These modes of vibration are the linearly independent solutions to the eigenvalue problems defined by the differential equations

$$EI \frac{d^4 x(z)}{dz^4} - \rho^* \omega_x^2 x(z) = 0 \tag{B1}$$

$$EI \frac{d^4 y(z)}{dz^4} - \rho^* \omega_x^2 y(z) = 0 \tag{B2}$$

$$C_W \frac{d^4 \varphi(z)}{dz^4} - C_T \frac{d^2 \varphi(z)}{dz^2} - I_s \omega_\varphi^2 \varphi(z) = 0 \tag{B3}$$

and their respective boundary conditions

$$x(0) = y(0) = \varphi(0) = 0 \tag{B4a, b, c}$$

$$\frac{dx(0)}{dz} = \frac{dy(0)}{dz} = \frac{d\varphi(0)}{dz} = 0 \tag{B5a, b, c}$$

$$\frac{d^2 x(L)}{dz^2} = \frac{d^2 y(L)}{dz^2} = \frac{d^2 \varphi(L)}{dz^2} = 0 \tag{B6a, b, c}$$

$$EI \frac{d^3 x(L)}{dz^3} + \frac{W_T}{g} \omega_x^2 x(L) = 0 \tag{B7a}$$

$$EI \frac{d^3 y(L)}{dz^3} + \frac{W_T}{g} \omega_x^2 y(L) = 0 \tag{B7b}$$

$$C_W \frac{d^3 \varphi(L)}{dz^3} - C_T \frac{d\varphi(L)}{dz} - I_T \omega_\varphi^2 \varphi(L) = 0 . \tag{B7c}$$

97

Since Equations B1 and B2 are identical in form and have the same boundary conditions, only the solutions to B1 and B3 will be outlined.

Bending Modes of Vibration

Let

$$\lambda^4 = \frac{\rho^* \omega_x^2}{EI} .$$

(B8)

Then Equation B1 may be rewritten as

$$\frac{d^4 x(z)}{dz^4} - \lambda^4 x(z) = 0 .$$

(B9)

The general solution to this equation is

$$x(z) = D_1 \cosh \lambda z + D_2 \sinh \lambda z + D_3 \cos \lambda z + D_4 \sin \lambda z .$$

(B10)

Directly substituting into the four boundary-condition Equations B4a, B5a, B6a, and B7a yields

$$0 = D_1 + D_3 ,$$

(B11)

$$0 = D_2 + D_4 ,$$

(B12)

$$0 = D_1 \cosh \lambda L + D_2 \sinh \lambda L - D_3 \cos \lambda L - D_4 \sin \lambda L ,$$

(B13)

$$0 = D_1 \left(\sinh \lambda L + \frac{W_T}{W_B} \lambda L \cosh \lambda L \right) + D_2 \left(\cosh \lambda L + \frac{W_T}{W_B} \lambda L \sinh \lambda L \right)$$

$$+ D_3 \left(\sin \lambda L + \frac{W_T}{W_B} \lambda L \cos \lambda L \right) + D_4 \left(-\cos \lambda L + \frac{W_T}{W_B} \lambda L \sin \lambda L \right) ,$$

(B14)

where

$$W_B = \rho^* L g .$$

(B15)

For a non-trivial solution of these equations to exist, the determinant of the coefficients of D_1, D_2, D_3, and D_4 must be equal to zero. The evaluation of this determinant yields what is commonly

referred to as the "frequency equation." It is found to be

$$\frac{W_T}{W_B} = \frac{1 + \sec \lambda L \operatorname{sech} \lambda L}{\lambda L (\tan \lambda L - \tanh \lambda L)} \cdot \tag{B16}$$

The nth solution to this equation (B16) in ascending order of magnitude will be written as $(\lambda L)_n$. It follows from Equation B8 that the nth natural frequency of the clamped free beam with tip weight is

$$\omega_{x_n} = \frac{(\lambda L)_n^2}{L^2} \sqrt{\frac{EI}{\rho^*}} \cdot \tag{B17}$$

Associated with each eigenvalue $(\lambda L)_n$ there exists an eigenvector. This eigenvector is the nth mode of vibration. It is obtained by substituting

$$\lambda_n = \frac{(\lambda L)_n}{L} \tag{B18}$$

into B10 to obtain

$$x_n(z) = D_{1n} \cosh \lambda_n z + D_{2n} \sinh \lambda_n z + D_{3n} \cos \lambda_n z + D_{4n} \sin \lambda_n z. \tag{B19}$$

Directly substituting B19 into the boundary-condition Equations B4a, B5a, and B6a and solving the equations simultaneously yield

$$x_n(z) = D_{1n} \cosh \lambda_n z \left[\sin \lambda_n z \operatorname{sech} \lambda_n z - \tanh \lambda_n z \right.$$
$$\left. - \left(\frac{\sin \lambda_n L \operatorname{sech} \lambda_n L + \tanh \lambda_n L}{\cos \lambda_n L \operatorname{sech} \lambda_n L + 1} \right) \left(\cos \lambda_n z \operatorname{sech} \lambda_n z - 1 \right) \right] \cdot \tag{B20}$$

In order to define uniquely the magnitude of D_{1n}, the modes must be normalized. The orthogonality relation that defines D_{1n} for this analysis will be taken to be

$$\int_0^L \rho^*(z) x_n(z) x_m(z) dz = \frac{W_T + W_B}{g} \delta_{m,n}, \tag{B21}$$

where

$$\rho^*(z) = \begin{cases} \rho^* & 0 < z < L \\ \dfrac{W_T}{g} & z = L \end{cases} \tag{B22}$$

99

$$\delta_{m,n} = \begin{cases} 1 & m = n \\ 0 & m \neq n \end{cases} .$$

(B23)

Torsional Modes of Vibration

For numerical computation and notational purposes it is convenient to solve Equation B3 in terms of dimensionless quantities.

Let

$$z = z^* L .$$

(B24)

$$k^2 = \frac{C_T L^2}{C_W} ;$$

(B25)

then Equation B3 becomes

$$\frac{d^4 \varphi(z^*)}{dz^{*4}} - k^2 \frac{d^2 \varphi(z^*)}{dz^{*2}} - \frac{I_s L^4 \omega_\varphi^2}{C_W} \varphi(z^*) = 0$$

(B26)

and the boundary conditions B4c, B5c, B6c, and B7c become

$$\varphi(0) = \frac{d\varphi(0)}{dz^*} = \frac{d^2 \varphi(1)}{dz^{*2}} = 0 ,$$

(B27, B28, B29)

$$\frac{d^3 \varphi(1)}{dz^{*3}} - k^2 \frac{d\varphi(1)}{dz^*} - \frac{I_T L^3 \omega_\varphi^3}{C_W} \varphi(1) = 0 .$$

(B30)

Equation B26 has the general solution

$$\varphi(z^*) = E_1 \sinh k\alpha z^* + E_2 \cosh k\alpha z^* + E_3 \sin k\gamma z^* + E_4 \cos k\gamma z^* ,$$

(B31)

where

$$\lambda^2 = \frac{I_s L^2 \omega_\varphi^2}{C_T} ,$$

(B32)

$$k^2 \lambda^2 = \frac{I_s L^4 \omega_\varphi^2}{C_W} ,$$

(B33)

100

$$\alpha = + \left(\frac{1}{2} + \frac{1}{2} \sqrt{1 + \frac{4\lambda^2}{k^2}} \right)^{1/2} , \tag{B34}$$

$$\gamma = + \left(-\frac{1}{2} + \frac{1}{2} \sqrt{1 + \frac{4\lambda^2}{k^2}} \right)^{1/2} . \tag{B35}$$

In a manner analogous to that of the preceding subsection Equation B31 is substituted into the four boundary-condition equations B27 through B30 to yield

$$0 = E_2 + E_4 , \tag{B36}$$

$$0 = k\alpha E_1 + k\gamma E_3 , \tag{B37}$$

$$0 = E_1 k^2 \alpha^2 \sinh k\alpha + E_2 k^2 \alpha^2 \cosh k\alpha - E_3 k^2 \gamma^2 \sin k\gamma - E_4 k^2 \gamma^2 \cos k\gamma , \tag{B38}$$

$$0 = E_1 \left(-k^3 \alpha\gamma^2 \cosh k\alpha + \frac{I_T}{I_s L} \lambda^2 k^2 \sinh k\alpha \right)$$

$$+ E_2 \left(-k^3 \alpha\gamma^2 \sinh k\alpha + \frac{I_T}{I_s L} \lambda^2 k^2 \cosh k\alpha \right)$$

$$+ E_3 \left(k^3 \gamma\alpha^2 \cos k\gamma + \frac{I_T}{I_s L} \lambda^2 k^2 \sin k\gamma \right)$$

$$+ E_4 \left(-k^3 \gamma\alpha^2 \sin k\gamma + \frac{I_T}{I_s L} \lambda^2 k^2 \cos k\gamma \right) . \tag{B39}$$

For a non-trivial solution of these equations to exist, the determinant of the coefficients of E_1, E_2, E_3, and E_4 must be equal to zero. The evaluation of this determinant yields the frequency equation

$$\frac{I_T}{I_s L} = \frac{2\lambda^2 \sec k\gamma \operatorname{sech} k\alpha + k^2 \left(1 + \frac{2\lambda^2}{k^2} \right) + k\lambda \tan k\gamma \tanh k\alpha}{\lambda k^2 \sqrt{1 + \frac{4\lambda^2}{k^2}} (\alpha \tan k\gamma - \gamma \tanh k\alpha)} \tag{B40}$$

If the substitutions

$$\lambda^{*2} = \lambda^2 k^2 \tag{B41}$$

101

$$\alpha^* \;=\; + \left(\frac{1}{2} + \frac{1}{2} \sqrt{1 + \frac{4\lambda^{*2}}{k^4}} \right)^{1/2} \tag{B42}$$

$$\gamma^* \;=\; + \left(-\frac{1}{2} + \frac{1}{2} \sqrt{1 + \frac{4\lambda^{*2}}{k^4}} \right)^{1/2} \tag{B43}$$

are made, the frequency Equation (B40) may be rewritten as

$$\frac{I_T}{I_s L} \;=\; \frac{2 \left(\frac{\lambda^*}{k} \right)^2 \operatorname{sech} k\alpha^* \sec k\gamma^* + k^2 \left(1 + \frac{2\lambda^{*2}}{k^4} \right) + \lambda^* \tan k\gamma^* \tanh k\alpha^*}{k\lambda^* \sqrt{1 + \frac{4\lambda^{*2}}{k^4}} \; (\alpha^* \tan k\gamma^* - \gamma^* \tanh k\alpha^*)} \tag{B44}$$

It is obvious that either Equation B40 or B44 can be used to determine the natural frequencies of the cylinder of open section with tip inertia when the tip is free to warp. It is convenient when numerically solving the frequency equation, however, to use Equation B40 for cases where $k^2 > 100$ and to use Equation B44 when $k^2 < 100$. This choice is made to avoid the inherent problems associated with digitally taking the difference between very large nearly equal numbers.

Let λ_n be the nth value of λ that satisfies the frequency equation in ascending order of magnitude. It follows then that the nth torsional natural frequency as defined in Equation B32 is

$$\omega_{\varphi_n}^2 \;=\; \frac{C_T \lambda_n^2}{I_s L^2}. \tag{B45}$$

The nth eigenvector, that is, the nth torsional mode of vibration, is obtained by substituting λ_n into the general solution given by Equation B31. This yields

$$\varphi_n(z^*) \;=\; E_{1n} \sinh k\alpha_n z^* + E_{2n} \cosh k\alpha_n z^* + E_{3n} \sin k\gamma_n z^* + E_{4n} \cos k\gamma_n z^*, \tag{B46}$$

where

$$\lambda_n^2 \;=\; \frac{I_s L^2 \omega_{\varphi_n}^2}{C_T}, \tag{B47}$$

$$\alpha_n \;=\; + \left(\frac{1}{2} + \frac{1}{2} \sqrt{1 + \frac{4\lambda_n^2}{k^2}} \right)^{1/2}, \tag{B48}$$

$$\gamma_n \;=\; + \left(-\frac{1}{2} + \frac{1}{2} \sqrt{1 + \frac{4\lambda_n^2}{k^2}} \right)^{1/2}. \tag{B49}$$

Substituting into Equations B27, B28, and B29 and solving for the unknown coefficients yield the nth torsional mode of vibration. This is

$$\varphi_n(z) = E_{1n} \cosh \frac{k\alpha_n}{L} z \left[\tanh \frac{k\alpha_n}{L} z - \frac{\alpha_n}{\gamma_n} \operatorname{sech} \frac{k\alpha_n}{L} z \sin \frac{k\gamma_n}{L} z \right.$$

$$\left. - G_n \left(1 - \operatorname{sech} \frac{k\alpha_n}{L} z \cos \frac{k\gamma_n}{L} z \right) \right] \qquad (B50)$$

where

$$z = z^* L , \qquad (B51)$$

$$G_n = \frac{\alpha_n \left(\alpha_n \tanh k\alpha_n + \gamma_n \operatorname{sech} k\alpha_n \sin k\gamma_n \right)}{\alpha_n^2 + \gamma_n^2 \operatorname{sech} k\alpha_n \cos k\gamma_n} . \qquad (B52)$$

The magnitude of E_{1n} can be specified by requiring that the mode shape satisfy the normalization condition

$$\int_0^L I_s(z) \varphi_n(z) \varphi_m(z) \, dz = \left(I_T + I_s L \right) \delta_{m,n} , \qquad (B53)$$

where

$$I_s(z) = \begin{cases} I_s & 0 < z < L \\ I_T & z = L \end{cases} . \qquad (B54)$$

List of Symbols

Lowercase English

$a_n(t)$	amplitude coordinate associated with the nth transverse bending mode in the (X_1, Z_1) plane
$b_n(t)$	amplitude coordinate associated with the nth transverse bending mode in the (Y_1, Z_1) plane
$c_n(t)$	amplitude coordinate associated with the nth torsion mode
c	specific heat of material
e_c	thermal expansion coefficient of material
e_s	distance between the geometrical center and the shear center of the cross-section
g	acceleration of gravity
h	thickness of cylinder wall
$[\vec{i}, \vec{j}, \vec{k}]$	orthonormal set of basis vectors parallel to body axes triad $[X, Y, Z]$ respectively at (z, t), but having their origin at $z = 0$
$[\vec{i}_1, \vec{j}_1, \vec{k}_1]$	orthonormal set of basis vectors parallel to inertial axes triad $[X_1, Y_1, Z_1]$ respectively, having their origin at $z = 0$
ℓ	positive integer
m	positive integer
n	positive integer
$\vec{n}(s)$	unit vector normal to the cross-section and directed outward at point s on the circumference
$q_n(z, t)$	nth generalized thermal coordinate at thermal station z and time t
r	radius of cross-section

s	arc length measured from outer to inner seam around the cross-section
t	coordinate used to measure time
$x_n(z)$	nth normalized transverse bending mode of vibration in the (X_1, Z_1) plane
$x_c(s)$	distance from the point s on the cross-section to the Y-axis
$y_n(z)$	nth normalized transverse bending mode of vibration in the (Y_1, Z_1) plane
$y_c(s)$	distance from the point s on the cross-section to the X-axis
z	coordinate used to measure arc length along the centroidal axis of the boom
z'	arbitrary point on centroidal axis between z and L

Uppercase English

$A_n(t)$	generalized displacement coordinate associated with the nth transverse bending mode in the X_1, Z_1 plane
$A_n^*(t)$	generalized force associated with the generalized displacement coordinate $A_n(t)$
$B_n(t)$	generalized displacement coordinate associated with the nth transverse bending mode in the (Y_1, Z_1) plane
$B_n^*(t)$	generalized force associated with the generalized displacement coordinate $B_n(t)$
$BM_x(z, t)$	thermal bending moment about the X-axis at (z, t)
$BM_y(z, t)$	thermal bending moment about the Y-axis at (z, t)
$C_n(t)$	generalized displacement coordinate associated with the nth torsional mode
$C_n^*(t)$	generalized force associated with the generalized displacement coordinate $C_n(t)$
C_T	torsional rigidity
C_W	warping rigidity
D_i	constants of integration ($i = 1, 2, \cdots$)
E	Young's modulus of elasticity
EI	bending stiffness

$\vec{F}$ resultant force distribution along boom

$[F_1, F_2, F_3]$ components of resultant force distribution with respect to basis vectors $[\vec{i}, \vec{j}, \vec{k}]$

G component of stress couple parallel to the X-axis at (z, t); "flexural couple"

G' component of stress couple parallel to the Y-axis at (z, t); "flexural couple"

G_s shear modulus of elasticity

H component of stress couple parallel to the Z-axis at (z, t); "torsional couple"

I average cross-sectional geometrical moment of inertia

I_x cross-sectional geometrical moment of inertia about the X-axis

I_y cross-sectional geometrical moment of inertia about the Y-axis

I_s mass rotational moment of inertia per unit length about the shear center axis

I_T mass rotational moment of inertia of the tip weight

J_s solar radiation intensity

K, K' components of resultant couple distribution per unit length parallel to the X-, Y-axes respectively at (z, t)

K_B, K_B' components of K, K' associated with kinetic reaction of transversely accelerating mass elements, respectively

K_C, K_C' sum of K_B, K_W and K_B', K_W' respectively

K_D, K_D' components of K, K' associated with the dissipative forces

K_H, K_H' components of K, K' associated with the thermal loading

K_W, K_W' components of K, K' associated with kinetic reaction of torsionally accelerating mass elements

K_T thermal conductivity of material

L antenna length

$\vec{M}$ moment of the internal stress distribution in the cross-section about its centroid

N component of stress resultant parallel to X-axis at (z, t)

N' component of stress resultant parallel to Y-axis at (z, t)

P	total perimeter of cross-section, tape width
$Q_n(z, t)$	generalized thermal input associated with the nth thermal mode and nth generalized thermal coordinate $q_n(z, t)$ at (z, t)
$\ddot{R}(z, t)$	transverse acceleration of the mass element at z at time t
$\overrightarrow{SL}(z, t)$	unit vector normal to Z-axis and directed toward sun at (z, t)
T	component of stress resultant parallel to Z-axis at (z, t); "tension"
T_0	steady state mean temperature of cross-section in thermal field
$\tilde{T}(s, z, t)$	absolute temperature of the point (s, z) on the surface of the boom at time t
$T(s, z, t)$	deviation of the absolute temperature $\tilde{T}(s, z, t)$ from the mean T_0
$T_n(s)$	nth normalized thermal mode
$T_{sc}(z, t)$	thermal torque at (z, t) about axis normal to cross-section
$\vec{V}$	resultant of the internal stress distribution on the cross-section
$V(z, t)$	thermal torque coefficient used to define $T_{sc}(z, t)$
W_B	boom weight
W_T	tip weight
[X, Y, Z]	body axes at (z, t)
X	body axis at (z, t); principal axis of inertia normal to axis of symmetry and longitudinal axis, directed so that X, Y, Z is a right-handed system
Y	body axis at (z, t); principal axis of inertia parallel to axis of symmetry and normal to longitudinal axis, directed away from overlap
Z	body axis parallel to longitudinal axis, directed positive from the point z toward the tip of the boom
$[X_1, Y_1, Z_1]$	inertially fixed axis system, coincident with the body axes at $z = 0$
$[X(z, t), Y(z, t), z]$	displacement coordinates of the point z along the centroidal axis at time t in the $[X_1, Y_1, Z_1]$ coordinate system
$[X_s(z, t), Y_s(z, t)]$	displacement coordinates of the point z along the centroidal axis of the boom when it is aligned along the instantaneous thermal equilibrium shape at time t measured in the $[X_1, Y_1, Z_1]$ coordinate system

Script Greek

$\alpha_n(t)$	amplitude of nth mode at time t in the modal expansion of $X_s(z, t)$
α_s	absorptivity of boom surface
$\beta_n(t)$	amplitude of nth mode at time t in the modal expansion of $Y_s(z, t)$
β_x	viscous damping coefficient for transverse motion
β_φ	viscous damping coefficient for torsional motion
$\gamma_n(t)$	amplitude of nth mode at time t in the modal expansion of $\varphi_s(z, s)$
δ_c	distance between geometrical center and centroid of cross-section
$\delta_{m,n}$	Kronecker delta function
ϵ	emissivity
ζ_x	transverse damping ratio
ζ_{x_n}	transverse damping ratio of nth transverse bending mode
ζ_φ	torsional damping ratio
ζ_{φ_n}	torsional damping ratio of nth torsional mode
η	defined constant $= \sqrt{C_T/C_W}$
$[\theta_1, \theta_2, \varphi]$	Euler angle sequence used to define rotational orientation of $[\vec{i}, \vec{j}, \vec{k}]$ relative to $[\vec{i}_1, \vec{j}_1, \vec{k}_1]$
κ, κ'	curvature component about the X-, Y-axes at (z, t)
λ_n	thermal decay constant of nth thermal mode
ρ	weight density of material
ρ^*	mass per unit length of boom
σ	Stefan-Boltzmann constant
τ	twist about Z-axis at (z, t)
τ_n	thermal time constant of nth thermal mode
ϕ	angular amount of overlap
$\varphi(z, t)$	angular amount of twist at (z, t) of the cross-section about its longitudinal axis

$\varphi_s(z, t)$	torsional coordinate of the point z along the boom when it is aligned along the instantaneous thermal equilibrium shape at time t
$\varphi_n(z)$	nth normalized torsional mode of vibration
$\psi(z, t)$	angular position of the sun measured relative to the cross-sectional principal axes of inertia
ω_{x_n}	nth natural frequency of transverse vibration
ω_{φ_n}	nth natural frequency of torsional vibration

Printed Greek

B	functions used in defining generalized thermal input $Q_n(z, t)$
Γ	defined parameter
$\overrightarrow{\Delta R}(z', z, t)$	vector connecting points z' and z along the centroidal axis at time t
E	functions used in defining generalized thermal input $Q_n(z, t)$
H	defined parameter
Θ	component of resultant couple distribution per unit length parallel to Z-axis at (z, t)
Θ_c	component of Θ associated with kinetic reaction of torsionally accelerating mass element
Θ_D	component of Θ associated with the dissipative force
Θ_H	component of Θ associated with the thermal loading
$\vec{K}$	applied resultant couple distribution along boom
$\Xi(s, z, t)$	defined to distinguish between sunlit and dark sides of boom
P_n	parameter used in generalized force expression; associated with nth torsional mode
T_n	parameter used in generalized force expression; associated with nth transverse mode
$\Upsilon(s, z, t)$	function used to define the heat input about the surface point (s, z) at time t
Ω_n	nth eigenvalue of the thermal characteristic equation
$\vec{\Omega}$	curvature vector; angular velocity vector expressed relative to $[\vec{i}, \vec{j}, \vec{k}]$ of the [X, Y, Z] axes when it slides at a constant rate along the longitudinal axis of the boom